博士論文

Development of Turn-on Biomolecule Sensors Utilizing Exciton-controlled Hybridization-sensitive Fluorescent Oligonucleotide Probes

(励起子制御された二重鎖形成感受性蛍光オリゴヌクレオチドプローブを用いたターンオン型生体分子センサーの開発**)**

国　立浩

Summary

Exciton-controlled hybridization-sensitive fluorescent oligonucleotide (ECHO) probes are hybridization-dependent fluorescent nucleotides regulated by the H-aggregation of incorporated thiazole orange homodimers. ECHO probes have been shown to be useful in nucleic acid detection. With an effort to expand applications of ECHO probes to more versatile biological systems, I carried out this study to develop new homodimer-attached fluorescent nucleic acid as exciton-controlled biosensors of specific bio-targets.

In chapter 1, I presented general introduction mainly divided into two sections. First, biosensors were overviewed on the basis of diverse bio-recognition elements and signal transduction components of biosensors. Nucleic acid-based biosensors were stressfully introduced including the importance, types, design and applications of fluorescent nucleic acid-based biosensors. Second section gave description of the new concept for ECHO probe design. This section also described a great quantity of applications of ECHO probes in real biological research and practice. Finally, the objectives of this thesis were put forward.

In chapter 2, I developed a fluorescent competition system that allows quantification of bacteria population by fluorescence-based analysis. RNA backbone ECHO probes were successfully synthesized and exhibited favorable hybridization based fluorescent turn-on responsiveness comparable to the previous DNA ECHO probes. Then, to provide direct information of bacterial amount, the neomycin RNA aptamer, served as the competitor of ribosome in *E. coli* to neomycin B, was covalently conjugated to two thiazole orange moieties and effectively quenched by neomycin B. As a proof of concept, I demonstrated that modified neomycin aptamers in neomycin B-containing solution showed apparently higher fluorescent intensity in the presence of *E. coli* compared to that in the absence of *E. coli*.

In chapter 3, I reported an ATP-sensitive fluorescent nucleic acid probe. The thiazole orange dimer was covalently conjugated to the site 13 of ATP RNA aptamer that is proximal to the duplex fragment of ATP RNA aptamer after forming the ATP/aptamer complex. The intensity of fluorescence from such an ATP-sensing aptamer system increased several times in the presence of ATP. This probe displayed the specificity to

ATP in contrast to UTP, GTP, CTP, ADP and AMP.

In chapter 4, I demonstrated a series of novel ECHO probes for two-photon-excited nucleic acid imaging. Three types of these probes were doubly conjugated with dyes stocked in our lab and six types were labelled with newly designed dyes. All novel ECHO probes showed nucleic acid hybridization-based fluorescent turn-on properties. The styryl cyanine probes have higher molar extinction coefficients while the fluorescent ON/OFF ratio of indole-based cyanine probes are more desirable for specific nucleic acid imaging. Interestingly, the indole-based cyanine probes performed excellent RNA sensitivities that have been quite problematic for the previously developed ECHO probes. Three of these probes attached with T2, T3 and T5 were identified to be suitable for two-photon-excited RNA imaging in live Hela cells and embryonic mouse brain at excitation wavelength 1030nm. These probes are also suitable for washing-free FISH imaging of specific DNA in fixed MEF7 cells washing-free two-photon-excitable FISH imaging of telomeres in adult mouse brain slices.

In chapter 5, conclusion and perspective of this thesis were described.

In summary, I have successfully expanded applications of ECHO probes into detection of bacterial population and ATP and two-photon-excited imaging of nucleic acids in cells and tissues.

Table of Contents

Chapter 1: General Introduction

1.1 Biosensors for biological analysis

1.1.1 Biosensors: translators of biological signals

1.1.2 Fluorescent aptamer-based biosensors

1.1.3 Detection of intracellular RNAs

1.2 Exciton-controlled hybridization-sensitive fluorescent oligonucleotide (ECHO) probes

1.2.1 Basis of aggregation-based probe design

1.2.2 Working principle of ECHO probes

1.2.3 Characterization and optimization of ECHO probes

1.2.4 Photo-physical functional expansions

1.2.5 Biological application expansions

1.3 Objectives of this thesis

1.4 References

Chapter 2: Bacterial Population Assessment in Solid-state Fermentation by Exciton-controlled Fluorescent RNA

2.1 Abstract

2.2 Introduction

2.3 Results and discussion

2.4 Conclusions

2.5 Experimental procedures

2.6 References

Chapter 3: ATP-sensitive Fluorescent Nucleic Acid Probes

3.1 Abstract

3.2 Introduction

3.3 Results and discussion

3.4 Conclusions

3.5 Experimental procedures

3.6 References

Chapter 4: Novel Exciton-controlled Hybridization-sensitive Fluorescent Probes for Two-photon Imaging of Nucleic Acid

4.1 Abstract

4.2 Introduction

4.3 Results and discussion

4.4 Conclusions

4.5 Experimental procedures

4.6 References

Chapter 5: Conclusion and Prospect

List of Achievements

Acknowledgements

Chapter 1

General Introduction

1.1 Biosensors for biological analysis

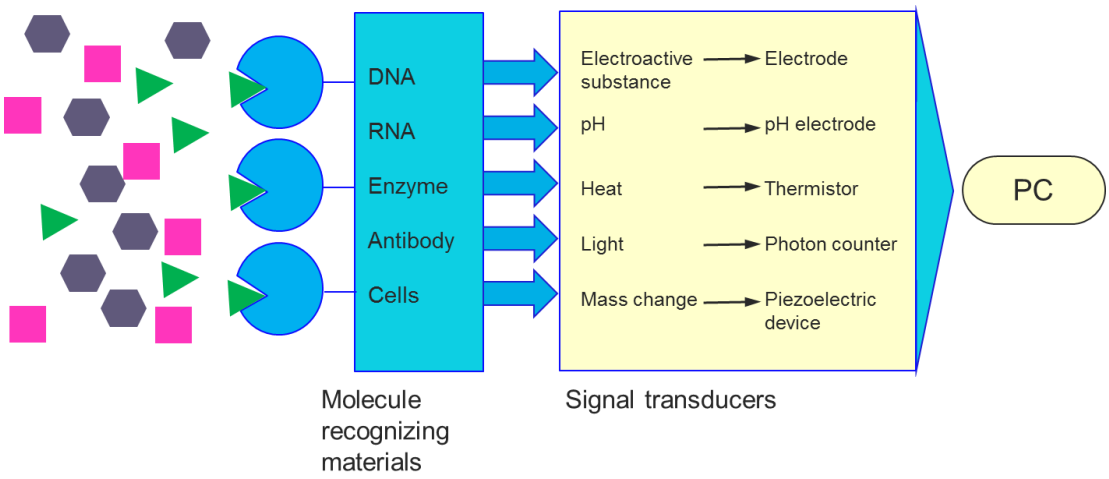

Figure 1-1. Schematic diagram of biosensor main components including molecular recognition components, signal transducers and readout.

1.1.1 Biosensors: translators of biological signals

A biosensor is an integrated system consisting of two main parts, the molecular recognizing element and the signal transducing element. The former element, recognizing element, firstly reacts or interacts with the analytes of the target samples and the latter one, signal transducing element, then effectively converts that signal into the readable data in computer or other electrical analysis systems (Figure 1-1). For these reasons, the selectivity of the biosensor is mainly determined by the bio-recognition element while the sensitivity is primarily affected by the transducing component. Bio-catalytic enzymes, microorganisms or tissues can be used for the bio-recognizing material. More common utilized recognition elements in bioassay are high affinity molecules, such as nucleic acids and antibodies [1]. Typical transducing elements include electrochemical, optical or thermal based detectors.

Recently, nucleic acid based biosensors have inspired increasing attention because of the variability and specificity of nucleic acid sequences. DNAs which can hybridize with the complementary strand possess high binding efficiency and good specificity, thus the detection of DNA or RNA can be easily achived. Broadly speaking, employing functional nucleic acids like aptamer as their recognition elements, nucleic acid based sensors put detection of other analytes into reality.

1.1.2 Fluorescent aptamer-based biosensors

Aptamers are oligonucleotides-based recognition components with high affinity and specificity to their corresponding molecular targets and the determinant of these properties is the specific base sequences in single-stranded DNA or RNA. Naturally, aptamers exist in RNA riboswitches of cells, but they can also be artificially isolated using the technology termed as systematic evolution of ligand by exponential enrichment (SELEX)[2]. Increased amounts of aptamers have been discovered and characterized, which can bind to various biological target molecules specifically including single molecules, proteins or cells. In the field of biosensors design, aptamers as the recognition components are being received more and more attentions. Although the monoclonal antibodies, as the conventional recognition components, have been widely used for bioassay, aptamers possess many distinguished properties[3-5]:

- The antibodies production needs repeated selection processes; aptamers can be chemically synthesized in a great quantity after identification or selection, that is more cost-effective.
- Thermally denaturing of aptamers is reversible and thus aptamer-based assays are more robust in the variable temperatures. Due to this reason, usage of aptamers can be widened to the high temperature assay conditions.
- Oligonucleotides in aptamers could readily be modified chemically either for the basic chemical structures of nucleic acid, such as bases, ribose or the backbones, or for the signal moieties, such as fluorophores and quenchers. The modification attributes of aptamer makes us smart design of biosensors more easily.
- By hybridizing with their complementary sequences, conformational switches of aptamers could be used as the signal transduction design.
- Generally, monoclonal antibodies recognize specific proteins or cells, other than ions or small molecules. For aptamers, except the proteins and cells, ions and small molecules can also be the substrates of aptamers that make the applications of the aptamer-based biosensors greatly expanded.
- The binding mechanism of aptamers is quite different with antibodies that are always explained in a way of lock and key. Aptamers have various conformations before and after binding to its specific molecular targets. This mechanism provides us a distinct, feasible approach for biosensor design: conformational switching based biosensor design.

Due to these unique advantages above, aptamers are being considered as the potential alternatives to monoclonal antibodies in both bioassays and diagnostic applications. For biomolecule detection, aptamers can be used in a simple binding way similar to that of

monoclonal antibodies. But more other unique assays for aptamers have been demonstrated. Until now, more than thousands of papers have been published on aptamer-based biosensors and it is impossible to be outlined in the short length. Therefore, I focus on the general design strategies of aptamer-based biosensors here.

Binding-based assays (Figure 1-2a)

Since aptamers show affinity to specific ligands or substrates, aptamers can be used as a recognition component directly. Similar to conventional antibody-based assays ELISA (enzyme linked immunosorbent assay), a pair of aptamers can be used in a sandwich assay[6-8]. However, multivalent aptamer-based nanoparticles could be created by conjugating several aptamers in to nanoparticles, such as AuNPs and thus novel ELISA approach using multivalent aptamer-nanoparticles perform higher sensitivities compared to the conventional antibody-based ELISA[9-12]. However, stringent washing steps are necessarily needed for the simple binding-based assays because the high concentration of serum proteins and a large amount of unbinding aptamers exist in the biomedical samples that may give rise to the false signal. One exception is aptamer-conjugated AuNPs. For some fluorophores, coupling to the gold surface will result in the color change and offer rational distinction between binding and unbinding aptamer via color.

Split aptamer sensors (Figure 1-2b)

In case splitting at the suitable site into two fragments, aptamers have the potential to be self-assembled after introducing the target ligands. Fluorophore and quencher pairs with the proximity induced fluorescent quenching can be labelled in the split aptamers and response the binding induced proximity. If the target ligands are present, the two pieces will be re-assembled and the fluorescent intensity will also change accordingly. The HIV-1 Tat protein has been detected using such kind of strategy[13]. One of the fragments of HIV-1 Tat aptamer is a hairpin structure conjugated with a pair of quencher and fluorophore at the two ends. The fluorescence is quenched without the addition of target molecules while the fluorescence is increased vastly with the addition of target substrates because the split fragments form a ternary complex disrupting the hairpin structure of the fragment and the fluorophore and quencher are enforced to separate with each other. Using the similar design, cocaine and adenosine have also been detected successfully by the split aptamers[14]. Pyrene excimer formation leads to fluorescent enhancement and has also been used for the development of split aptamer based biosensors[15] and split aptamer immobilized nanoparticles with the ligand induced

re-assembly render a more sensitive detection[16]. However, the drawbacks of split aptamer based design are also very notable. Firstly, the splitting site is quite difficult to control and that always destroy the original binding affinity of target molecule. Secondly, the interaction mechanisms turn from the dual-molecule reaction into a tri-molecular reaction and the binding affinity declines to a relatively low level.

Structure-switching aptamers (Figure 1-2c)

The conformations of aptamers, as one kind of nucleic acid, are mainly determined by the hybridization of oligonucleotides. Once the additional complementary DNA or RNA is introduced, the original structures of aptamers will be significantly changed. Thus, the distinct binding and unbinding structures could be used for aptamer-based biosensor design. The quencher conjugated complementary DNA is a rational design to hybridize with the fluorophore conjugated aptamer. Due to the close distance between the fluorophore and the quencher, the fluorescence is almost totally quenched in the absence of target ligands. After addition of the target ligand, the complementary DNA with a quencher is released by competition, resulting in restoration of original aptamer conformation and the corresponding fluorescent enhancement[17]. The prime merit of conformation switching based design is the artificial controlling of large distance change and the marked fluorescent increase[18-24]. Restraining the initial aptamer conformation may also be implemented by other materials, such as the inorganic surface graphene oxide. Graphene oxide has dual functions towards fluorophore labelled aptamers: efficient absorbance of single-stranded aptamers and valid quenching the fluorescence in the probes. Without target molecules, the labelled aptamer attaches to the graphene oxide and little fluorescence could be observed, whereas the adsorbed aptamer can disassociate to perform high fluorescent increase after adding the specific target substrate (Figure 1-2f)[25]. Due to the distinguished artificial switching ability of nucleic acid based aptamers comparing with monoclonal antibodies, the conformation switching based design is a quite unique strategy for biosensor development.

Folding based aptamer sensors (Figure 1-2d)

Compared with antibody, aptamer binding to the cognate ligands has another distinct property: aptamer-based binding involves a global conformation variation. This difference provides a possibility to tell the signals from the binding and unbinding aptamers[26]. One design is to use an aptamer with a conjugated fluorophore that is sensitive to the changed local environment due to the conformational change of aptamers and was confirmed successfully[27]. This type of labelled aptamer can be easily

synthesized but the modified site and the according fluorescent change should be carefully considered and estimated and always the signal transduction is inefficient or modest. The fluorophore and quencher pair used in conformation switching based design can also be introduced to folding based design and improve the performance of target sensing. In the folding based aptamer design to test magnesium ion, cocaine, adenosine/ATP and proteins, the fluorophore and quencher are respectively labelled at the two end of the aptamer[28-31]. The ligand induced end-toe-end distance change could response as the florescent increase from the de-quenched fluorophore. Due to the much stronger adsorbing ability to nanoparticles of free aptamers than the folded aptamers, many researchers have used AuNPs to detect the folded aptamers in a similar way for split aptamer conjugated nanoparticles[32-33]. One weak point of folding-based aptamer design is the relatively small distance change compared to the much larger distance change in conformational switching based design.

Fused aptamers (Figure 1-2e)

Different with the conformational switching design that introduces an artificial linear nucleic acid to disrupt the original structure of analyte aptamer, the fused aptamer design fused an analyte aptamer and a fluorophore aptamer, in which the former one is used to stabilize the conformation of the latter. The common used fluorophore aptamer is the malachite green (MG) aptamer. The free MG in water solution is non-fluorescent and the bound MG to the MG aptamer can emit strong fluorescent intensity via the inhibition of structural rotation by the RNA aptamer[34]. MG aptamers have been fused to FMN aptamers, ATP aptamers and theophylline aptamers and displayed substrate-induced fluorescent turn-on[35]. In these designs, the malachite green binding pocket in the RNA aptamer can only be formed after the formation of stable analyte aptamer by adding target analytes and thus generate bright fluorescence of MG. Compared the another four methods mentioned above, fused aptamers are labelling-free aptamers and therefore suitable for detection of analytes in live cell. Except for the small molecules, fused aptamers have been also applied to detect large molecules, such as proteins[36-37].

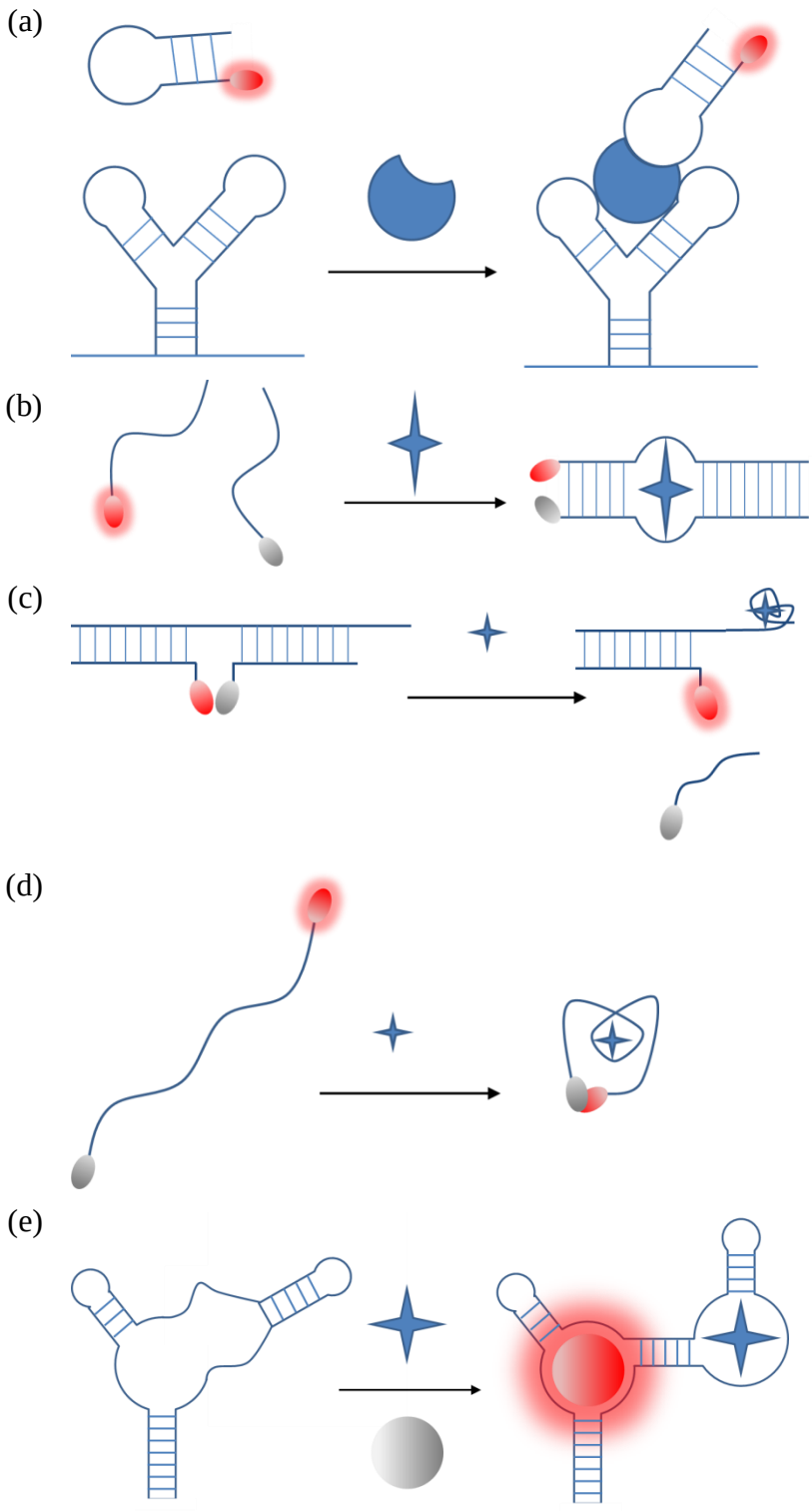

Figure 1-2. Versatile strategies of aptamer-based biosensor design. (a) Binding-based assays. (b) Self-assembly of split aptamers. (c) Switching-based design. (d) Folding-based sensors. (e) Induced reassembly of fused aptamers.

1.1.3 Detection of intracellular RNAs

RNAs are very crucial genetic biomolecules that involve the delivery of genetic information as messenger RNAs, and regulation of many important biological processes. Detection of RNAs, especially the intracellular RNAs, is essential to elucidate the biological functions of RNAs. To monitor the temporal and spatial dynamics of RNAs in live cells, many RNA imaging approaches have been developed, generally divided into two types: genetic vector-based method and chemically synthesized nucleic acid probes. The genetic vector-based methods use vector to insert specific protein binding sequences or the dye interacting sequences into RNAs of interest before imaging. The fluorescent proteins or dyes then specifically image target RNAs via the inserted RNA sequences. This approach can only image the artificial endogenous RNAs or the exogenous RNAs. The synthesized nucleic acid probes specifically hybridize with the target RNAs other than the inserted sequences. Therefore, chemically synthesized nucleic acid probes could be used for endogenous RNA imaging.

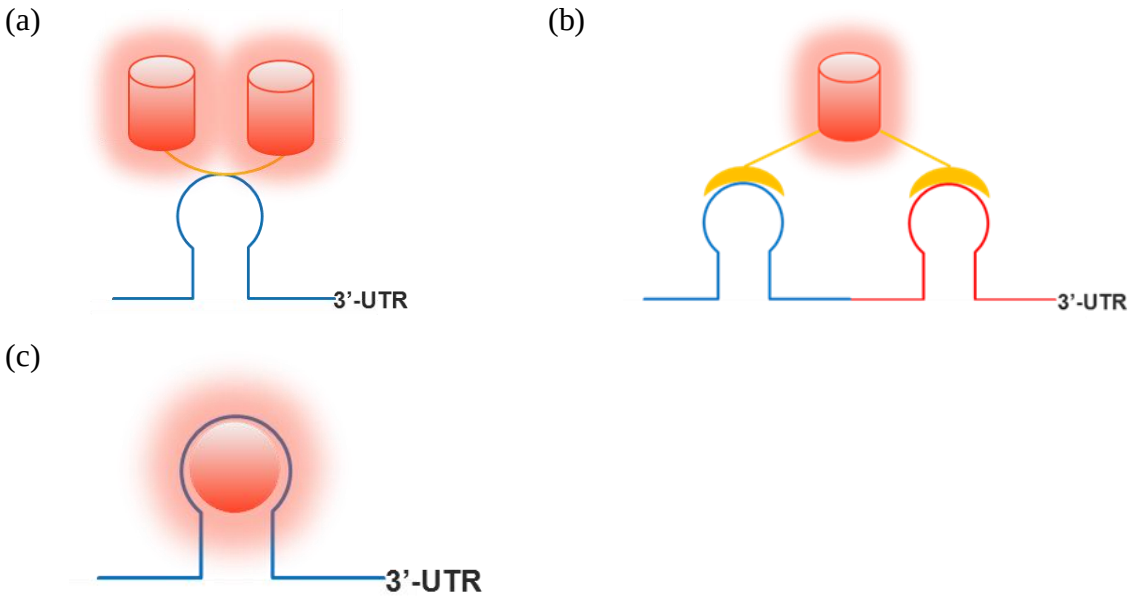

Figure 1-3. Schematic diagrams of genetic vector-based RNA imaging. (a) RBP-FP system. (b) split fluorescent protein system. (c) fluorophore RNA aptamer system.

Genetic vector-based RNA imaging

Currently, three types of genetic vector-based RNA imaging systems have been developed: RNA binding protein-fluorescent protein (RBP-FP) system, split fluorescent protein system, and fluorophore RNA aptamer system.

RNA binding protein-fluorescent protein system (RBP-FP system) (Figure 1-3a)

The commonly used RBP is the MS2 coat protein (MCP) that can recognize a specific RNA sequence MS2 binding sequence (MBS). To observe target RNAs in cells, a series of tandem MBSs are inserted into the 3'-UTR of target RNAs and meanwhile the MCPs are fused with fluorescent proteins, such as GFP. After transfection of MCP-GFP fusion protein containing vectors into target cells, the MCP-GFP fusion proteins bind to target RNAs and demonstrate the location of target RNAs specifically. The RBP-FP system has been introduced to ASH1 RNA and the location and transportation of this RNA have been visualized in live cells[38].

Split fluorescent protein system (Figure 1-3b)

Although RBP-FP system is very useful for imaging target RNAs, the fluorescent backgrounds are high and sometimes are not negligible that would affect the next functional analysis. To solve this problem, the split fluorescent proteins are introduced into the imaging system to substitute the complete fluorescent proteins[39-42]. The split fluorescent proteins include two complementary fragments that are non-fluorescent: N-terminal fluorescent proteins (N-FPs) and C-terminal fluorescent proteins (C-FPs). To reconstitute the split FPs to be functional, MCP-PCP based reconstitutions were firstly introduced[43]. PCP is PP7 bacteriophage coat protein that can specifically binds to the PP7 binding sequence (PBS). To visualize target RNAs, MBS and PBS are rationally inserted into the target RNAs at the 3'-UTR. After transfecting N-FP-MCPs and C-FP-PCPs into target cells, the binding of these fusion proteins to the inserted MBS and PBS facilitates the two fragments of FPs close to each other and reconstruct the complete FPs to visualize the target RNA. The second reconstitution of FPs is using the bio-orthogonal peptides[45]. HTLV-Rex peptide and 1N peptide can specifically bind to HTLV-Rex RNA aptamer and 1N RNA aptamer, respectively. The fused proteins, HTLV-Rex-N-FP and 1N-C-FP, have successfully imaged the target RNAs in live bacterial cells by binding the corresponding RNA aptamers. Different with these two described methods, the third reconstitution of split fluorescent proteins employs the split RBP. Eukaryotic initiation factor 4A (eIF4A) is a protein that specifically binds to the

eIF4A interactive aptamer sequence. Interestingly, the two fragments of split eIF4A could automatically reconstruct by recognition of the target aptamer. By fusing the split eIF4A and the split FPs, the eIF4A interactive aptamer inserted target RNAs could be fluorescently readable in live cells with high sensitivity[44].

Fluorophore RNA aptamer system (Figure 1-3c)

Fluorophore RNA aptamer system is another vector based RNA imaging system. The fluorophore are generally non-fluorescent in water solutions and strongly enhance their fluorescence in the presence of specific RNA aptamers. The fluorophore RNA aptamer system utilizes the fluorophores to image the aptamer inserted target RNAs other than the RBPs used in the RBP-FP system and split fluorescent protein system and thus is quite suitable for real-time imaging because the binding of fluorophore to the aptamer is quick. Difluoro-4-hydroxybenzylidene imidazolinone (DFHBI) is most used fluorophores in fluorophore RNA aptamer imaging system[46]. Spinach aptamer, the DFHBI-binding aptamer, can specifically increase the fluorescence intensity of this fluorophore up to about 2000 times. However, the light-on property of DFHBI in the presence of Spinach aptamer will be modest in the incubated cells. To solve these challenges, alternative aptamers and fluorophores were screened. PFP-DFHBI and Spinach2 are another pairs for fluorophores aptamer imaging system and perform 5-fold higher binding affinity than the pair of DFHBI and Spinach aptamer. In addition, Spinach2-PFP-DFHBI is more resistant to salt concentration than Spinach-DFHBI [48]. DFHBI-1T is another alternative fluorophore and it shows lower fluorescent background than DFHBI in the incubated cells[47]. Thiazole orange 1 (TO1) can specifically binds to G4 quadruplex containing aptamers such as RNA Mango aptamer and the fluorescence can be significantly increased in the presence of G4 quadruplex containing aptamers. RNA Mango aptamer-TO1 has been successfully applied to track the process of the binding and release of 6S RNA in tubes[49].

RNA imaging using chemically synthesized nucleic acid probes

To image endogenous RNAs effectively, the incorporation of certain RNA sequences into the RNAs of interest should be avoided. Chemically synthesized nucleic acid probes recognize target RNA sequences via base-pairing hybridization and are suitable for endogenous RNA imaging.

Simply dye-labeling probes (FISH probes) (Figure 1-4a)

Although simply dye-labelling probes can hybridize the complementary RNA sequences, it is difficult for users to tell the hybridized and unhybridized probes directly. To read the hybridization signals of probes, the unhybridized probes as the fluorescent background signals should be removed specially. Therefore, the simply dye-labelling probes can only visualize RNAs in fixed cells using a process call fluorescence in situ hybridization (FISH)[50]. A typical FISH process is described as follows. Firstly, cells or tissues are fixed and permeabilized. Considering nucleic acid probes are negatively charged that makes it challenging to penetrate the lipid bilayers in the membrane, it is necessary to remove the lipids in the membrane as to improve the permeability of fixed cells. After cell permeabilization, the nucleic acid probes or FISH probes can easily go through the holes on cell surface. Secondly, proteins in fixed cells should be digested by pepsin and washed away due to the obstacle to the next RNA hybridization with FISH probes. Thirdly, FISH probes are introduced into the fixed cells to hybridize with the RNAs of interest. Stringent washing in this step is very crucial because the remained background signals may confuse us to observe target RNAs. Finally, the probe hybridized fixed cells are then imaged and analyzed using a fluorescent microscopy. One exception for FISH probes in the washing step is the FRET-based probes[51].

FRET-based probes (Figure 1-4b)

Fluorescence (Förster) resonance energy transfer (FRET) is a photo-physical phenomenon in which the energy from one fluorophore is transferred to a proximal fluorophore. There are two kinds of performances during FRET. For the common style, fluorescence from the donor fluorophore is transferred to the acceptor dye accordingly emitting fluorescence with longer wavelength. Particularly, the donor fluorophore is arranged close to a quencher thus quenching the fluorescence of the donor. To decrease the background signal intensity of FISH probes, FRET was used to design target-dependent turn-on probes[52]. The molecular beacons are the most studied FRET based nucleic acid probes. The molecular beacon is a stem-loop hairpin structure riothe

loop region of the molecular beacon, the hairpin structure is disrupted and the pair of the FRET dyes at the two ends is separated apart, thereby restoring the fluorescence of the donor fluorophore. Yet a serious flaw is the difficult controlling of the stem-loop structure, especially for the usage of molecular beacons in the living cells. To avoid the use of hairpin structure, the pair of two probed that hybridize with target RNAs side by side always renders improved results[53-54]. Another FRET-controlling probes pairs are the quenched autoligation (QUAL) probe pairs. One probe is modified with a donor fluorophore and a quencher through a nucleophile attackable group. The other probe is conjugated with a nucleophile thiol group. When the two probes bind to the target RNA side by side, the nucleophile thiol group in one probe will catalyze the removing of the quencher from the other probe and the fluorescence of fluorophore will be restored[55].

Self-quenching Probes

Unlike FRET-based probes, the fluorophores in these self-quenching probes are quenched by themselves. FIT probes (Figure 1-4c) and ECHO probes (Figure 1-4d) are typical self-quenching probes.

The FIT (single dye forced intercalation) probe is a signle-stranded linear DNA conjugated with a single thiazole orange (TO) dye. Via the intercalator TO, the fluorescence of FIT probe is controlling rationally which is non-fluorescent in the absence of the target RNA and strongly fluorescent after forming the nucleic acid duplex with the target RNA. Two variations, PNA-FIT and LNA-FIT probes, have been developed to image target RNAs. The PNA-FIT probe was designed to detect influenza H1N1 mRNA and a 11-fold enhancement of fluorescence was observed in the presence of target RNAs attributing to both the TO structure control and the specific PNA structure[56]. The probes of LNA-FIT also have good fluorescent response to target RNAs[57]. Due to relative low fluorescent brightness of TO dyes, some newly designed self-quenching probes were introduced. TO/JO-FIT probes conjugate a JO dye close to the TO dye in the general FIT probe. As JO (oxazolopyridine analogue) is a bright fluorophore, the light collected by TO dyes could be transferred to JO and emit bright fluorescence[58]. LNA-QB probes are probes similar with FIT probes and contain a bright intercalator QB other than TO in the single strand LNA[59]. Different with single-stranded FIT probes, AP probes are double-stranded DNA-based probes. In AP probes, the double-stranded DNA is conjugated with a 2-aminopurine (2-AP) dye that is quenched by the nucleic acid duplex. Competition of the complementary strand by targeted RNAs will release the fluorescence from the 2-AP modified strand[60].

A practical development of FIT probes is the exciton-controlled hybridization-sensitive

fluorescent oligonucleotides (ECHO) probes that exhibit improved signal-to-background ratio. The exciton coupling theory based ECHO probes will be introduced in the next section.

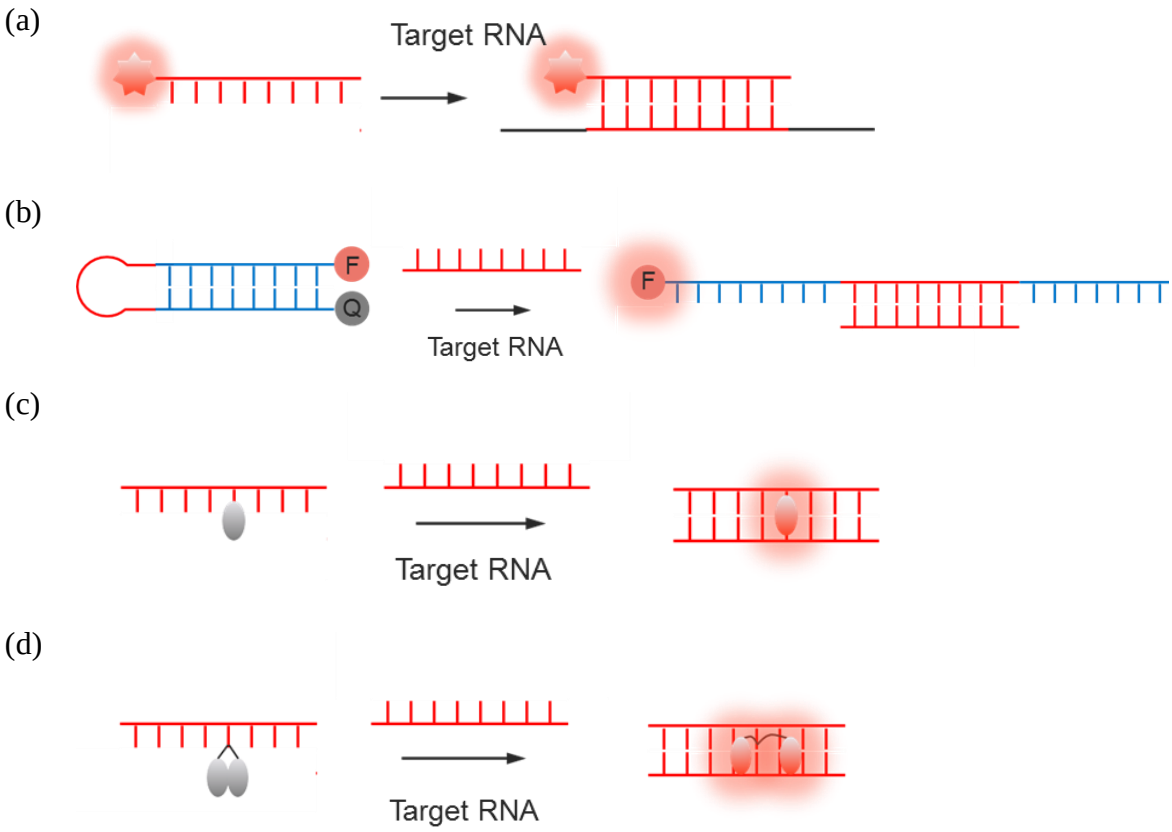

Figure 1-4. Schematic diagrams of RNA imaging using chemically synthesized nucleic acid probes. (a) FISH probes. (b) FRET-based probes. (c) FIT probes. (d) ECHO probes.

1.2 Exciton-controlled hybridization-sensitive fluorescent oligonucleotide (ECHO) probes

1.2.1 Basis of ECHO probes: aggregation control

Types of aggregation: Aggregation means a dynamic process during which the molecular states change from uniformly distributed individual molecules into clusters of a larger number of particle groups. Aggregation frequently happens when the probes in the solution are at a high concentration and this is particularly true in the case of organic probes in the aqueous solutions. The phenomena of aggregation could be explained properly by the attractive van der Waals forces and the hydrophobic attribute of organic probes[61]. Many types of aggregation exist but the two basic fashions are H-aggregation and J-aggregation[62-66]. Both H-aggregate and J-aggregate are arranged in one-dimension orientation and their dipole moments are parallel between the proximal molecules (Figure 1-5a). However, the dipole moments of individual molecules in H-aggregate are perpendicular with the line connecting their molecular centers (face-to-face) while the dipole moments of individual molecules in J-aggregate are parallel with the line connecting their molecular centers (end-to-end).

Absorption properties of aggregates: These aggregated organic molecules and individual organic molecules have distinct electronic properties and exhibit different absorption changes due to their different intermolecular interactions. The energetic shifts of the absorbance for these two aggregated types could be explained by the exciton coupling theory[67-70] (Figure 1-5a). As this theory, each monomer in the aggregate is regarded as a dipole. The parallel dipoles and the anti-parallel dipoles in the aggregates make the excited states of the aggregated molecules two possible energetic levels (Higher level S1 and lower level S2). For H-aggregation, the two dipoles are arranged face-to-face that put the paralleled dipoles repel each other and the anti-paralleled dipoles attract each other. Therefore, the paralleled dipoles correspond to a higher excitonic energy level and the anti-paralleled dipoles a lower excitonic energy level in H-aggregate. For J-aggregation, the two dipoles are arranged end-to-end that put the paralleled dipoles attract each other and the anti-paralleled dipoles repel each other. Therefore, the paralleled dipoles correspond to a lower excitonic energy level and the anti-paralleled dipoles a higher excitonic energy level in J-aggregate. But it is impossible to exhibit two excited states in one aggregate. Based on the exciton coupling theory, the transition dipole moment should be larger than zero after excitation. Thus,

the excited H-aggregate transits into the higher energy state (S1) and displays a blue shifted absorption spectra whereas the excited J-aggregate transits into the lower energy state (S2) and performs a red shifted absorption spectra.

Fluorescence properties of aggregates (Figure 1-5a):

The fluorescent emission from organic fluorophores derives from the electric conjugation. To obtain good fluorescence property, the aromatic rings were generally incorporated into the fluorophores as to generate the larger extent of π-conjugation. Due to the planar shape of aromatic rings, organic fluorophores have high possibility to aggregate in the form of excimer if they have high concentration in the aqueous solutions[71]. In this case, a disfavored fluorescence quenching may be observed due to the π-π interaction between the proximal dyes. This phenomenon has been termed as aggregation caused quenching[72]. Aggregation caused quenching may happen for most of organic dyes in the aqueous solutions. However, a reversed phenomenon called aggregation induced emission can also be observed for a small number of special fluorophores with intramolecular rotation[73].

Aggregation-based probe design: Considering aggregation caused quenching (ACQ) is a much more usual phenomenon than aggregation induced emission (AIE) in the organic fluorophore family, here I will mainly introduce the ACQ-based probe design although some groups have designed many AIE-based probes[74]. Since ACQ is a generally disapproved intermolecular interaction, one feasible way is to design turn-off probes: the aggregation of probes is induced by the target of interest, and the resulting ACQ effect renders signal attenuation[75]. Alternatively, another orientation to obtain turn-on probes is more useful for the practical biological applications. Although aggregates will not easily be disrupted once aggregates have formed, some smart designed structures can dramatically change the environment of the aggregate and dissociate the aggregates into individual molecules after recognizing the targets of interest. As a reverse process, disaggregation will enhance and recover the fluorescent signal. The induced disaggregation is a quite applicable way to design aggregation-based turn-on probes. Exquisite designs have utilized aggregation to generate many biological applications. The aggregation property of BODIPY has been employed for the specific protein detection[76-77] (Figure 1-5b). The authors have synthesized a BODIPY-based fluorescent probe which is structurally composed of three functional parts: the fluorophore, the linker and the recognition ligand. The red shifted absorption spectra and the quenched fluorescence of this probe were observed in buffer

due to the formation of J-aggregate of probes. When the probe was introduced to a system with the target protein human carbonic anhydrase I (hCA), the absorbance band moved to a position similar with the free BODIPY and the fluorescence of this probe was strongly enhanced. Therefore, this aggregation-based hCA probes showed high sensitivity and specificity. A squaraine homodimer has also been used to detect the objective membrane proteins[78] (Figure 1-5c). The squaraine dimer was chemically conjugated to carbetocin in order to generate a fluorescent probe targeting to the oxytocin G protein coupled receptor. In aqueous media, a shorter absorption peak from this probe was observed indicating that the H-aggregate formed and accordingly little fluorescence could be emitted. However, the strong fluorescence from the probe exhibited in the organic media. When introduced to the media with cells, the probe displayed the high selectivity to the target receptor as well as minimal nonspecific recognition to lipid bilayer membranes and other proteins. Many other biomolecules, including lysozyme[79], GBL[80], caffeine[81], phosphate[82], cysteine[83], were also fluorescently monitored by aggregation-based probe design.

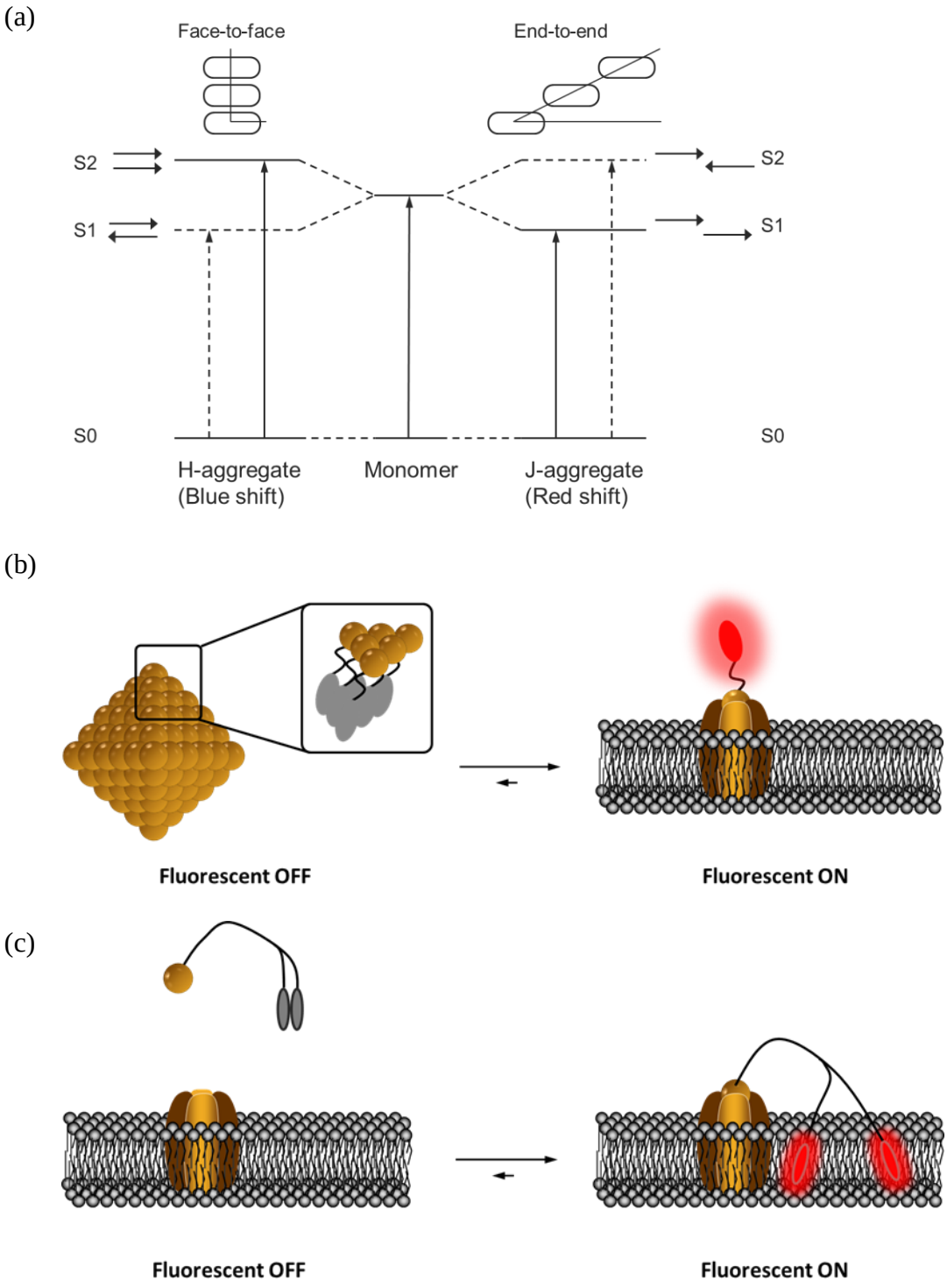

Figure 1-5. Aggregation and its role for probe design. (a) The relationship between dye molecule arrangement and spectral shift of H-aggregate and J-aggregate; (b) Fluorescent turn-on protein imaging based on recognition-driven disaggregation; (c) Specific membrane protein imaging based on recognition-driven disaggregation.

1.2.2 Working principle of ECHO probes

Singly TO-labeled oligonucleotide: As a kind of commercialized nucleic acid staining dye, thiazole orange (TO) exhibits a fine photo-physical behavior that is the enhancement of fluorescent intensity upon binding to DNA via insertion into the DNA duplex structure[84-85]. In water solution, TO is largely non-fluorescent due to the rotation around the methane bond between the two heterocyclic systems (Figure 1-6a). After inserting into DNA duplex, the rotation in TO dyes is restricted accordingly leading to the fluorescent increase. This superior photo-physical property of TO inspired many researchers to link a TO dye to the artificial DNA, DNA analogue or peptide nucleic acid and made many genetic applications[86-94]. However, the inescapable background fluorescence vastly affected the precise biological analysis. A more effective nucleic acid probes with higher suppress efficiency is required.

Doubly TO-labeled oligonucleotide: As mentioned in 1.2.1, aggregation-based probe design is suitable to many probes. Luckily, TO emission can be largely inhibited when several TO dyes are arranged in parallel (H-aggregate) compared to free TO dye[62-64]. The interaction among aggregated TOs decreases fluorescence evidently explainable by the exciton coupling theory (Figure 1-6b). To further reducing the fluorescent background of the TO conjugated nucleic acid probes, the ODN probes were labelled with TO dimers (Figure 1-6c and 1-6d)[95]. Under the exciton coupling effect, the single-stranded probe should exhibit suppressed fluorescence emission because the TO dimer are aggregated. The excited state of TO aggregated dimer splits into two energy levels (E' and E"). The transition from the upper energy (E") level to lower energy state is achieved quickly by system conversion while the transition from the lower energy level (E') to the ground level (G) is blocked. Thus, the paralleled TO dyes in single-stranded probes harvested their self-quenching properties by exciton coupling effect. After hybridizing with the corresponding DNA or RNA sequence, the fluorescent turn-on was followed by the bis-intercalation of TO dyes into the formed duplex structure through hybridization to both disrupt the H-aggregation of TO dimer and restriction of each TO rotation. This rational design combined both kinds of TO fluorescent controlling mechanisms, exciton coupling effect and restriction of rotation, to provide more precise target nucleic acid readout for nucleic acid imaging and analysis.

In the newly designed probe, a single pyrimidine, termed as nucleoside D_{514}, was attached with the homodimer of TO which was excited at 514 nm (Figure 1-6d).

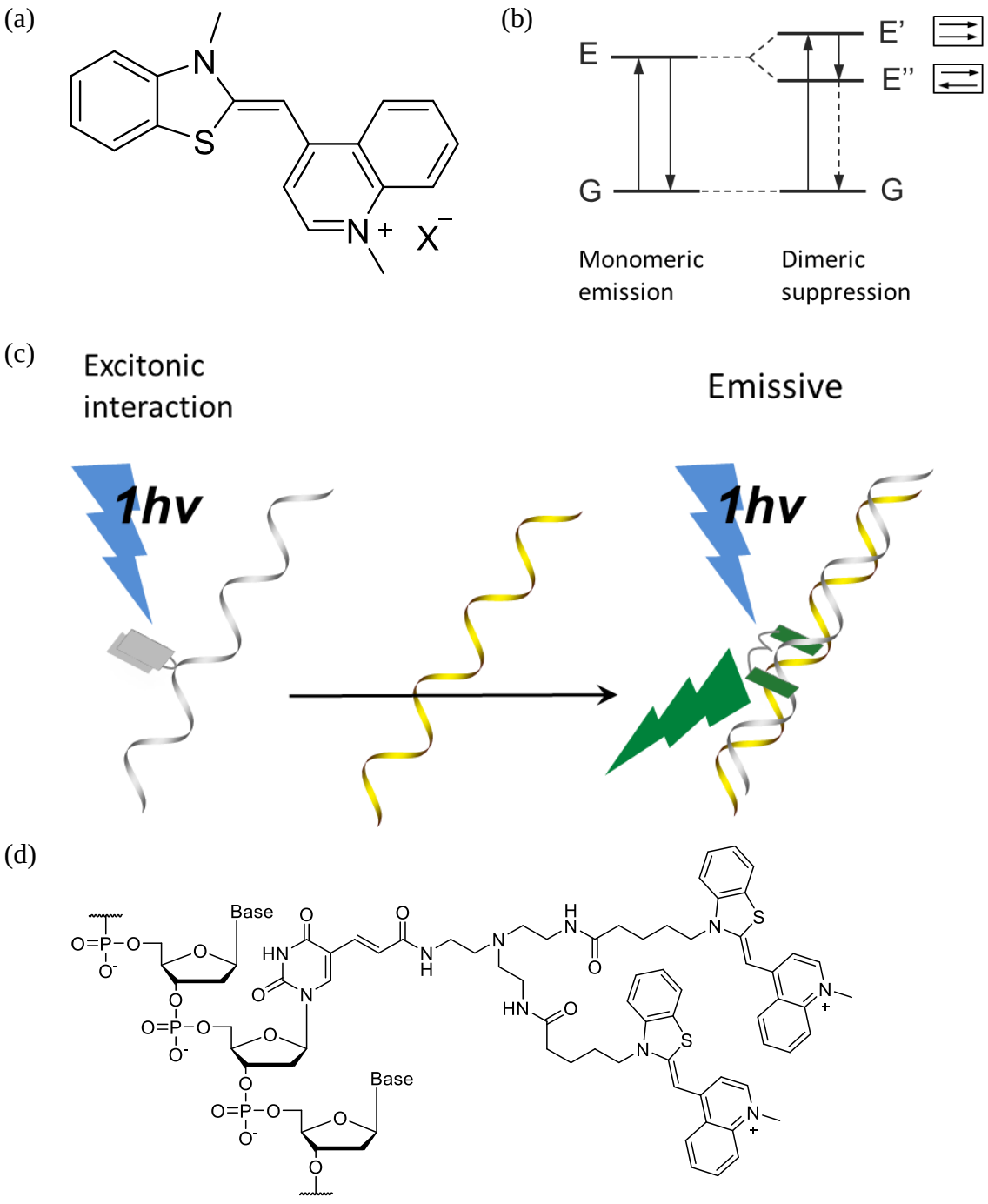

Figure 1-6. Fluorescence-controllable oligonucleotide D_{514}. (a) Chemical structure of thiazole orange; (b) Splitting excited state of TO aggregates. The arrows in the right of the energy levels are the transition dipoles of the dye molecules; (c) Schematic illustration of target nucleic acid detection by exciton-controlled hybridization-sensitive fluorescent oligonucleotide (ECHO) probes. (d) A common structure of ECHO probes D_{514}.

1.2.3 Characterization and optimization of ECHO probes

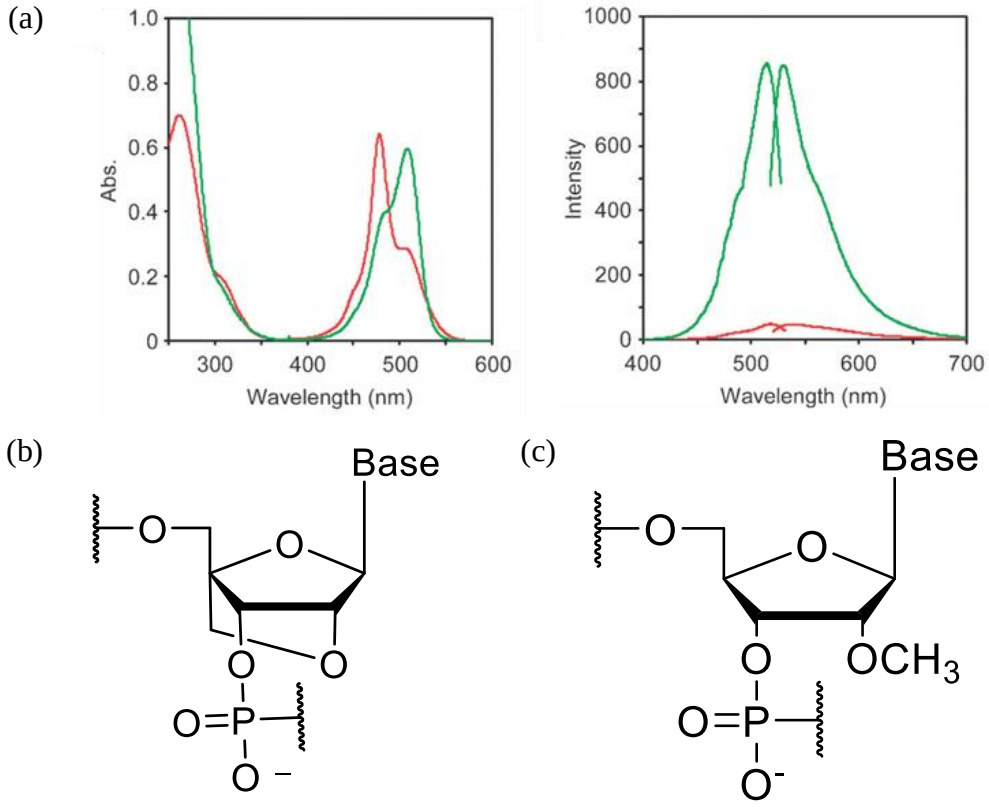

Figure 1-7. (a) A typical absorption, excitation and emission spectra of ECHO probes; (b) Chemical structure of LNA-modified nucleotides; (c) Chemical structure of 2'-O-methyl modified nucleotides

Hybridization-dependent absorption and emission and LNA ECHO probes

To analyze photo-physical behavior of the exciton coupling effect, the absorption, excitation and emission spectra of OND probes labelling with D_{514} in the absence and presence of their complementary DNA were measured[95-96]. The typical absorption spectra had two major bands at 480 nm (derived from TO dimer) and 510 nm (derived from TO monomer) respectively with different peak intensity. However, the ECHO probes, in spite of the absence and presence of the complementary sequences, only displayed the excitation peaks at about 510 nm, suggesting that only the absorption at the longer wavelength practically attributes to fluorescent increase. The changes of absorption intensities and excitation peaks at 510 nm before and after hybridization are consistent with the corresponding emission intensities, indicating that hybridization-induced exciton control predominantly affected absorption and fluorescence emission (Figure 1-7a).

However, DNA ECHO probes are sometimes thermodynamically difficult to access and hybridize with many RNA molecules, because of the higher-order structures of RNAs. To overcome this challenge, locked nucleic acid (LNA) were incorporated into ECHO probes because chimeric probes with selected positions modified with LNA nucleotides have been reported to enhance the thermos-stability of formed duplexes with complementary sequences (Figure 1-7b)[97-98]. The incorporation sites of LNAs were designed away from the TO dye conjugated site more than three nucleotide residues to avoid the inhibition of dye intercalation. The ECHO-LNA probes performed improved fluorescent emission in the presence of complementary sequences.

Sequence-dependent quenching and I/E-substituted ECHO probes

The hybridization-based fluorescent turn-on property of ECHO probes is flavorful for expression analysis and living cell imaging. However, another disfavored property also exhibited in the self-quenching fluorescent probes: the fluorescent intensity changes are always dependent with the varied sequences[99]. A conclusion for the design of effective ECHO probes with a high fluorescent ratio is that sequences that form self-dimers should be avoid because they induce fluorescence emission in the absence of target nucleic acid. To attenuate self-dimerization of nucleic acid probes, alternative bases of nucleic acid were introduced into DNA probes. Two kinds of artificial nucleosides, 2'-deoxyinosine (I) and N^4-ethyl-2'-deoxycytidine (E) were chose as the alternatives[100] (Figure 1-8). Base pairs of 2'-deoxyinosine/ cytosine (I/C) and N^4-ethyl-2'-deoxycytidine/ guanine (E/G) are fairly stable comparable with base pairs A/T and C/G, respectively while the base pair I/E are less stable. For this reason, the replacements of C and G with E and I largely decreased the intermolecular or intramolecular self-dimerization but rather hold enough abilities to hybridize with the complementary sequences. The ratio of fluorescent intensity in the presence and absence of target sequences clearly improved after replacing G and C with I and E in ECHO probes. Therefore, the I/E-substituted ECHO probes are very robust design and provide superior performance at random target sequences. However, the position of the replaced nucleotides should be carefully decided and the cytosine base close to D_{514} could not be replaced by an E because of the steric blocking with the intercalation of TO dyes into the probe-target duplex.

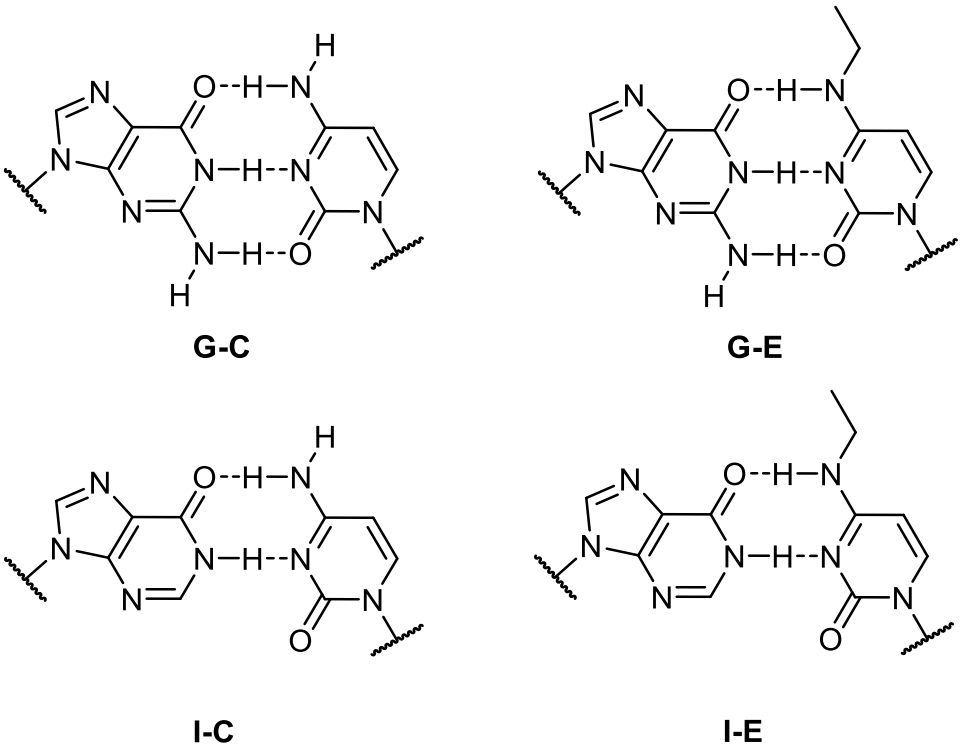

Figure 1-8. ECHO probes with unnatural nucleobase analogs: Four possible base pairs.

2'-O-methyl (2'-OMe) RNA backbone ECHO probes

Since the ODN ECHO probes are quite risky to be cleaved by nucleases that widely exist in live cells, ODN ECHO probes are only suitable for in vitro or short-term observations[101]. To improve the nuclease resistance of ECHO probes, the ODN ECHO probes were replaced by 2'-OMe RNA ECHO probes in which all nucleotides were modified by 2'-OMe groups[102]. The 2'-OMe modification at the backbone of ECHO probes did almost not affect the TO intercalation into the duplex and the fluorescent controlling is maintained commendably. In a 12-h nuclease-incubating in vitro experiment, ECHO probes with 2'-OMe backbone modification maintained intact while more than 80 % of DNA-based ECHO probes were cleaved. The decreased and sustained fluorescence were respectively observed in Hela cells transfected with ECHO probes with a DNA or a 2'-OMe RNA backbone (Figure 1-7c). Therefore, the 2'-OMe modified ECHO probes are better choice for imaging RNAs in living cells or tissues.

1.2.4 Photo-physical functional expansions

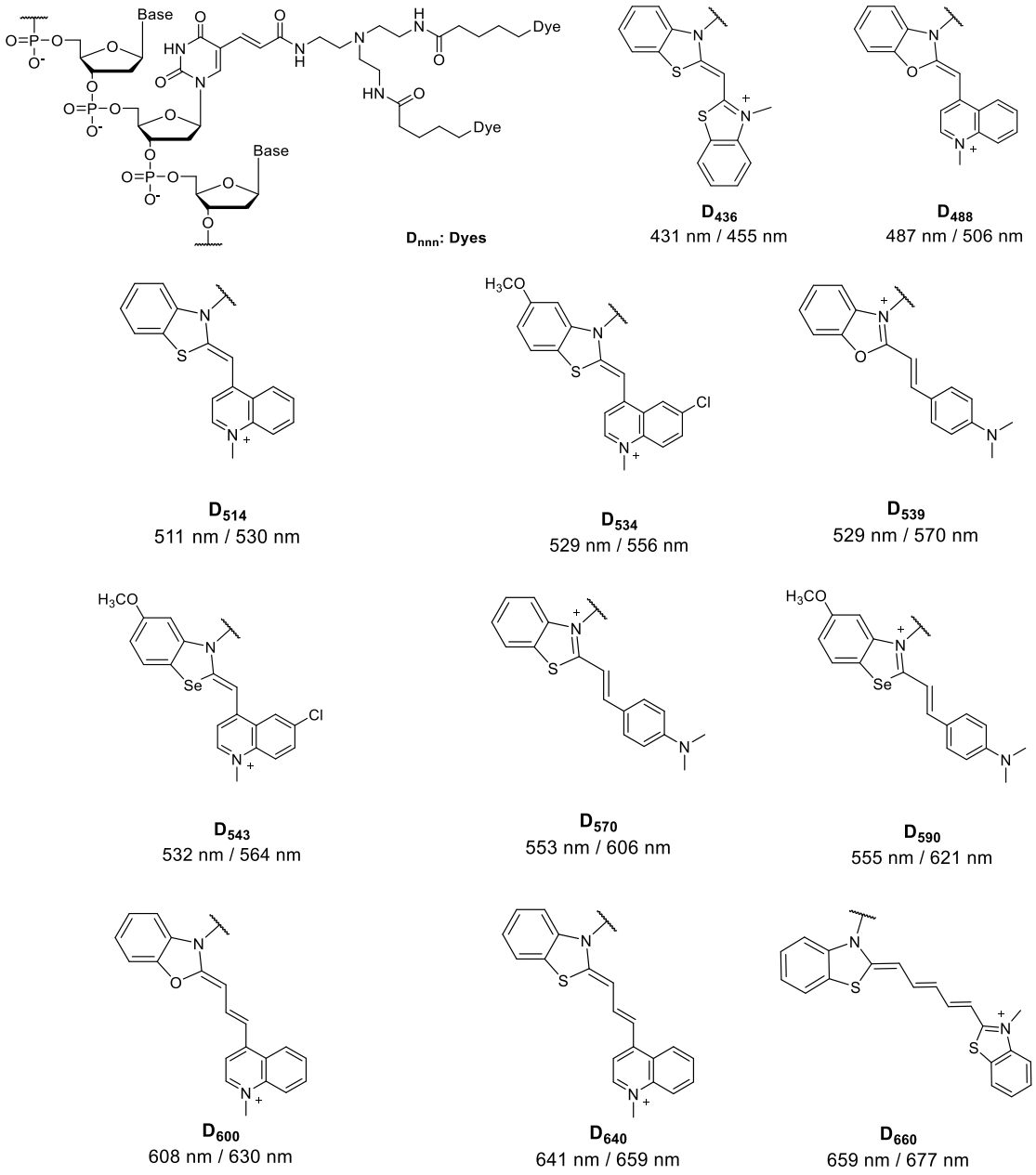

Figure 1-9. Versatile ECHO probes for multicolor imaging

Multicolor detection by D_{514} variants

To imaging versatile RNAs in a single cell simultaneously, a series of newly designed ECHO probes were introduced in which the fluorescent nucleotides were conjugated by newly designed cyanine dyes with varied excitation and emission wavelengths(Figure 1-9)[103]. These fluorescent moieties were termed as Dnnn based on their distinct excitation wavelength. After hybridization with their complementary sequences, these new ECHO probes showed red shifts in the absorption spectra and intensity increase in the emission spectra, indicating that these newly designed ECHO probes control fluorescence emission via the same mechanism, the exciton coupling effect, as ECHO probe D_{514}. In a model experiment of multicolor live cell RNA imaging, three colors were observed simultaneously in a cell injected with the mixtures including three differently colored ECHO probes (D_{514}, D_{543} and D_{640}).

FRET energy transfer analysis within ECHO probes

Förster resonance energy transfer (FRET) is a photon-physical phenomenon in which energy from a donor is transferred to a close acceptor dye[104]. The distance changed can be indicated by FRET due to the robust distance-based energy transfer efficiency[105]. However, if the acceptor dyes are photo-bleached by a strong laser, the interaction between the proximal chromophores can be irreversibly disrupted and the donor dye could be activated only at the irradiated areas. Considering the importance of tracking a RNA dynamics spatiotemporally in cell of interest, a FRET-type ECHO probe, 5'-Cy5-s-s-$U_2D_{514}U_6$-3', were synthesized to image poly-A RNAs in a single cell (Figure 1-10a)[98]. After transfection of the probes into Hela cells, weak fluorescence from TO and strong fluorescence from Cy5 were observed when excited at 488nm, indicating that the distance between TO and Cy5 is suitable for FRET occurring. After scanning one transfected cell with a strong laser at 633 nm, only strong fluorescence from TO happened suggesting that Cy5 was photo-bleached effectively and the FRET process were disrupted. Thus, the FRET-type ECHO probes allowed us to observe RNA dynamics in a single cell spatially and temporally.

Ratiometric analysis by binary labelled probes

Unlike the FRET-type ECHO probes, the fluorophore Cy5 can also be labelled at the end of ECHO probes far from D_{514}[106]. In the binary labelled probes, fluorescent signals from Cy5 indicated the distribution of the probes and the signals from TO meant the dynamic RNAs hybridized with the probes. Using this system, the quantity of hybridization and dynamic distribution of the probes themselves can be determined

effectively and this type of probes provide more information about probe to make researches explain imaging data more properly.

Fluorescent caged ECHO probes

Except for FRET-type ECHO probes, fluorescent caged ECHO probes are also applicable for imaging target RNAs in spatiotemporal manners. In caged ECHO probes, a photo-labile nitrobenzyl (NB) group was conjugated to the fluorescent nucleotide D_{514} (Figure 1-10b)[107]. The caging mechanism of NB unit to ECHO probe is to reduce the hybridization ability of ECHO probes to the complementary sequences. Thus, almost little fluorescence of caged ECHO probes could be observed even when the target DNAs or RNAs were added. Conversely, the caged ECHO probes restored the fluorescent emission in the presence of complementary sequences after irradiation and the hybridization-based fluorescent control of decaged ECHO behaved as the conventional ECHO probes.

(a)

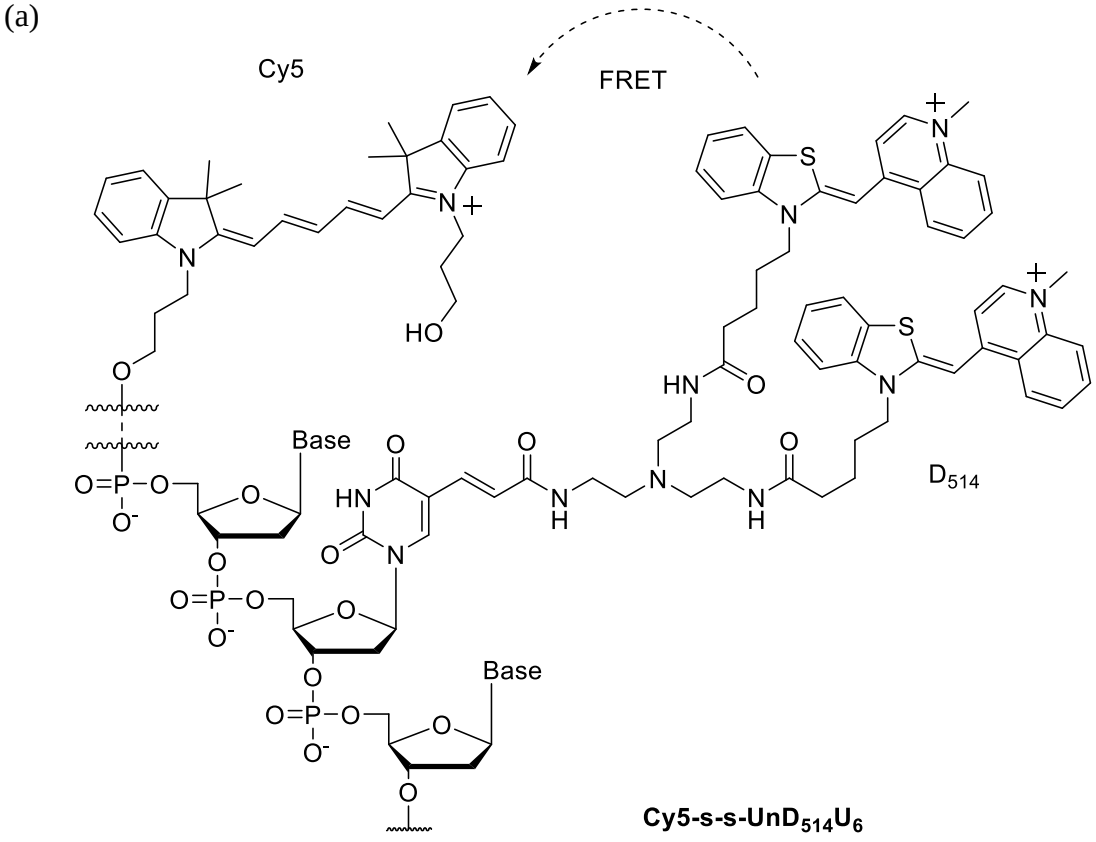

(b)

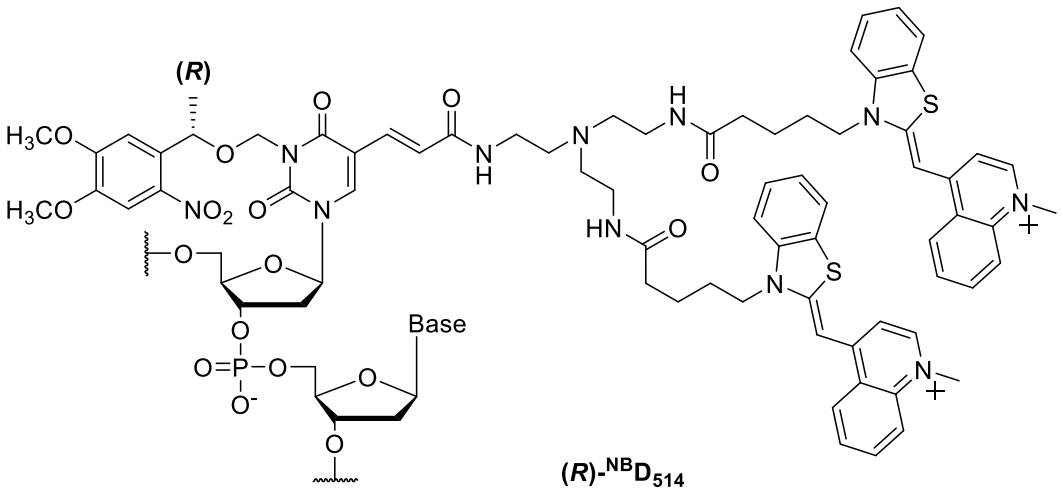

Figure 1-10. (a) Binary energy transfer emission control within ECHO probes. (b) Design of caged ECHO probes.

1.2.5 Biological application expansions

Because of the superior signal-to-noise ratio of ECHO probes compared with conventional ODN probes, many biological applications were successfully performed. In vitro, ECHO probes give a more concise and simple operation; in live cells, nonspecific signals from probes can be slacked to an extreme. These developed applications cover a wide range from tubes to live cells: real-time PCR detection, SNP detection, fluorescence in situ hybridization, endogenous and exogenous RNA detection in live cells or even in the tissue.

Real-Time PCR monitoring

Real-time PCR is a very important and basic method for quantifying DNAs or RNAs and this technique has been widely used in the academic researches and the medical molecular diagnostics. A new kind of ECHO based probe, Eprobe, was developed that blocks ECHO probe at the 3' end. The Eprobe has a very unique feature that real-time PCR amplification and melting curve analysis can be monitored in one operation[108-110]. The PCR amplification could be monitored by Eprobes in a sequence-dependent manner

that guarantees the sensitivity and specificity of target DNA or RNA detection. The melting analysis curve analysis can further estimate the quality of PCR product in specificity. This Eprobe real-time PCR technique provides a more accurate and easier approach to account the target nucleic acid in the practical sample, such as the analysis of mutation.

SNP detection by Exciton Primer-mediated SmartAmp2 system

The smart amplification process2 (SmartAmp2) is a facile primer design to amplification target sequences in which the product of isothermal amplification can be used as an intramolecular primer to continue the amplifying reaction and elongate the product effectively[111]. The SYBR Green I stained SmartAmp2 has been developed to monitor the DNA SNPs in the blood samples in real time. Compared with SYBR Green I, the ECHO probe can transduce the accurate amplification of target nucleic acid (DNA or RNA) in a sequence-dependent way and renders superior specificity and sensitivity to the desired nucleic acid target[112]. There are two fashions to monitor SmartAmp2 using ECHO probes. The first fashion is the ECHO primers that involve the extensions of DNA polymerase. The second fashion just serves ECHO probes as a specific sensor to read the amplified PCR product specifically.

Simplified fluorescent in situ hybridization

Fluorescence in situ hybridization (FISH) is a wide used technique in the academic and diagnostic researches and its role for bio-analysis include gene expression, karyotyping, cytogenotyping and medical diagnosis. Due to the requirement of the stringent washing step, conventional FISH procedures are very time-consuming and operation-dependent. Using the unique property of sequence-dependent fluorescent responsiveness of ECHO probes, a simple FISH protocol was introduced[113]. This simple FISH only need three steps: fixation, mounting and observation of target RNAs. Due to the avoidance of cumbersome washing step, the ECHO-based simple FISH could be finished in 25 min. Except for RNA detection in fixed cells, three typical repeated DNA sequences, telomeres, centromeres and pericentromeres, were also conveniently detected using simple FISH in the mouse chromosomes.

Monitoring endogeneous RNA dynamics in living cells

RNA distribution and dynamics in living cells are quite function-related and tracing RNAs in the complex living cell environment was keeping challenging. ECHO probes perform target-dependent fluorescent turn-on and particular suitable for endogeneous

RNA monitoring. ECHO probes conjugated with three different colors (D_{514}, D_{543}, and D_{640}) have been designed to target three microRNAs, miR-20, miR-17, and miR-30 [103]. The orthogonal fluorescent signal from these three probes can be assigned to the corresponding microRNAs and mutual signal interferences between probes could be specifically avoided. FRET-type probes and NB-caged ECHO probes are suitable for spatial and temporal analysis[98, 107]. Though light irradiation, a cell or single subcellular structures could be tracked specifically by a color from donor dyes D_{514} that are of particularly helpful to understand RNA dynamics in different culturing conditions or environmental factor.

Monitoring tagged RNA dynamics in living cells

Due to the varying size and conformation of RNAs and the interaction with many protein partners, ECHO probes were blocked to access the desired target regions. For this reason, detailed information about the conformational structures of target RNAs should be known in advance when designing the nucleic acid. To overcome the challenge, the RNA tagging technology was used for RNA function research. A few copies of orthogonal tag sequences that can be specifically hybridized by the predesigned ECHO probes were genetically inserted into the 3'-end of target RNAs[114]. After transfection ECHO probes into the pretreated cells, the dynamic manners of target RNAs were fluorescently monitored. For simultaneous observation of multiple RNAs, multicolor ECHO probes targeting to orthogonal tag sequences were also designed and applied successfully. Compared with other tagging systems, ECHO-based tagging requires shorter tag length, fewer tag copies and offer lower fluorescent background.

***in vivo* RNA imaging**

RNAs existed more copies in some regions of a live cell than other regions and RNA distribution is various in different cells and divergent cell conditions. However, this difference is not easy to be visualized and identified in live tissues or bodies due to limited tools. After introducing ECHO probes into the brain of live mice, the researchers succeeded in observing targeted RNAs at the cell nucleus[115]. Using ECHO probes, RNA concentration levels were indicated by the variational intensities of fluorescence and quantified the various local RNA amounts in the live tissue or living bodies. A very important finding using this live ECHO-FISH method is that RNA distribution and dynamics in live tissue is different from the RNA behavior in the cultured cells. Thus, the live ECHO-FISH technique is a powerful tool to reveal the natural state and dynamic of RNAs.

1.3 Objectives of this thesis

The aim of this thesis is to develop fluorescent turn-on biosensors using the concept of exciton controlling that have been demonstrated in ECHO probes. Based on the introductions above, ECHO probes exhibit excellent hybridization-based turn-on properties when used for linear nucleic acid monitoring. As one of the most important carriers, aptamers have favorable specific recognition to target molecules. Energy transfer, particularly FRET, is the most useful approach to converse this recognition into readable fluorescent signals. However, this process frequently non-effective due to the distance-based design and our insufficient understanding about the three-dimensional structures of aptamer. Compared with the distance-based design by energy transfer, the hybridization-based design employed in ECHO probe just requires us to find the duplex structures. This secondary structure is only a two-dimensional concept that is much easier for us to identify and exploit. For introducing this new designing notion into aptamer-based biosensor, doubly thiazole orange conjugated nucleotides are newly designed and synthesized. RNAs, very special and important biomolecules, can be detected by ECHO probes more effectively and simply than other common biomolecules. However, the special detection environments, tubes or cells, make researchers achieve limited or even incorrect RNA information using ECHO probes because of the removed or changed physiological and environmental factors. Thus, it is quite essential for us to expand the usage of ECHO probes into a more complex and natural bio-system, such as tissues or whole bodies. Actually, elaborate biosensor design needs many considerations. In this doctor thesis, I just tried to provide insight for the biosensor design by expanding the applications of ECHO probes. Briefly, the objectives of this study include: i) design exciton-controlled neomycin aptamer for bacterial assessment; ii) synthesize exciton-controlled ATP aptamer for ATP monitoring and iii) develop two-photon-excited ECHO probes for DNA or RNA imaging in tissues.

1.4 References

1. Arnold M. A., Meyerhoff M. E., *CRC Crit. Revs. Anal. Chem.* 1988, **20**, 149-196.
2. Irvine D., Tuerk C., Gold L. J., *Mol. Biol.* 1991, **222**, 739-761.
3. Que-Gewirth N.S., Sullenger B.A., *Gene Therapy.* 2007, **14**, 283-291.
4. Zhou W., Huang P.J., Ding J., Liu J., *Analyst*. 2014, **139**, 2627-2640.
5. Dollins C.M., Nair S., Sullenger B.A., *Hum. Gene Ther.* 2008, **19**, 443-450.
6. Gokulrangan G., Unruh J.R., Holub D.F., Ingram B., Johnson C.K., Wilson G.S., *Anal. Chem*. 2005, **77**, 1963-1970.
7. Kirby R., Cho E.J., Gehrke B., Bayer T., Park Y.S., Neikirk D.P., McDevitt J.T., Ellington A.D., *Anal. Chem.* 2004, **76**, 4066-4075.
8. Kato T., Yano K., Ikebukuro K., Karube I., *Analyst*. 2000, **125**, 1371-1373.
9. Pavlov V., Xiao Y., Shlyahovsky B., Willner I., *J. Am. Chem. Soc*. 2004, **126**, 11768-11769.
10. Liu J., Lu Y., *Angew. Chem. Int. Ed. Engl*. 2005, **45**, 90-94.
11. Yu S., Dong R., Chen J., Chen F., Jiang W., Zhou Y., Zhu X., Yan D., *Biomacromolecules*, 2014, **15**, 1828-1836.
12. Zhou J., Soontornworajit B., Martin J., Sullenger B.A., Gilboa E., Wang Y., *Macromol. Biosci.* 2009, **9**, 831-835.
13. Lubin A.A., Plaxco K.W., *Acc. Chem. Res.* 2010, **43**, 496-505.
14. Jhaveri S.D., Kirby R., Conrad R., Maglott E.J., Bowser M., Kennedy R.T., Glick G., Ellington A.D., *J. Am. Chem. Soc.* 2000, **122**, 2469-2473.
15. Hou X., Guo W., Xia F., Nie F.Q., Dong H., Tian Y., Wen L., Wang L., Cao L., Yang Y., Xue J., Song Y., Wang Y., Liu D., Jiang L., *J. Am. Chem. Soc*. 2009, **131**, 7800-7805.
16. Stojanovic M.N., de Prada P., Landry D.W., *J. Am. Chem. Soc*. 2001, **123**, 4928-4931.
17. Urata H., Nomura K., Wada S., Akagi M., *Biochem. Biophys. Res. Commun.* 2007, **360**, 459-463.
18. Yang C.J., Jockusch S., Vicens M., Turro N.J., Tan W. *Proc. Natl. Acad. Sci. USA.* 2005, **102**, 17278-17283.
19. Sharma A.K., Kent A.D., Heemstra J.M., *Anal. Chem*. 2012, **84**, 6104-6109..
20. Wang J., Wang L.H., Liu X.F., Liang Z.Q., Song S.P., Li W.X., Li G.X., Fan C.H., *Adv. Mater.* 2007, **19**, 3943-3946.
21. Nutiu R., Li Y., *Angew. Chem. Int. Ed. Engl*. 2005, **44**, 1061-1065..
22. Nutiu R., Li Y., *Chemistry.* 2004, **10**, 1868-1876.

23. Sudarsan N., Lee E.R., Weinberg Z., Moy R.H., Kim J.N., Link K.H., Breaker R.R., *Science*. 2008, **321**, 411-413.
24. Lau P.S., Coombes B.K., Li Y., *Angew. Chem. Int. Ed. Engl.* 2010, **49**, 7938-7942.
25. Desai S.K., Gallivan J.P., *J. Am. Chem. Soc.* 2004, **126**, 13247-13254.
26. Topp S., Gallivan J.P., *J. Am. Chem. Soc.* 2007, **129**, 6807-6811.
27. Shen Y., Chiuman W., Brennan J.D., Li Y., *Chembiochem.* 2006, **7**, 1343-1348.
28. Lai R.Y., Plaxco K.W., Heeger A.J. *Anal. Chem.* 2007, **79**, 229-233.
29. Wang Y., Li Z., Hu D., Lin C.T., Li J., Lin Y., *J. Am. Chem. Soc*. 2010, **132**, 9274-9276.
30. Li N., Ho C.M., *J. Am. Chem. Soc*. 2008, **130**, 2380-2381..
31. Stojanovic M.N., de Prada P., Landry D.W., *J. Am. Chem. Soc*. 2000, **122**, 11547-11548.
32. Wu C., Yan L., Wang C., Lin H., Wang C., Chen X., Yang C.J., *Biosens Bioelectron.* 2010, **25**, 2232-2237.
33. Wu S., Duan N., Wang Z., Wang H., *Analyst*. 2011, **136**, 2306-2314.
34. Stojanovic M.N., Kolpashchikov D.M., *J. Am. Chem. Soc.* 2004, **126**, 9266-9270.
35. Kolpashchikov D.M., *J. Am. Chem. Soc*. 2005, **127**, 12442-12443.
36. Bang G.S., Cho S., Lee N., Lee B.R., Kim J.H., Kim B.G., *Biosens. Bioelectron.* 2013, **39**, 44-50.
37. Xu W., Lu Y., *Anal. Chem.* 2010, **82**, 574-578.
38. Bertrand E., Chartrand P., Schaefer M., Shenoy S.M., Singer R.H., Long R.M., *Mol. Cell*, 1998, **2**, 437-445.
39. Hu C.D., Chinenov Y., Kerppola T.K., *Mol. Cell.* 2002, **9**, 789-798.
40. Kodama Y., Hu C.D., *BioTechniques*. 2010, 49, 793-805.
41. Rath A.K., Rentmeister A., *Curr. Opin. Biotechnol*. 2015, **31**, 42-49.
42. Dictenberg J., *Trends Biotechnol.* 2012, **30**, 621-626.
43. Wu B., Chen J., Singer R.H., *Sci. Rep.* 2014, **4**, 3615.
44. Kelley S.O., Mirkin C.A., Walt D.R., Ismagilov R.F., Toner M., Sargent E.H., *Nat. Nanotechnol.* 2014, **9**, 969-980.
45. Wu B., Chen J., Singer R.H., *Sci. Rep.* 2014, **4**, 3615.
46. Paige J.S., Wu K.Y., Jaffrey S.R., *Science*. 2011, **333**, 642-646.
47. Song W., Strack R.L., Svensen N., Jaffrey S.R., *J. Am. Chem. Soc.* 2014, **136**, 1198-1201.
48. Ilgu M., Ray J., Bendickson L., Wang T., Geraskin I.M., Kraus G.A., Nilsen-Hamilton M., *Methods.* 2016, **98**, 26-33.
49. Dolgosheina E.V., Jeng S.C., Panchapakesan S.S.S., Cojocaru R., Chen P.S., Wilson

P.D., Hawkins N., Wiggins P.A., Unrau P.J., *ACS Chem. Biol.* 2014, **9**, 2412-2420.
50. Urbanek M.O., Nawrocka A.U., Krzyzosiak W.J., *Int. J. Mol. Sci.* 2015, **16**, 13259-13286.
51. Huang J., Wang H., Yang X., Quan K., Yang Y., Ying L., Xie N., Ou M., Wang K., *Chem. Sci.* 2016, **7**, 3829-3835.
52. Tyagi S., Kramer F.R., *Nat Biotechnol.* 1996, **14**, 303-308.
53. Gaylord B.S., Heeger A.J., Bazan G.C., *Proc. Natl. Acad. Sci. USA.* 2002, **99**, 10954-10957.
54. Tsuji A., Koshimoto H., Sato Y., Hirano M., Sei-Iida Y., Kondo S., Ishibashi K., *Biophys. J.* 2000, **78**, 3260-3274.
55. Sando S., Kool E.T., *J. Am. Chem. Soc.* 2002, **124**, 9686-9687.
56. Kummer S., Knoll A., Socher E., Bethge L., Herrmann A., Seitz O., *Angew. Chem., Int. Ed.* 2011, **50**, 1931-1934.
57. Hövelmann F., Gaspar I., Loibl S., Ermilov E.A., Röder B., Wengel J., Ephrussi A., Seitz O., *Angew. Chem., Int. Ed.* 2014, **53**, 11370-11375.
58. Hövelmann F., Gaspar I., Ephrussi A., Seitz O., *J. Am. Chem. Soc.* 2013, **135**, 19025-19032.
59. Hövelmann F., Gaspar I., Chamiolo J., Kasper M., Steffen J., Ephrussi A., Seitz O., *Chem. Sci.* 2016, **7**, 128-135.
60. Liao R., He K., Chen C., Chen X., Cai C., *Anal. Chem.* 2016, **88**, 4254-4258.
61. Yuan L., Lin W., Zheng K., Zhu S., *Acc. Chem. Res.* 2013, **46**, 1462-1473.
62. Sagawa T., Tobata H., Ihara H., *Chem. Commun.* 2004, 2-4.
63. Fürstenberg A., Julliard M.D., Deligeorgiev T.G., Gadjev N.I., Vasilev A.A., Vauthey E., *J. Am. Chem. Soc.* 2006, **128**, 7661-7669.
64. Khairutdinov R.F., Serpone N., *J. Phys. Chem. B.* 1997, **101**, 2602-2610.
65. Cosa G., Focsaneanu K.S., McLean J.R.N., McNamee J.P., Scaiano J.C., *Photochem. Photobiol.* 2001, **73**, 585-599.
66. Simon L.D., Abramo K.H., Sell J.K., McGown L.B., *Biospectroscopy.* 1998, **4**, 17-25.
67. McRae E.G., Kasha M., *J. Chem. Phys.* 1958, **28**, 721-722.
68. Kasha M., Rawls H.R., El-Bayoumi M.A., *Pure Appl. Chem.* 1965, **11**, 371-392.
69. Levinson G.L., Simpson W.T., Curtis W., *J. Am. Chem. Soc.* 1957, **79**, 4314-4320.
70. Kasha M., *Radiat. Res.* 1963, **20**, 55-70.
71. Jares-Erijman E.A., Jovin T.M., *Nat. Biotechnol.* 2003, **21**, 1387-1395.
72. Hecht S., Frechet J.M., *Angew. Chem. Int. Ed.* 2001, **40**, 74-91.
73. Luo J., Xie Z., Lam J.W., Cheng L., Chen H., Qiu C., Kwok H.S., Zhan X., Liu Y.,

Zhu D., Tang B.Z., *Chem. Commun.* 2001, 1740-1741.
74. Hong Y., Lam J.W., Tang B.Z., *Chem. Soc. Rev.* 2011, **40**, 5361-5388.
75. Adachi K., Chayama K., Watarai H., *Langmuir*. 2006, **22**, 1630-1639.
76. Mizusawa K., Ishida Y., Takaoka Y., Miyagawa M., Tsukiji S., Hamachi I., *J. Am. Chem. Soc.* 2010, **132**, 7291-7293.
77. Mizusawa K., Takaoka Y., Hamachi I., *J. Am. Chem. Soc.* 2012, **134**, 13386-13395.
78. Karpenko I.A., Collot M., Richert L., Valencia C., Villa P., Mély Y., Hibert M., Bonnet D., Klymchenko A.S., *J. Am. Chem. Soc.* 2015, **137**, 405-412.
79. Wang B., Yu C., *Angew. Chem. Int. Ed.* 2010, **49**, 1485-1488.
80. Zhai D., Agrawalla B.K., Eng P.S., Lee S.C., Xu W., Chang Y.T., *Chem. Commun.* 2013, **49**, 6170-6172.
81. Xu W., Kim T.H., Zhai D., Er J.C., Zhang L., Kale A.A., Agrawalla B.K., Cho Y.K., Chang Y.T., *Sci. Rep.* 2013, **3**, 2255.
82. Zhao H.X., Liu L.Q., Liu Z.D., Wang Y., Zhao X.J., Huang C.Z., *Chem. Commun.* 2011, **47**, 2604-2606.
83. Ruan Y.B., Li A.F., Zhao J.S., Shen J.S., Jiang Y.B., *Chem. Commun.* 2010, **46**, 4938-4940.
84. Nygren J., Svanvik N., Kubista M., *Biopolymers.* 1998, **46**, 39-51.
85. Lee L.G., Chen C.H., Chiu L.A., *Cytometry.* 1986, **7**, 508-517.
86. Hanafi-Bagby D., Piunno P.A.E., Wust C.C., Krull U.J., *Anal. Chim. Acta*. 2000, **411**, 19.
87. Wang X., Krull U.J., *Anal. Chim. Acta*. 2002, **470**, 57-70.
88. Wang X., Krull U.J., *Bioorg. Med. Chem. Lett.* 2005, **15**, 1725-1729.
89. Asseline U., Chassignol M., Aubert Y., Roig V., *Org. Biomol. Chem.* 2006, **4**, 1949-1957.
90. Lartia R., Asseline U., *Chemistry*. 2006, **12**, 2270-2281.
91. Svanvik N., Nygren J., Westman G., Kubista M., *J. Am. Chem. Soc.* 2001, **123**, 803-809.
92. Köhler O., Jarikote D.V., Seitz O., *Chem. Commun. (Camb).* 2004, **23**, 2674-2675.
93. Marin V.L., Armitage B.A., *Biochemistry.* 2006, **45**, 1745-1754.
94. S, Wagenknecht H.A., *Angew. Chem. Int. Ed.* 2009, **48**, 2418-2421.
95. Ikeda S., Okamoto A., *Chem. Asian J.* 2008, **3**, 958-968.
96. Okamoto A. *Chem. Soc. Rev.* 2011, **40**, 5815-5828.
97. Petersen M., Wengel J., *Trends Biotechnol.* 2003, **21**, 74-81.
98. Sugizaki K., Okamoto A., *Bioconjug. Chem.* 2010, **21**, 2276-2281.
99. Ikeda S., Kubota T., Kino K., Okamoto A., *Bioconjug. Chem.* 2008, **19**, 1719-1725.

100. Ikeda S., Kubota T., Yuki M., Yanagisawa H., Tsuruma S., Okamoto A., *Org. Biomol. Chem.* 2010, **8**, 546-51.

101. Majlessi M., Nelson N.C., Becker M.M., *Nucleic. Acids. Res.* 1998, **26**, 2224-2229.

102. Kubota T., Ikeda S., Yanagisawa H., Yuki M., Okamoto A., *Bioconjug. Chem.* 2009, **20**, 1256-1261.

103. Ikeda S., Kubota T., Yuki M., Okamoto A., *Angew. Chem. Int. Ed. Engl.* 2009, **48**, 6480-6484.

104. Maki A.H., Co T., *Biochemistry.* 1976, **15**, 1229-1235.

105. Stryer L., Haugland R.P., *Proc. Natl. Acad. Sci. U.S.A.* 1967, **58**, 719-726.

106. Kubota T., Ikeda S., Yanagisawa H., Yuki M., Okamoto A., *Bioconjug. Chem.* 2011, **22**, 1625-1630.

107. Ikeda S., Kubota T., Wang D.O., Yanagisawa H., Umemoto T., Okamoto A., *Chembiochem.* 2011, **12**, 2871-2880.

108. Hanami T., Delobel D., Kanamori H., Tanaka Y., Kimura Y., Nakasone A., Soma T., Hayashizaki Y., Usui K., Harbers M., *PLoS One*. 2013, **8**, e70942.

109. Atsumi J., Hanami T., Enokida Y., Ogawa H., Delobel D., Mitani Y., Kimura Y., Soma T., Tagami M., Takase Y., Ichihara T., Takeyoshi I., Usui K., Hayashizaki Y., Shimizu K., *Oncol. Rep.* 2015, **33**, 2719-2727.

110. Kimura Y., Soma T., Kasahara N., Delobel D., Hanami T., Tanaka Y., de Hoon M.J., Hayashizaki Y., Usui K., Harbers M., *PLoS One.* 2016, **11**, e0146950.

111. Mitani Y., Lezhava A., Kawai Y., Kikuchi T., Oguchi-Katayama A., Kogo Y., Itoh M., Miyagi T., Takakura H., Hoshi K., Kato C., Arakawa T., Shibata K., Fukui K., Masui R., Kuramitsu S., Kiyotani K., Chalk A., Tsunekawa K., Murakami M., Kamataki T., Oka T., Shimada H., Cizdziel P.E., Hayashizaki Y., *Nat. Methods.* 2007, **4**, 257-262.

112. Lezhava A., Ishidao T., Ishizu Y., Naito K., Hanami T., Katayama A., Kogo Y., Soma T., Ikeda S., Murakami K., Nogawa C., Itoh M., Mitani Y., Harbers M., Okamoto A., Hayashizaki Y., *Hum. Mutat.* 2010, **31**, 208-217.

113. Wang D.O., Matsuno H., Ikeda S., Nakamura A., Yanagisawa H., Hayashi Y., Okamoto A., *RNA.* 2012, **18**, 166-175.

114. Kubota T., Ikeda S., Yanagisawa H., Yuki M., Okamoto A., *PLoS One*. 2010, **5**, e13003.

115. Oomoto I., Suzuki-Hirano A., Umeshima H., Han Y.W., Yanagisawa H., Carlton P., Harada Y., Kengaku M., Okamoto A., Shimogori T., Wang D.O., *Nucleic. Acid Res.* 2015, **43**, e126.

Chapter 2

Bacterial Population Assessment in Solid-state Fermentation by Exciton-controlled Fluorescent RNA

2.1 Abstract

Municipal and agricultural solid-waste composting and bioenergy conversion through biomass processes allows recyclable and sustainable methods to obtain materials and energy. These solid-state fermentation (SSF) bioprocesses are performed in complex solid-rich systems that present significant challenges for effective monitoring of bacterial population dynamics. We have developed a simple and efficient chemical system that allows quantification of bacteria population by fluorescence-based analysis. The key component in the system is the exciton-controlled fluorescent RNA aptamer, which was covalently conjugated to two thiazole orange moieties and serves as a competitor of bacterial ribosome. The intensity of fluorescence from such a ribosome-sensing system was controlled by the excitonic interaction between dyes in the RNA aptamer and it increased drastically in the presence of *Escherichia coli*. This innovative fluorescence-based competition system is valuable for quantification without any extraction of bacterial nucleic acids, enables the relationship between the bacterial population and physical factors to be determined, and provides the simplest and most feasible way to optimize SSF bioprocesses.

2.2 Introduction

Solid-state fermentation (SSF) is a biomolecule manufacturing process driven by microbial populations growing on either a solid support or on a slurry with high solid content.[1] These cost-effective processes have been widely used for city waste treatment and for agricultural residue recycling by composting and biorefinery.[2–6] Abiotic and biotic byproducts that may be generated as a result of the use of raw materials as feedstock in SSF lead to various effects on the microbial population, which results in a complex feedback system.[7] Identification of the relationship between bacterial population size and physical factors will make it possible to understand the ecological processes and adjust the processing efficiency and orientation for specific purposes. However, the vast ranges of the heterogeneous solid particles that are involved in SSF make tracking and quantifying bacterial populations quite challenging for these bioprocesses.[8] Plating techniques have been developed to quantify bacterial populations in the presence of an uncontrolled bacterial inoculum.[9,10] However, operational variation in material handling, air conditioning, and substrate composition limits its application. Most current methods for monitoring bacterial population dynamics involve techniques based on molecular biology such as 16S-rRNA-based denaturing gradient gel electrophoresis,[11–14] terminal restriction fragment length polymorphism,[15] microarray,[16] and sequencing of clone libraries.[17–19]

Although these approaches have achieved some success in monitoring microbial communities during different SSF phases, all of them need to extract DNA or RNA from raw fermentation samples and cost- and time-intensive steps, including many preparation processes, are required to obtain quantitative information. Although hybridization techniques using oligonucleotides specific to regions of 16S and 18S rRNA or their genes have been attempted to describe the changes in microbial populations of sedentary environmental processes,[20] they also require extraction of either DNA or RNA from the heterogeneous matrix, which is labor-intensive, time-consuming, and may result in loss of DNA and RNA, which consequently reduces accuracy.

A conceptually new approach would involve a simple and efficient fluorescence assay that does not require extraction of bacterial nucleic acids; such a system could be used for quantitative detection of bacterial population dynamics and would be suitable for the analysis of sedentary matrix systems and for

composting and bioenergy studies. Here, we report the first simple and feasible fluorescence-based RNA system that can be used to assess bacteria proliferation from a sedentary matrix directly. Although the fluorescence the synthetic RNA in the system is usually quenched by dye interaction, fluorescence is emitted with an intensity that can be used to quantify the number of bacterial ribosome present, which makes fluorescence analysis of the proliferation of *Escherichia coli* in SSF simple and practical (Fig. 2-1).

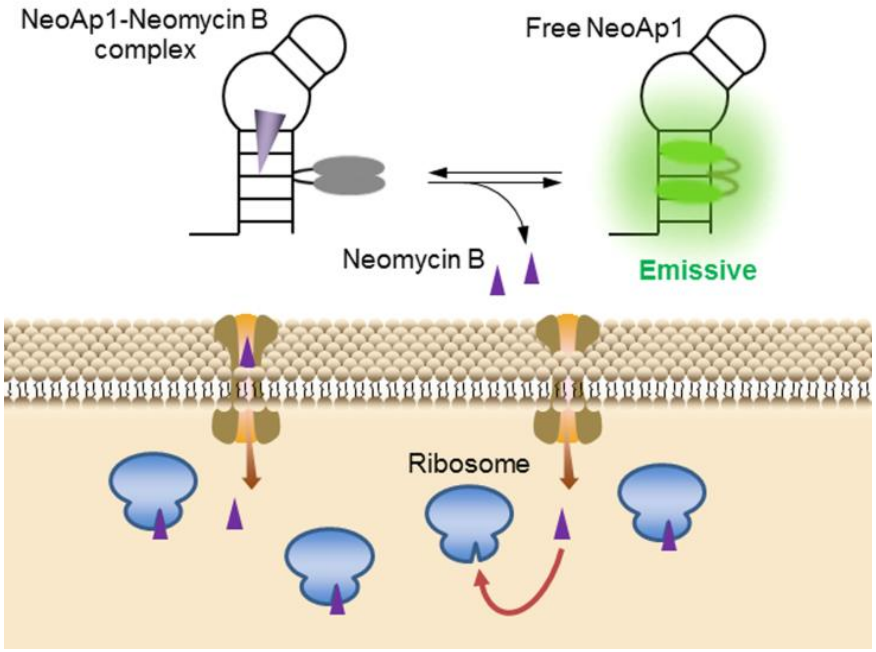

Figure 2-1. Competition for neomycin B between bacterial ribosomes and exciton-controlled fluorescent neomycin B RNA aptamer.

2.3 Results and discussion

Rationale

For simple biomolecule-monitoring fluorescence systems, the design of an effective target-specific turn-on fluorescent molecule is required. An example of a well-designed target-specific turn-on fluorescent molecule is the exciton-controlled hybridization-sensitive fluorescent oligonucleotide probe, which is composed of a DNA sequence linked covalently to two molecules of thiazole orange (TO); this probe has made numerous biological applications possible, including RNA imaging,[21–23] RNA tag-labeling,[24] simple fluorescent *in situ* hybridization (FISH),[25] and "live FISH".[26] Compared with the TO monomer-labeled probes, the fluorescence of TO homodimer-linked DNA probes was restrained because of the exciton coupling effect between the two TO units. Upon hybridization, two fluorescence-suppressed TO molecules intercalate into formed nucleic acid duplex structures to both robustly reduce the interaction between the dyes and simultaneously restrict the free rotation of TO around the methine bonds, giving rise to drastic fluorescence enhancement of the two TO units.[27,28] Considering the similarity between DNA and RNA, we envisaged that RNA sequences conjugated with the homodimer of TO may lead to a similar fluorescence response by controlling the intercalation of TO into double-stranded RNA (Fig. 2-2).

Neomycin B is an aminoglycoside antibiotic that can bind to bacterial ribosome-relating RNAs, such as rRNA A-site, *E. coli* ribosome, and synthetic neomycin RNA aptamers.[29–32] The binding affinities are not fully equivalent to rRNA A-site mimics obtained when employing intact ribosomes *in vitro* or *in vivo*,[33–35] indicating that the *E. coli* ribosome may have higher binding affinity with neomycin B compared with rRNA A-site mimics. Ribostamycin, a derivative of neomycin B, also showed affinity to an engineered neomycin B aptamer, and its ribose group was quite proximal to the end duplex region (Fig. 2-3).[36] Based on such chemistry, we can rationally infer that neomycin B, with an additional amino-modified glycoside into the ribose group of ribostamycin, may also interact directly with the end duplex of the neomycin aptamer. Therefore, we hypothesized that if a homodimer of TO dyes were linked to the end duplex region of the aptamer, the dyes may show strong fluorescent emission due to dye intercalation into the RNA duplex. On the other hand, upon neomycin B addition, neomycin B binding with the aptamer would inhibit the dye intercalation and

reduce the intensity of the fluorescence. Accordingly, in a system consisting of both neomycin B and the TO-homodimeric RNA aptamer, fluorescence emission might be recovered through neomycin B competition between aptamer and bacterial ribosome (Fig. 2-1).

Exciton-controlled hybridization-sensitive fluorescent RNA

Differences between the steric structures of the DNA and RNA duplex[37] mean that the intercalation characteristics of TO dyes conjugated to RNAs and the resultant fluorescent emission must be estimated after hybridizing with its complementary RNAs. To establish its photophysical properties, we selected 13nt repeated and base-mixed RNA sequences (ON1 and ON2, respectively) and a 20nt RNA sequence (ON3), labeled with a homodimer of TO (Table 1). To construct the RNA probe containing the TO homodimer, compound **8**, which is a uridine phosphoramidite with two amino ends connected through a blanched acrylamide linker at position C5, was first synthesized from uridine (**1**) (Scheme 1). The modified uridine phosphoramidite **8** was then quantitatively incorporated into single-stranded RNAs **9** (ssRNAs) by using an automated DNA/RNA synthesizer. The synthetic diamino-modified ssRNA **9** was coupled with an excess of carboxylate-activated TO dye in a postsynthetic process for 1.5 h. The ssRNA containing two TO dye moieties **10** was then purified by HPLC and its identity was confirmed by MALDI-TOF MS analysis.

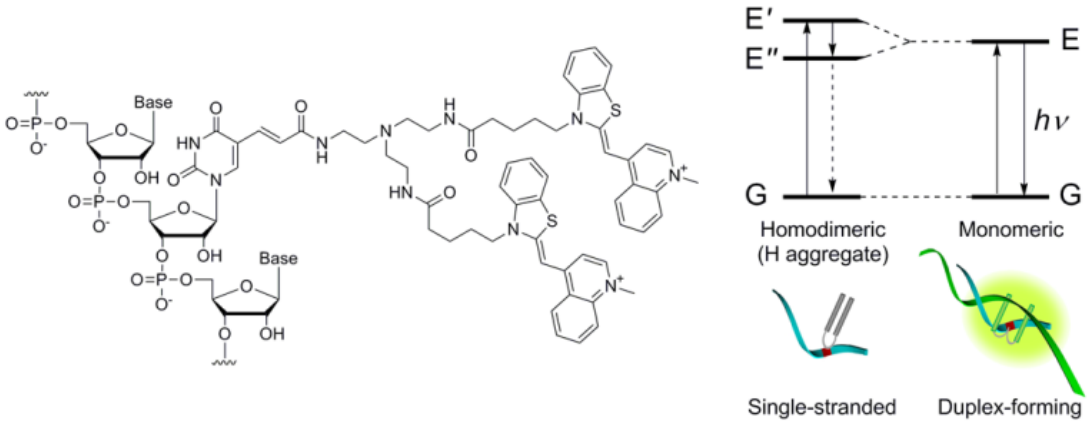

Figure 2-2. Chemical structure of the TO homodimer-labeled nucleotide D in exciton-controlled hybridization-sensitive fluorescent RNA strands (left) and control of the fluorescence emission by the exciton coupling effect of an H aggregation in D (right).

A

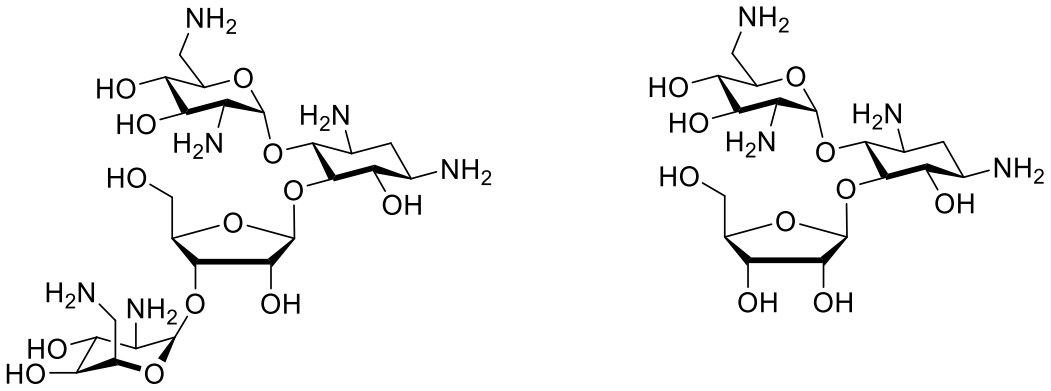

B

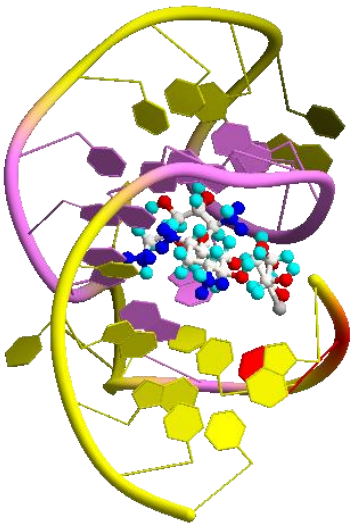

Figure 2-3. Aminoglycoside antibiotics neomycin B and ribostamycin. (**A**) Structures of neomycin B and ribostamycin; (**B**) Crystal structure of engineered neomycin B RNA aptamer binding with ribostamycin (PDB 2KXM). The interaction bases with ribostamycin are highlighted in purple, and the base modified in NeoAp1 is highlighted in red.

Scheme 1. Synthesis of an exciton-controlled hybridization-sensitive fluorescent RNA.

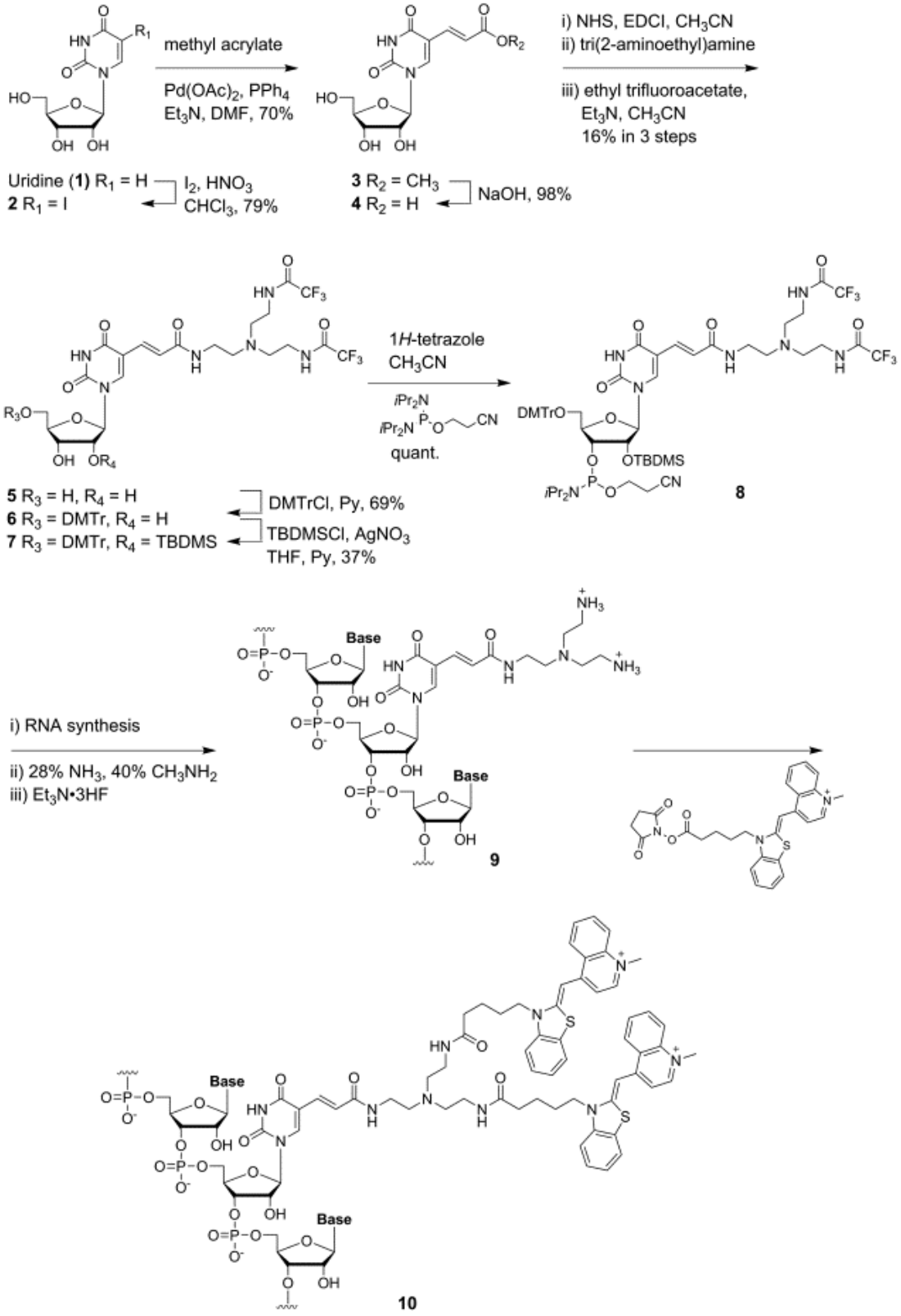

Table 1. Artificial RNA strands with short sequences used in this study.

	Sequences[a]
ON1	5′-r(UUUUUUDUUUUUU)-3′
ON1'	5′-r(AAAAAAAAAAAAA)-3′
ON2	5′-r(CGCAAUDUAACGC)-3′
ON2'	5′-r(GCGUUAAAUUGCG)-3′
ON3	5′-r(UGAAGGGCUUDUGAACUCUG)-3′
ON3'	5′-r(CAGAGUUCAAAAGCCCUUCA)-3′

[a]D represents the TO homodimer-labeled nucleotide as shown in Fig. 2-2.

The homodimeric-TO-labeled RNA strands exhibited a good response to hybridization with the complementary RNA (Figs 2-4a and 2-4b). The absorption spectra gave two bands at 479 and 507 nm. The former absorption band was stronger when these RNA strands were in the single-stranded states, whereas the latter absorption band became dominant after hybridization with the complementary RNA strands. The absorption band at 479 nm arises from H-aggregation of homodimeric TO, which suppresses fluorescence emission through the excitonic interaction between TOs.[21] On the other hand, the absorption band at 507 nm, similar with the monomeric TO, was observed after hybridization, suggesting that TO intercalation into the RNA duplex, leading to disruption of dye H-aggregation, was the emission mechanism.[21] Although the fluorescent emission was restrained in the single-stranded states, the fluorescence intensity at 535 nm increased dramatically after the homodimeric-TO-labeled RNA was mixed with the complementary RNA strands. For all homodimeric-TO-labeled RNA strands, irrespective of their hybridization states, the excitation spectra displayed a single peak at approximately 510 nm, which is in good accord with the absorption band at longer wavelengths. The coincident intensity of the excitation and emission further indicated that dye intercalation states control both the exciton states of the dyes and the fluorescent emission. These data were also supported by measuring the absorption spectra under various temperatures and probe concentrations. With increased temperature, the absorption band at 478 nm decreased gradually and the absorption band at 506 nm increased (Fig. 2-4c). The TO homodimer tethered to an RNA strand is

mainly aggregated and in the excitonic interaction state in room temperature. The concentration of the homodimeric-TO-labeled RNA did not alter the value of $\log(A_{476})/\log(A_{506})$; thus, an intramolecular H-aggregation was formed by the bichromophoric system of RNA (Fig. 2-7a). In the circular dichroism spectra recorded after hybridization with its complementary RNA, an induced circular dichroism was observed with broad negative signals and a sharp positive signal at 450-550 nm, which are characteristic signals of intercalation into the RNA duplex (Fig. 2-4d). In addition, the higher T_m values of the duplex of homodimeric-TO-labeled RNA and its complementary RNA strand were reflected in higher fluorescence intensity (Fig. 2-7b). A good response to RNA hybridization was observed for all three RNA samples (ON1, ON2 and ON3) with diverse sequences and lengths, indicating that the fluorescence of the homodimeric-TO-labeled RNA is controlled and is emitted in response to hybridization by excitonic interaction between two TO dyes (Fig. 2-5, and 2-6). The fluorescence intensity of the conjugated homodimer of TO in RNA can be controlled by adjusting its equilibrium between intercalation and intramolecular H-aggregation to change its exciton coupling state; this is the basis for designing the neomycin B-responsive fluorescent RNA aptamers described in the next section.

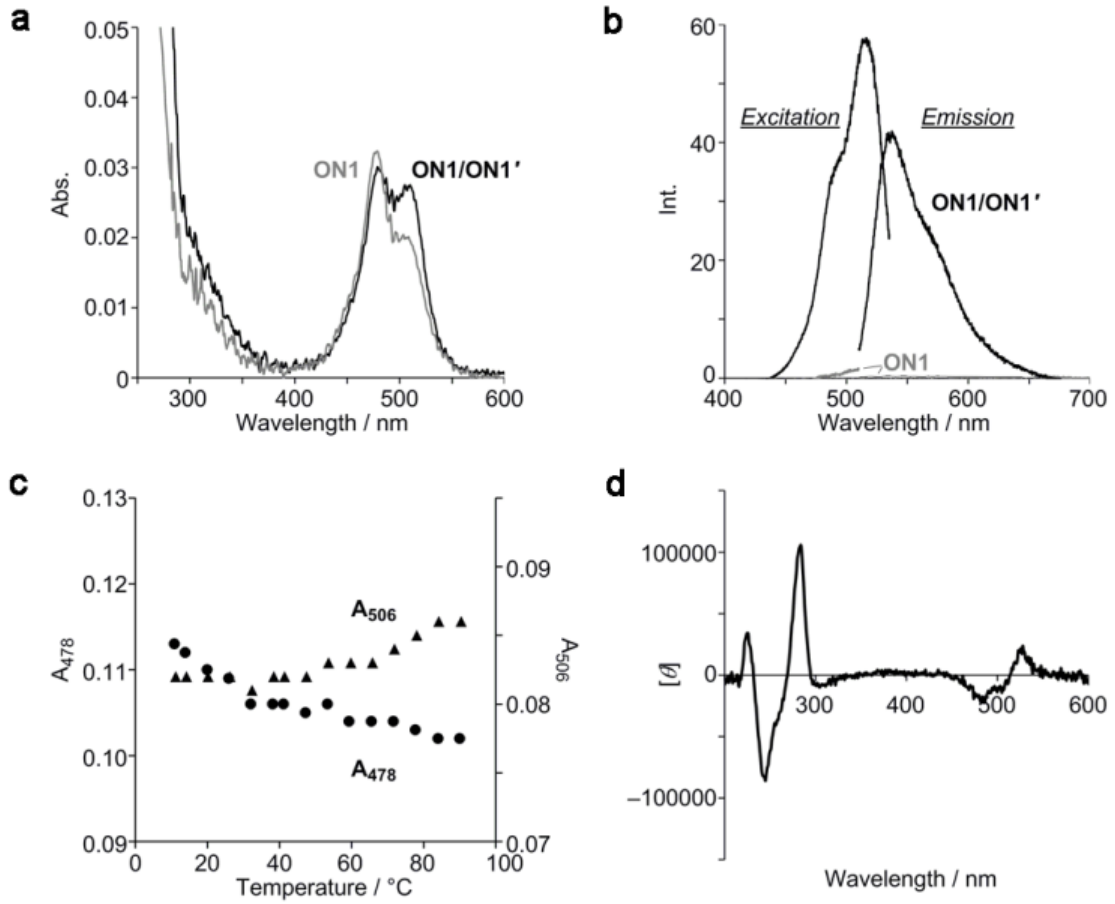

Figure 2-4. Analysis of the functions of exciton-controlled hybridization-sensitive fluorescent RNA strands. (a) The absorption spectra of ON1 before and after hybridization with the complementary RNA ON1. Spectra of ON1 (1 μM) were measured in 50 mM sodium phosphate (pH 7.0) containing 100 mM sodium chloride at 25 ^{o}C. (b) Excitation and emission spectra of ON1 before and after hybridization with the complementary RNA ON1. Spectra of ON1 (1 μM) were measured in 50 mM sodium phosphate (pH 7.0) containing 100 mM sodium chloride at 25 ^{o}C. The excitation spectra were measured for emission at a wavelength of 530 nm, and the emission spectra were obtained by excitation at 506 nm. (c) Changes of the absorbance at 478 and 506 nm of single-stranded ON1 at different temperatures. Spectra of ON1 (1 μM) were measured in 50 mM sodium phosphate (pH 7.0) containing 100 mM sodium chloride. (d) Circular dichroism spectrum of an ON1/ON1 duplex. The duplex (2.5 μM) was measured in 50 mM sodium phosphate (pH 7.0) containing 100 mM sodium chloride at 25 ^{o}C. [θ] is shown in deg cm^{2} dmol^{-1}.

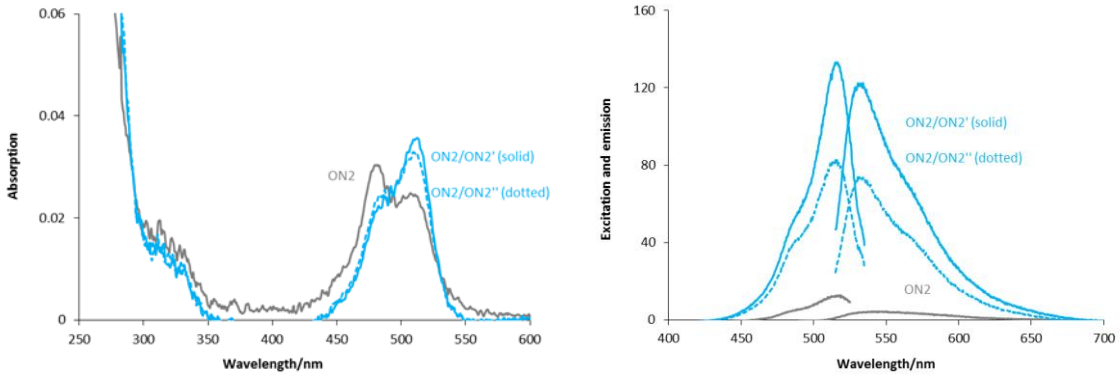

Figure 2-5. Photochemical behavior of ON2. (left) Absorption spectra; (right) Excitation and emission spectra. Spectra of ON2 (0.5 μM) were measured in 50 mM sodium phosphate (pH 7.0) containing 100 mM sodium chloride at 25 ℃. Emission spectra were measured on excitation at 510 nm. Excitation spectra were measured for emission at 530 nm. ON2: 5'-r(CGCAAUD$_{514}$UAACGC)-3'; ON2': 5'-r(GCGUUAAAUUGCG)-3'; ON2'': 5'-r(GCGUUAGAUUGCG)-3'.

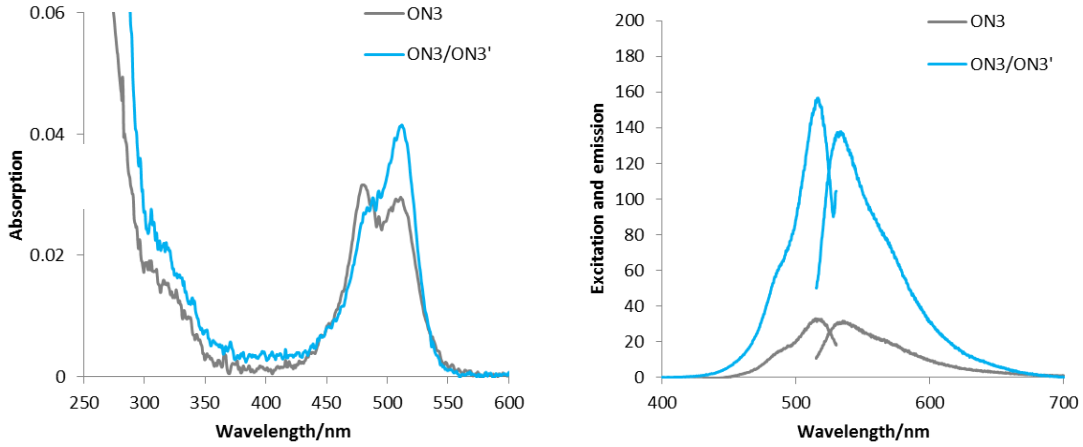

Figure 2-6. Photochemical behavior of ON3. (left) Absorption spectra; (right) Excitation and emission spectra. Spectra of ON3 (0.5 μM) were measured in 50 mM sodium phosphate (pH 7.0) containing 100 mM sodium chloride at 25 ℃. Emission spectra were measured on excitation at 510 nm. Excitation spectra were measured for emission at 530 nm.

A

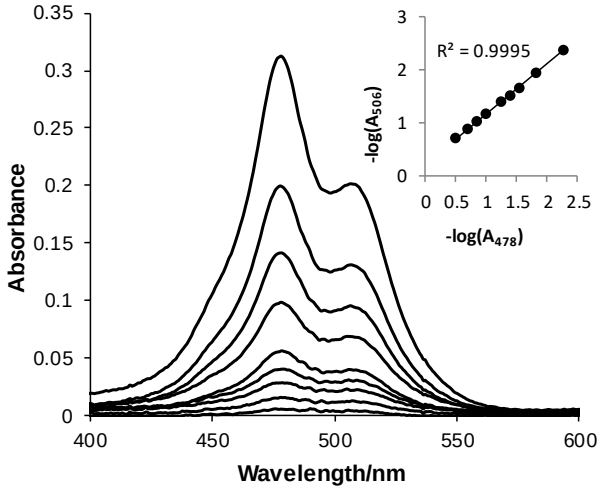

B

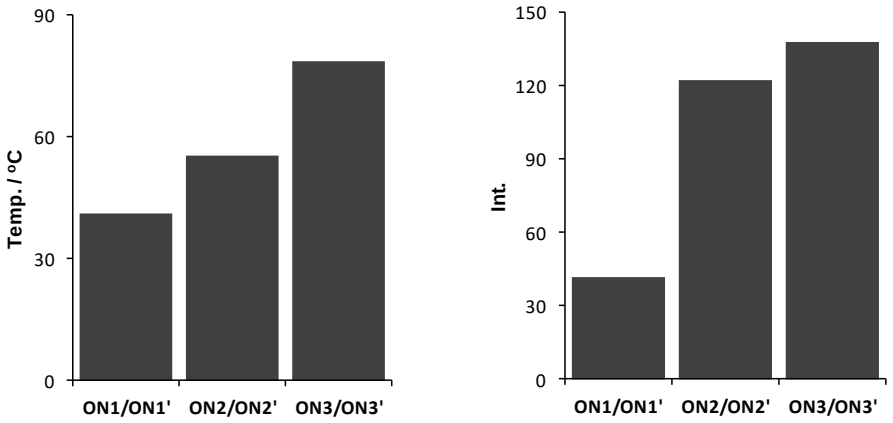

Figure 2-7. Analysis of the functions of exciton-controlled hybridization-sensitive fluorescent RNA strands. (**A**) Absorption spectra of single-strand ON1 under different concentrations. Spectra of ON1 (0.5, 0.75, 1.0, 1.2, 1.5, 2.0, 2.5, 3.0, 4.0 μM) were measured in 50mM sodium phosphate (pH 7.0) containing 100 mM sodium chloride at 25 ℃. Inset: plot of $-\log(A_{506})$ against $-\log(A_{478})$; (**B**) T_m values (left) and maximum fluorescent intensity (right) of ON1/ON1′, ON2/ON2′ and ON3/ON3′. The T_m values of the duplexes (1 μM, final duplex concentration) were measured in 50 mM sodium phosphate (pH 7.0) containing 100 mM sodium chloride. The absorbance of the samples was monitored at 260 nm from 10 to 90 ℃ with a heating rate of 0.5 ℃/min. The data for maximum fluorescent intensities come from Figure 2-2 and Figure 2-6.

Fluorescence suppression by neomycin B

An engineered neomycin B aptamer was selected to construct the neomycin B-responsive fluorescent RNA probe.[29] The loops in the aptamer structure are the core region for binding of ribostamycin, a neomycin B derivative, and the short end stem region has negligible interaction with the bound ribostamycin molecule. Neomycin B has an additional aminoglycoside group attached to the ribose side of ribostamycin that is close to the aptamer end stem duplex (Fig. 2-3). The additional aminoglycoside might interact with the end duplex because neomycin B has higher affinity to the aptamer than ribostamycin. Based on this assumption, we designed three neomycin B-based RNA aptamers with decreasing fluorescence (NeoAp1, NeoAp2, and NeoAp3; Fig. 2-8) by replacing the short end RNA stem with an RNA duplex labeled with TO homodimer. The requirements for neomycin B fluorescence suppression are: (i) neomycin B can bind to the replaced RNA aptamer, (ii) the replaced stem is long enough to maintain intercalation of TO effectively, and (iii) the modified site should be proximal to the neomycin B-binding site.

The homodimeric-TO-labeled RNA aptamers were also synthesized by using an automated DNA/RNA synthesizer and subsequently coupled with succinimidylated TO dyes. The purity of synthesized RNA was confirmed by HPLC chart and MALDI-TOF-MS (Fig. 2-9a and 2-9b). These synthetic RNA strands exhibited neomycin B-sensitive suppression of fluorescence (Fig. 2-8). In particular, the fluorescence intensity of NeoAp1 decreased drastically upon addition of neomycin B, although the fluorescence from NeoAp2 and NeoAp3 were also weakened. The dramatic reduction in fluorescence intensity results from the stem-binding competition between neomycin B and TO dyes in NeoAp1. The absorption spectra of NeoAp1 (Fig. 2-9c) reveals blue-shifted bands after the addition of neomycin B, which indicates that the fluorescent TO moieties transform their exciton states from noncoupling to coupling states because of intercalation disruption of TO dyes into NeoAp1 upon neomycin B binding. The neomycin B binding can be further confirmed by the increased Tm value of NeoAp1 in neomycin-B-containing solution (77.5 ^{o}C) compared with the neomycin-free solution (72 ^{o}C). Given that NeoAp1 showed a high fluorescence intensity ratio in the presence/absence of neomycin B, the NeoAp1–neomycin B complex was chosen for the neomycin B competition assays with *E. coli* ribosome.

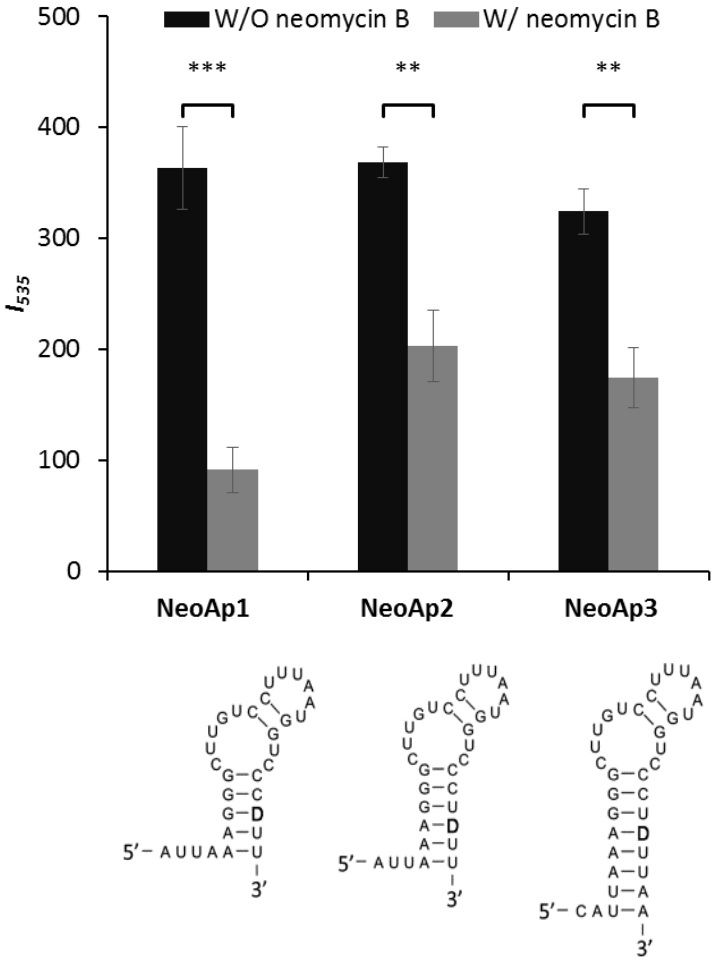

Figure 2-8. Secondary structures of engineered fluorescent neomycin B aptamers and their fluorescence intensities at 535 nm in the presence and absence of neomycin B. D denotes the TO homodimer-labeled nucleotide as shown in Fig. 2. Spectra of NeoAp1, NeoAp2, and NeoAp3 (0.5 μM each) were measured in 50 mM potassium phosphate (pH 6.2) containing 100 μM neomycin B and 100 mM potassium chloride at 25 ^{o}C. All emission spectra were measured with excitation at 510 nm. The mean values of triplicate samples are given. Error bars, mean ± standard deviation. Stars indicate significance in Student's t-test, *P < 0.05, **P < 0.01, ***P < 0.001.

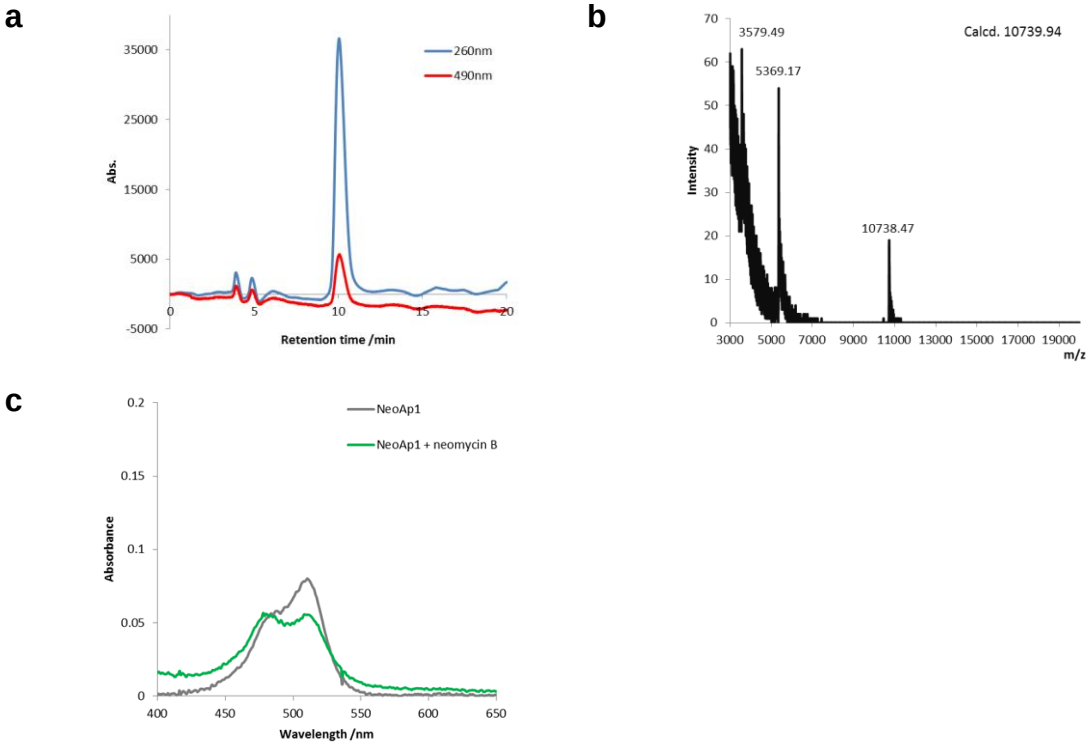

Figure 2-9. (a) HPLC spectra of NeoAp1. Condition: gradient 10-30 % in 20min with flow rate of TEAA buffer 1 mL/min; (b) MALDI-TOF mass spectrum showing desired mass value of NeoAp1; (c) Absorption spectra of NeoAp1 in the presence/absence of Neomycin B. Spectra of NeoAp1 (1.5 μM) were measured in 50 mM potassium phosphate (pH 6.2) containing 200 μM neomycin B and 100 mM potassium chloride at 25 ℃.

Fluorescence recovery by addition of *E. coli* ribosome

The binding affinity of neomycin B to its aptamer does not correlate linearly with inhibition of translation *in vitro* or antibacterial potency *in vivo*,[33–35] indicating that *E. coli* ribosome has a higher affinity to neomycin B than the aptamer. Based on this, we expected that *E. coli* ribosome would compete for neomycin B with NeoAp1 in the mixed solution, leading to recovery of the fluorescence of NeoAp1. Indeed, coincubation of the NeoAp1–neomycin B complex with *E. coli* ribosome showed marked fluorescent recovery from NeoAp1 suppressed by neomycin B. The intensity of fluorescence increased linearly with increased concentration of *E. coli* ribosome (Fig. 2-10a).

The recovery in fluorescence is specific to *E. coli* ribosome. The NeoAp1–neomycin B complex was incubated with *E. coli* ribosome, ON3′ (a random RNA

sequence) and polyA (the most common sequences in mRNA) (Fig. 2-10b). There was little fluorescence increase after the addition of ON3′ and polyA, whereas co-incubation of *E. coli* ribosome and the NeoAp1–neomycin B complex led to a remarkable increase, up to approximately eight times, in fluorescence.

Bacterial population quantification

NeoAp1 effectively recovered its fluorescence intensity through competition for neomycin B by *E. coli* ribosomes. The clear variation in fluorescence of NeoAp1 strongly depends on the existence of *E. coli* (Fig. 2-10c). The efficient bacterial cell penetration property of neomycin B[38,39] were expected to be useful for quantification of bacteria and concentration variation of neomycin after *E. coli* addition was monitored by agar diffusion assay (Fig. 2-10d). This was further verified by confirming the linear relationship over a defined range between the intensity of fluorescence of NeoAp1 and the OD_{600} of *E. coli* growing in LB medium. The fluorescence intensity of NeoAp1 in a neomycin B-containing solution increased in proportion to the amount of *E. coli* from 0 to 4.5 of OD_{600}, and the increase essentially stopped when the OD_{600} of *E. coli* was more than 4.5 because of complete removal of neomycin B from NeoAp1 by *E. coli* (Fig. 2-10f). The presence of *E. coli* in the NeoAp1–neomycin B complex-containing solution thus resulted in clear fluorescence emission (Fig. 2-10e). As neomycin B is a common antibiotic against bacteria, NeoAp1-neomycin-containing solution also performed to response environmental bacteria (Fig. 2-10g).

The establishment of the bacteria-population-dependent fluorescence properties of NeoAp1 made it possible to monitor *E. coli* population dynamics in an SSF process using NeoAp1 (Fig. 2-10h). Fish food containing large amounts of insoluble solid particles was incorporated into LB media to imitate SSF. When *E. coli* was cultured at 40 °C, fluorescence intensity started to increase at about 12 h and went through a maximum fluorescence intensity of more than 400 at 26 h. However, the fluorescence intensity started to increase at 26 h with a culturing temperature of 26 °C, and remained nearly constant during the entire monitored time period with a culturing temperature of 4 °C. The fluorescence intensity arising from NeoAp1 reflected the proliferation of *E. coli* in SSF at 40 °C and reduced cell viability at lower temperatures. NeoAp1 thus worked as a simple and practical fluorescence-based molecular tool to assess bacterial population dynamics during SSF.

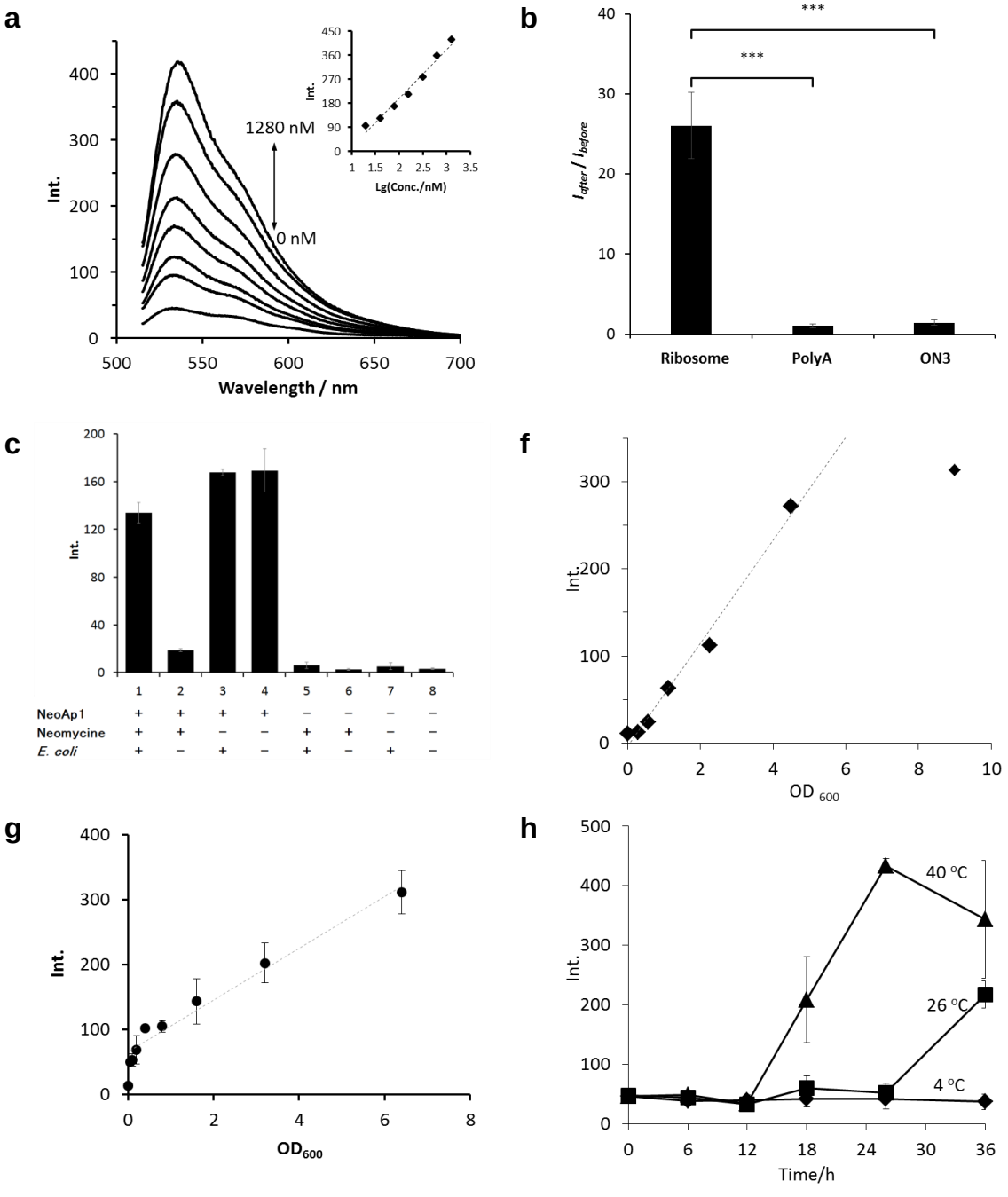
a
Int.
Wavelength / nm
1280 nM
0 nM
Lg(Conc./nM)
b
***
***
Ribosome
PolyA
ON3
c
Int.
NeoAp1
Neomycine
E. coli
f
Int.
OD 600
g
Int.
OD600
h
Int.
40 °C
26 °C
4 °C
Time/h
d

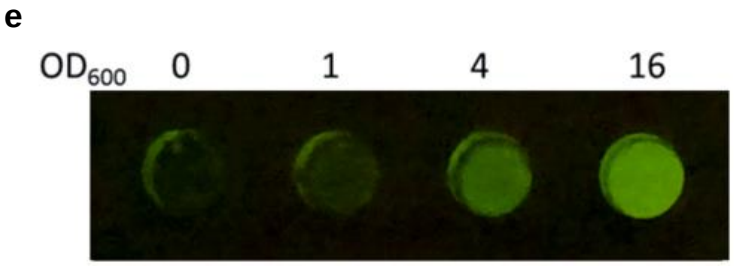

Figure 2-10. Neomycin B-competitive fluorescence assay using an exciton-controlled fluorescent RNA NeoAp1. (a) The emission spectra of NeoAp1 in the presence of *E. coli* ribosome. The spectra of NeoAp1 (20 nM) were measured in 50 mM potassium phosphate (pH 6.2) containing 200 μM neomycin B, 100 mM potassium chloride, and *E. coli* ribosomes (0, 20, 40, 80, 160, 320, 640 or 1280 nM) at 25 ^{o}C. The emission spectra were measured with excitation at 510 nm. Inset: fluorescent intensity against lg(Concentration/nM). (b) Fluorescence changes of NeoAp1 in the presence of competitors. Spectra of NeoAp1 (20 nM) were measured in 50 mM potassium phosphate (pH 6.2) containing 640 nM competitors, 200 μM neomycin B and 100 mM potassium chloride at 25 ^{o}C. The emission spectra were measured with excitation at 510 nm. The mean values of triplicate samples are given. Error bars, mean ± standard deviation. Stars indicate significance in Student's t-test, *P < 0.05, **P < 0.01, ***P < 0.001. (c) The fluorescent intensities at 530 nm in the presence of NeoAp1, neomycin and *E. coli* (lane 1), NeoAp1 and neomycin (lane 2), NeoAp1, and *E. coli* (lane 3), neomycin and *E. coli* (lane 5), NeoAp1 (lane 4), neomycin (lane 6), *E. coli* (lane 7), and absent of NeoAp1, neomycin and *E. coli* (lane 8). The fluorescence intensity of NeoAp1 (0.4 μM) at 526 nm was measured in 50 mM potassium phosphate (pH 6.2) containing 400 μM neomycin B, 25 times diluted RNAsecure solution and 100 mM potassium chloride at 25 ^{o}C. NeoAp1 stock solution and LB medium with *E. coli* at 3 of OD_{600} were mixed with equivalent volume. The emission spectra were measured with excitation at 510 nm. (d) Agar diffusion assay for determination of the inhibition zones of growth of *E. coli* with filtered solutions in (c). Left: trial 1; right: trial 6. (e) Fluorescence emission of NeoAp1 (1 μM) in 50 mM potassium phosphate (pH 6.2) containing 400 μM neomycin B and 100 mM potassium chloride at 25 ^{o}C. The emission was observed upon irradiation with 254 nm light. The *E. coli* OD_{600} of each well was 0, 1, 4, and 16 from left to right. (f) Relationship between OD_{600} of *E. coli* and the fluorescence intensity of NeoAp1. The fluorescence intensity of NeoAp1 (0.4

μM) at 526 nm was measured in 50 mM potassium phosphate (pH 6.2) containing 400 μM neomycin B, 25 times diluted RNAsecure solution and 100 mM potassium chloride at 25 ^{o}C. NeoAp1 stock solution and fresh LB medium were mixed with equivalent volume. The emission spectra were measured with excitation at 510 nm. The linear dashed line is a linear approximation of the data from OD_{600} = 0 to 4.5 (R^2 = 0.9867). (g) Relationship between OD_{600} of environmental bacteria and the fluorescence intensity of NeoAp1. The fluorescence intensity of NeoAp1 (0.4 μM) at 526 nm was measured in 50 mM potassium phosphate (pH 6.2) containing 400 μM neomycin B, 25 times diluted RNAsecure solution and 100 mM potassium chloride at 25 ^{o}C. NeoAp1 stock solution and fresh LB medium were mixed with equivalent volume. The emission spectra were measured with excitation at 510 nm. (h) The growth time courses of *E. coli* in compost reactors at different culturing temperatures monitored by using the NeoAp1-neomycin B fluorescence-based system (λ_{exc} = 510 nm, λ_{em} = 530 nm). The mean values of duplicate samples are given. Error bars, mean ± standard deviation.

2.4 Conclusions

The development of chemistry that can be used to monitor bacteria proliferation is an urgent issue in SSF. We have described a conceptually new fluorescence assay to quantify bacterial population. Synthetic RNAs labelled with an exciton-controlled TO dimer revealed a hybridization-sensitive fluorescence increase. Based on the principle of the intercalation adjustment of homodimeric-TO-labelled RNA, a NeoAp1 fluorescent probe was designed for neomycin B-competitive ribosome fluorescence assessment. This fluorescence-based competition assay made it simple and practical to monitor bacterial population dynamics in SSF, compared with other current methods based on analysis of the nucleic acids extracted from bacteria. The assay presented herein is expected to be used to help monitor the change of bacterial physical state and to optimize bioprocesses in SSF. The technique is suitable for the analysis of sedentary matrix and also for composting and bioenergy studies.

2.5 Experimental procedures

General. All chemicals were purchased from Sigma-Aldrich, Wako chemicals, and Tokyo Chemical Industry. ^{1}H and ^{13}C NMR spectra were measured with a Bruker Avance 600 (600 MHz). Electrospray ionization mass spectra ESI-MS spectra were recorded by a Bruker microTOF II-NAC. MALDI-TOF mass spectra were recorded by a Bruker microflex-NAC. RNA was synthesized on a NTS H-8 DNA/RNA synthesizer (Nihon Techno Service). RNA oligonucleotides were purified by HPLC system composed by GILSON Inc. and JASCO Inc. modules. Absorption and fluorescence spectra were recorded on Shimadzu UV-2550 spectrophotometer and RF-5300PC spectrofluorophotometer, respectively.

Compound 2. In a round bottom flask, uridine (**1**) (2.0 g, 8.2 mmol) and iodine powder (2.3 g, 9.0 mmol) were dissolved in a mixture of chloroform (110 mL) and 1 M nitric acid (20 mL). The mixture was heated at 80 ^{o}C for 5h. The reaction progress was monitored by TLC (30 % methanol in chloroform). After cooling down the reaction mixture to 0 ^{o}C, the precipitate was collected by filtration and dried under vacuum overnight to provide **2** as colorless needles (2.4 g, 79 %). ^{1}H NMR (600 MHz, DMSO-d_6) δ 11.70 (s, 1H), 8.50 (s, 1H), 5.72 (d, 1H, J = 4.4 Hz), 4.03 (t, 1H, J = 4.7 Hz), 3.99 (t, 1H, J = 4.4 Hz), 3.87 (m, 1H), 3.70 (q, 1H, J = 12.1 Hz), 3.59 (q, 1H, J = 12.0 Hz); ^{13}C NMR (600 MHz, DMSO-d_6) δ 161.3, 151.2, 146.0, 89.2, 85.6, 74.8, 70.3, 70.1, 61.1; ESI-MS $[M-H]^-$ $C_9H_{10}IN_2O_6$ 368.9584 (calcd.), 368.9589 (found).

Compound 3. To a solution of **2** (2.0 g, 5.6 mmol) in *N*, *N*-dimethylformamide (30 mL) was added palladium(II) acetate (60.0 mg, 0.36 mmol), triphenylphosphine (148.0 mg, 0.76 mmol), triethylamine (1.0 mL, 7.2 mmol) and methyl acrylate (0.9 mL, 10.8 mmol). The mixture was heated at 100 ^{o}C for 4 h. The mixture was filtered and the filtrate was concentrated *in vacuo*. The residue was recrystallized using methanol to provide **3** as a white solid (1.3 g, 70 %). ^{1}H NMR (600 MHz, DMSO-d_6) δ 11.68 (s, 1H), 8.53 (s, 1H), 7.34 (t, 1H, J =8.5 Hz), 6.85 (t, 1H, J = 8.5 Hz), 5.78 (s, 1H), 5.49 (s, 1H), 5.35 (s, 1H), 5.10 (s, 1H), 4.09 (s, 1H), 4.03 (s, 1H), 3.89 (s, 1H), 3.74 (s, 1H), 3.68 (s, 3H), 3.63 (s, 1H); ^{13}C NMR (150 MHz, DMSO-d_6) δ 168.0, 162.6, 150.3, 144.8, 138.7, 117.1, 109.1, 89.5, 85.5, 74.8, 69.9, 61.0, 52.1; ESI-MS $[M-H]^-$ $C_{13}H_5N_2O_8$ 327.0828 (calcd.), 327.0821 (found).

Compound 4. In a round bottom flask, **3** (1.3 g, 4.0 mmol) was dissolved in 3.0 M sodium hydroxide in 1:1 water/ethanol (12 mL) and this mixture was stirred at room temperature for 3 h. 1M HCl solution was added into the mixture on cooling ice bath to give white precipitate. The precipitate was filtered and washed with hexane. The product was dried *in vacuo* to yield white powder (1.2 g, 98 %). ^{1}H NMR (600 MHz, DMSO-d_6) δ 11.64 (s, 1H), 8.51 (s, 1H), 7.30 (d, 1H, J = 15.8 Hz), 6.79 (d, 1H, J = 15.8 Hz), 5.79 (d, 1H, J = 4.1 Hz), 4.11 (d, 1H, J = 4.4 Hz), 4.06 (t, 1H, J = 4.7 Hz), 3.90 (s, 1H), 3.75 (d, 1H, J = 11.7 Hz), 3.63 (d, 1H, J = 10.0 Hz); ^{13}C NMR (150 MHz, DMSO-d_6) δ 168.9, 162.6, 150.4, 144.3, 138.1, 118.7, 109.3, 89.5, 85.6 74.9, 70.0, 61.0; ESI-MS $[M-H]^-$ $C_{12}H_{13}N_2O_8$ 313.0672 (calcd.), 313.0677 (found).

Compound 5. *N*-Hydroxysuccinimide (732.6 mg, 6.4 mmol) and 1-ethyl-3-(3-dimethylaminopropyl)carbodiimide hydrochloride (1.2 g, 6.4 mmol) were added to a solution of **4** (1.0 g, 3.2 mmol) in acetonitrile (80 mL) and stirred at 25 ^{o}C for 24 h. Tris(2-aminoethyl)amine (4.8 mL, 32.0 mmol) was added to the suspension and was stirred at 25 ^{o}C for 2 h. Ethyl trifluoroacetate (19.0 mL, 160 mmol) and triethylamine (22.3 mL, 160 mmol) were added to the suspension and stirred at 25 ^{o}C for 48 h. The mixture was concentrated *in vacuo* and purified by silica gel column chromatography (5 % − 10 % methanol/dichloromethane). The fraction containing **5** was concentrated *in vacuo*. The residue was dissolved in a small amount of acetone. A white powder precipitated from the mixture upon the addition of diethyl ether. The precipitate was filtered and washed with ether and then dried *in vacuo* to give **5** as a colorless oil (527.1 mg, 16 %). ^{1}H NMR (600 MHz, CD_3OD) δ 8.49 (s, 1H), 7.26 (d, 1H, J = 15.6 Hz), 7.10 (d, 1H, J = 15.6 Hz), 5.95 (s, 1H), 4.23 (s, 2H), 4.07 (s, 1H), 3.96 (d, 1H, J = 12.0 Hz), 3.82 (d, 1H, J = 12.0 Hz), 3.38 (d, 6H, J = 6.2 Hz), 2.74 (t, 6H, J = 6.2 Hz); ^{13}C NMR (150 MHz, CD_3OD) δ 168.3, 162.7, 158.3, 158.0, 150.4, 142.9, 133.2, 121.1, 117.5, 115.6, 110.0, 90.1, 85.4, 75.1, 69.9, 60.9, 53.4, 52.9, 46.8, 38.0, 37.7, 8.3. ESI-MS $[M-H]^-$ $C_{22}H_{27}F_6N_6O_9$ 633.1744 (calcd.), 633.1737 (found).

Compound 6. A solution of **5** (508.0 mg, 0.8 mmol) and 4,4'-dimethoxytrityl chloride (101.7 mg, 0.3 mmol) in pyridine (20 mL) was stirred at 25 ^{o}C for 16 h. Water (2 mL) was added to the reaction mixture and then the mixture was concentrated *in vacuo*. The residue was purified by silica gel column chromatography (5 % methanol and 1 % trimethylamine in dichloromethane). The fraction containing **6** was then concentrated. Saturated aqueous sodium bicarbonate was added to the residue, and then extracted with ethyl acetate,

washed with brine, and dried *in vacuo* to give **6** as a white foam (516.7 mg, 69 %). ^{1}H NMR (600 MHz, DMSO-d_6) δ 11.69 (s, 1H), 9.33 (s, 1H), 7.96 (s, 1H), 7.40−6.89 (15H), 5.80 (s, 1H), 5.50 (s, 1H), 5.14 (s, 1H), 4.18 (s, 1H), 4.02 (s, 1H), 3.95 (s, 1H), 3.72 (s, 6H), 3.61 (s, 1H), 2.10 (m, 12H); ^{13}C NMR (150 MHz, DMSO-d_6) δ 166.5, 162.6, 158.9, 157.3, 157.1, 150.3, 145.6, 144.1, 136.5, 136.4, 133.0, 130.6, 130.5, 128.6, 128.6, 127.5, 127.2, 122.9, 119.6, 117.8, 115.8, 114.1, 110.5, 90.2, 86.4, 83.6, 73.5, 70.7, 64.8, 55.8, 55.8, 53.8, 52.9, 38.3, 37.8, 31.5; ESI-MS $[M-H]^-$ $C_{43}H_{45}F_6N_6O_{11}$ 935.3051 (calcd.), 935.3049 (found).

Compound 7. A solution of **6** (468.0 mg, 0.5 mmol), silver nitrate (93.4 mg, 0.6 mmol) in pyridine (201 μL) and THF (4 mL) was stirred at 25 ^{o}C for 1 h, and then *tert*-butyldimethylsilyl chloride (82.9 mg, 0.6 mmol) was added. The solution was stirred at 25 ^{o}C for 24 h. The reaction mixture was concentrated *in vacuo* and purified by silica gel column chromatography (2% methanol and 1% trimethylamine in dichloromethane). The fraction containing **7** was concentrated. Saturated aqueous sodium bicarbonate was added to the residue, and then extracted with ethyl acetate, washed with brine, and dried *in vacuo* to give **7** as a white foam (194.3 mg, 37 %). ^{1}H NMR (600 MHz, DMSO-d_6) δ 7.98 (s, 1H), 7.87 (s, 1H), 7.48−6.53 (15H), 6.00 (s, 1H), 5.37 (s, 1H), 4.43(s, 1H), 4.16 (s, 2H), 3.79 (s, 6H), 3.67 (s, 1H), 3.62 (s, 1H), 3.35−2.07 (12H), 0.92 (9H), 0.15 (3H); ^{13}C NMR (150 MHz, DMSO-d_6) δ 167.0, 161.7, 159.2, 159.1, 158.4, 158.2, 149.6, 145.0, 140.0, 135.9, 135.8, 132.1, 130.4, 130.3, 128.6, 128.3, 127.6, 122.2, 117.2, 115.3, 113.9, 111.1, 89.6, 87.2, 84.3, 76.3, 71.2, 71.0, 63.67, 60.8, 55.7, 55.1, 53.5, 38.1, 26.0, 18.4; ESI-MS $[M-H]^-$ $C_{49}H_{59}F_6N_6O_{11}Si$ 1049.3915 (calcd.), 1049.3908 (found).

Compound 8. Acetonitrile (1 mL) and 2-cyanoethyl *N*,*N*,*N*',*N*'-tetraisopropylphosphordiamidite (155 μL, 0.49 mmol) were added to a mixture of **7** (171 mg, 0.16 mmol) and 1*H*-tetrazole (23 mg, 0.33 mmol) dried in a round-bottom flask. The mixture was stirred at 25 ^{o}C for 2 h. After identification of the end of the reaction by TLC, the reaction mixture was passed through a 0.45 μm filter and was used for automated RNA synthesis without further purification.

Succinimidylation of TO dyes.[21] *N*-Hydroxysuccinimide (4.6 mg, 40 μmol) and 1-ethyl-3-(3-dimethylaminopropyl) carbodiimide hydrochloride (7.7 mg, 40 μmol) were added to a solution of TO dye (20 μmol) in DMF (0.50 mL) and stirred at 25 ℃ for 16 h. The reaction mixture was used for the next reaction with RNA oligomers without further purification.

Synthesis of fluorescent RNA. RNA oligomers were synthesized by a conventional phosphoramidite method from **8** and commercially available A, G, C, and U phosphoramidites (Glen Research) using a NTS H-8 DNA/RNA synthesizer. The synthesized RNA oligomer was cleaved from the support by the hydrolysis in a solution of 1:1 (*v*/*v*) 28% aqueous ammonia/40% methylamine for 20 min, and then synthetic oligonucleotides were deprotected at 65 ^{o}C for 5 min. After concentration of the solution *in vacuo*, 2'−silyl groups were removed with triethylamine trihydrofluoride at 65 ^{o}C for 2 h. After diluting with distilled water, RNA was purified by reversed-phase HPLC on a 5-ODS-H column (10 mm × 150 mm, elution with a solvent mixture of 0.1 M triethylammonium acetate (TEAA), pH 7.0, linear gradient over 30 min from 5% to 30% acetonitrile at a flow rate of 3.0 mL/min).

A solution of the succinimidyl ester of TO dye (100 *eq*. to an active amino group of RNA) in *N*, *N*-dimethylformamide was added to a solution of diamino-modified RNA in 100 mM sodium carbonate buffer (pH 9.0), and incubated at 25 ^{o}C for 1.5 h. The reaction mixture was diluted with ethanol. After centrifuging at -20 ^{o}C for 20 min, the supernatant was removed. The residue was dissolved in a small volume of water and the solution was passed through a 0.45 um filter. The product was purified by reversed-phase HPLC on a 5-ODS-H column (10 mm × 150 mm, elution with a solvent mixture of 0.1 M TEAA, pH 7.0, linear gradient over 30 min from 5 % to 30 % acetonitrile at a flow rate of 3.0 mL/min). The concentration of the fluorescent RNA was determined at Nanodrop 1000 spectrophotometer. The fluorescent RNA was identified by MALDI-TOF mass spectrometry.

Absorption, fluorescence and circular dichroism spectra measurements. Absorption, fluorescence and circular dichroism spectra of the fluorescent probes of the fluorescent RNA samples (0.5-2.5 μM) were measured in 50 mM sodium phosphate buffer (pH 7.0) containing 100 mM sodium chloride using a cell with a 1 cm path length. The excitation and emission bandwidths were 1.5 nm.

Melting temperature (T_m) measurements. The T_m values of duplexes (1 μM) were measured in 50 mM sodium phosphate buffers (pH 7.0) containing 100 mM sodium chloride. The absorbance of the samples was monitored at 260 nm from 10 to 90 ^{o}C with a heating rate of 0.5 ^{o}C /min. From these absorbance profiles, the first derivatives were calculated to determine the value of T_m.

***E. coli* culture.** To test the relationship between fluorescent intensity of NeoAp1 and OD_{600} of *E. coli*, *E. coli* cells were cultured at 37 ^{o}C in LB medium. LB

medium was purchased from Becton, Dickinson and Company and autoclaved at 120 ^{o}C for 20 min before use. A stock solution containing 40 nM NeoAp1, 400 μM neomycin B and 2× RNAsecure^{TM} (Thermo Fisher Scientific) in 50 mM sodium phosphate buffer (pH 7.0) containing 100 mM sodium chloride was made in advance. The stock solution (20 μL) and the culturing solution with different OD_{600} (20 μL) were mixed for fluorescence intensity measurement. The excitation and emission bandwidths were 3 nm.

Bacteria population assessment. The experiment was performed in a 200 mL glass flask with synthetic food waste. The synthetic food waste was a mixture of fish food (Japan Pet Design Co., Ltd., Tokyo) and LB medium with a final solid content of approximately 50% (*w*/*w*). *E. coli* was cultured in the synthetic food waste at 4, 26, and 40 °C without shaking. 20 μL NeoAp1 stock solution (40 nM NeoAp1, 400 μM neomycin B and 2-times-diluted RNAsecure^{TM} (Thermo Fisher Scientific) in 50 mM sodium phosphate buffer (pH 7.0) containing 100 mM sodium chloride) and 20 μL culturing slurry at different time points were mixed for fluorescence intensity measurements. The excitation and emission bandwidths were 3 nm.

2.6 References

1 R. R. Singhania, A. K. Patel, C. R. Soccol and A. Pandey, *Biochem. Eng. J.* 2009, **44**, 13–18.

2 E. Varga, H. B. Klinke, K. Reczey and A. B. Thomsen, *Biotechnol. Bioeng.* 2004, **88**, 567–574.

3 H. Jørgensen, J. Vibe-Pedersen, J. Larsen and C. Felby, *Biotechnol. Bioeng.* 2007, **96**, 862–870.

4 J. Zhang, D. Chu, J. Huang, Z. Yu, G. Dai, and J. Bao, *Biotechnol. Bioeng.* 2010, **105**, 718–728.

5 E. R. Viéitez, J. Mosquera and S. Ghosh, *Water Sci. Technol*. 2000, **41**, 231–238.

6 B. Xi, X. He, Q. Dang, T. Yang, M. Li, X. Wang, D. Li, and J. Tang, *Bioresour. Technol*. 2015, **196**, 399–405.

7 P. D. Schloss, A. G. Hay, D. B. Wilson and L .P. Walker, *Trans. ASAE.* 2003, **46**, 919–927.

8 J. P. Tamang, K. Watanabe and W. H. Holzapfel, *Front. Microbiol*. 2016, **7**, 377.

9 K. Nakasaki, M. Shoda and H. Kubota, *Appl. Environ. Microbiol*. 1985, **50**, 1526–1530.

10 J. Ryckeboer, J. Mergaert, J. Coosemans, K. Deprins and J. Swings, *J. Appl. Microbiol*. 2003, **94**, 127–137.

11 Z. H. Yang, Y. Xiao, G. M. Zeng, Z. Y. Xu and Y. S. Liu, *Appl. Microbiol. Biotechnol*. 2007, **74**, 918–925.

12 N. Yamamoto, R. Asano, H. Yoshii, K. Otawa and Y. Nakai, *Appl. Microbiol. Biotechnol*. 2011, **90**, 1501–1510.

13 X. Yong, Y. Cui, L. Chen, W. Ran, Q .Shen and X. Yang, *Appl. Microbiol. Biotechnol*. 2011, **92**, 717–725.

14 Z. Yu, B. Dong and W. Lu, *Lett. Appl. Microbiol*. 2009, **49**, 166–172.

15 A. J. Székely, R. Sipos, B. Berta, B. Vajna, C. Hajdú and K. Márialigeti, *Microb. Ecol*. 2009, **57**, 522–533.

16 I. H. Franke-Whittle, B. A. Knapp, J. Fuchs, R. Kaufmann and H. Insam, *Microb. Ecol*. 2009, **57**, 510–521.

17 P. M. Dees and W. C. Ghiorse, *FEMS Microbiol. Ecol*. 2001, **35**, 207–216.

18 J. Hultman, T. Vasara, P. Partanen, J. Kurola, M. H. Kontro, L. Paulin, P. Auvinen and M. Romantschuk, *J. Appl. Microbiol*. 2010, **108**, 472–487.

19 V. L. Tkachuk, D. O. Krause, N. C. Knox, A. C. Hamm, F. Zvomuya, K. H. Ominski and T. A. McAllister, *J. Appl. Microbiol*. 2014, **116**, 1181–1194.

20 P. D. Schloss, A. G. Hay, D. B. Wilson, J. M. Gossett and L. P. Walker, *Appl. Microbiol. Biotechnol*. 2005, **66**, 457–463.
21 S. Ikeda and A. Okamoto, *Chem. Asian J*. 2008, **3**, 958–968.
22 S. Ikeda, H. Yanagisawa, A.Nakamura, D. O. Wang, M. Yuki and A. Okamoto *Org. Biomol. Chem*. 2011, **9**, 4199–4204.
23 S. Ikeda, T. Kubota, M. Yuki and A. Okamoto, *Angew. Chem. Int. Ed. Engl*. 2009, **48**, 6480–6484.
24 T. Kubota, S. Ikeda, H. Yanagisawa, M. Yuki and A. Okamoto, *PLOS ONE*. 2010, **5**, e13003.
25 D. O. Wang, H. Matsuno, S. Ikeda, A. Nakamura, H. Yanagisawa, Y. Hayashi and A. Okamoto, *RNA* 2012, **18**, 166–175.
26 I. Oomoto, A. Suzuki-Hirano, H. Umeshima, Y. W. Han, H. Yanagisawa, P. Carlton, Y. Harada, M. Kengaku, A. Okamoto, T. Shimogori and D. O. Wang, *Nucleic Acids Res*. 2015, **43**, e126.
27 A. Okamoto, *Chem. Soc. Rev*. 2011, **40**, 5815–5828.
28 D. O. Wang and A. Okamoto, *J. Photochem. Photobiol., C* 2012, **13**, 112–123.
29 J. E. Weigand, M. Sanchez, E. B. Gunnesch, S. Zeiher, R. Schroeder and B. Suess, *RNA* 2008, **14**, 89–97.
30 D. Moazed and H. F. Noller, *Nature* 1987, **327**, 389–394.
31 A. A. Bastian, A. Marcozzi and A. Herrmann, *Nat. Chem*. 2012, **4**, 789–793.
32 D. N. Wilson, *Nat. Rev. Microbiol*. 2014, **12**, 35–48.
33 W. A. Greenberg, E. S. Priestley, P. S. Sears, P. B. Alper, C. Rosenbohm, M. Hendrix, S. C. Hung and C. H. Wong, *J. Am. Chem. Soc*. 1999, **121**, 6527–6541.
34 S. Huang, X. Zhu and C. E. Melan ̧on, III. *ACS Chem. Biol*. 2016, **11**, 31–37.
35 J. L. McGinnis, Q. Liu, C. A. Lavender, A. Devaraj, S. P. McClory, K. Fredrick and K. M. Weeks, *Proc. Natl. Acad. Sci. USA*. 2015, **112**, 2425–2430 .
36 E. Duchardt-Ferner, J. E. Weigand, O. Ohlenschlager, S. R. Schmidtke, B. Suess and J. Wohnert, *Angew. Chem. Int. Ed. Engl*. 2010, **49**, 6216–6219.
37 J. A. Brown and Z. Suo, *Biochemistry* 2011, **50**, 1135–1142.
38 C. Foster and W. S. Champney, *Arch. Microbiol*. 2008, **189**, 441–449.
39 B. Llano-Sotelo, R. P. Hickerson, L. Lancaster, H. F. Noller and A. S. Mankin, *RNA* 2009, **15**, 1597–1604.

Chapter 3

ATP-sensitive Fluorescent Nucleic Acid Probes

3.1 Abstract

ATP is regarded as the molecular unit of currency for intracellular energy transfer. Many fundamental activities of life, including the glycolysis, protein transportation, Kreb's cycle and activation of ion channels, involve ATP for energy metabolism. Here I developed an aptamer-base ATP biosensor by the exciton-controlling approach. The thiazole orange dimer was covalently conjugate to the site 13 of ATP RNA aptamer that is proximal to the duplex fragment of ATP RNA aptamer after forming the ATP/aptamer complex. The intensity of fluorescence from such an ATP-sensing aptamer system increased several times in the presence of ATP. This probe displayed the specificity to ATP in contrast to UTP, GTP, CTP, ADP and AMP.

3.2 Introduction

Adenosine triphosphate (ATP) is the most active energy transporting biological molecule and exists in all organisms. The mitochondria in animals and the chloroplasts in plants are the main organelles producing ATPs via a couple of reactions. After generation, ATPs function as the energy currency to regulate basic cellular metabolism and biochemical reactions in living organisms[1-2]. ATP quickly and effectively provides energy via the active triphosphate at the end of ATP molecules and is circularly utilized in the cells. ATP molecules involve almost all important biological processes as energy currency in the assembly of large molecules (protein, lipid or nucleic acid) and ion transportation among different subcellular regions. Additionally, it plays crucial roles as electrical signals in the nervous systems and as chemical signal molecules in signal transduction[3-8].

As the importance of ATP in such many biological processes, many research groups focused on developing the tools for measuring ATP concentrations in vitro or in vivo. ATP-dependent bioluminescence method is the most sensitive in the developed approaches. In this process, light is emitted using ATP as a substrate of the reaction and thereby the light intensity directly correlates to the ATP concentration [9]. Although this method has shown its usefulness in the detection of ATP, it may provide false results since the bioluminescence reaction dramatically affect the physiological conditions. Another available fluorescent probes are ATP-sensitive chemical probes. A variety of such kinds of probes have been developed: pyrene, anthracene, acridone, xanthenes, coumarin, naphthalimide and other kind of probes[10-17]. However, other biomolecule responses are always concurrent and thus their biological applications are restrained. After ATP aptamers were reported[18-19], the interaction between aptamer and ATP has been systematically explored indicating that both the ribose and the bases involve the recognition of ATP and the interaction significantly changed conformation of the ATP aptamer[20]. The specificity and variable local environments have inspired the generation of fluorescent aptamer-based biosensor[21]. Yet, the unreasonable fluorescent control made that ATP detection very insensitive. Here I introduced another fluorescent controlling mechanism into ATP aptamers and the sensitivity of the fluorescent ATP aptamer was improved greatly.

3.3 Results and discussion

There have been several published three-dimensional structures of aptamers that bind ATP[22-23]. One of the ATP RNA aptamers, showing high affinity and specificity to the cognate ligand ATP, was chose for the design of "signaling aptamers"[21]. In their models, an acridine moiety was incorporated into residue 13 of the RNA aptamer that is adjacent to the binding pocket but does not participate in interactions with ATP and instead points outward into solution (Figure 3-1). Although avoiding blocking or disrupting interaction between aptamer and ATP, ligand-induced conformational changes in aptamer structure were monitored by the fluorescent intensity increase that can be explained by the ligand-induced local environment change. However, the sensitivity of acridine dyes to the ATP-induced aptamer structure is low and only 45 % fluorescent increase was showed upon the addition of ATP. After addition of ATP into the aptamer solution, stem duplexes were formed in the most part of RNA sequences (Figure 3-1a). Replacing acridine into aptamer using a more sensitive moiety to nucleic acid duplex may provide a more effective way to response ATP molecules. Exciton-controlled hybridization-sensitive fluorescent oligonucleotide (ECHO) probes[24-25] have been introduced in Chapter 1 and Chapter 2. The thiazole orange (TO) dimer in ECHO probes are generally quenched due to the exciton coupling effect and the fluorescence can be vastly restored when the probes hybridize with their complementary DNAs or RNAs. The concept of exciton controlling may also work in this ATP RNA aptamer. We rationally predicted that the two TO dyes will be in the H-aggregation state and show little fluorescence in the absence of ATP whereas the TO dyes will intercalate into the duplex structure and emit strong fluorescence in the presence of ATP after conjugating a homodimer of TO dyes in the site 13 of ATP RNA aptamer.

To get the ATP RNA aptamer containing TO homodimer, uridine phosphoramidites with two amino linkers via an acrylate group that have been obtained in Chapter 2 were used to substitute adenine in site 13 that was inferred no significant affect to ATP/aptamer interaction (Figure 3-2a). The modified uridine phosphoramidites were incorporated into ATP RNA aptamer using an automated DNA/RNA synthesizer. The synthesized ssRNAs were coupled with TO dyes by the postsynthetic process at basic condition similar as the process for DNA ECHO probe synthesis. Due to instability of RNA in basic condition, higher equivalent of carboxylate-activated TO dyes (200 equivalents) and shorter reaction time (1.5 h) were used during the reaction with diamino-modified RNA compared with DNA ECHO probe synthesis. The purified aptamers containing two TO dyes were confirmed pure by HPLC (Figure 3-2c) and identified by

MALDI-TOF MS (Figure 3-2b). The Tm value of modified ATP RNA aptamer is 74 ^{o}C.

(a)

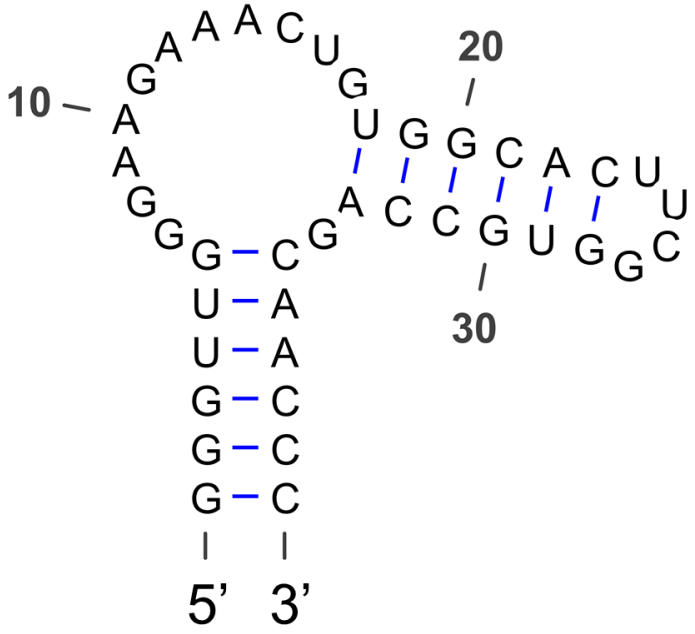

(b)

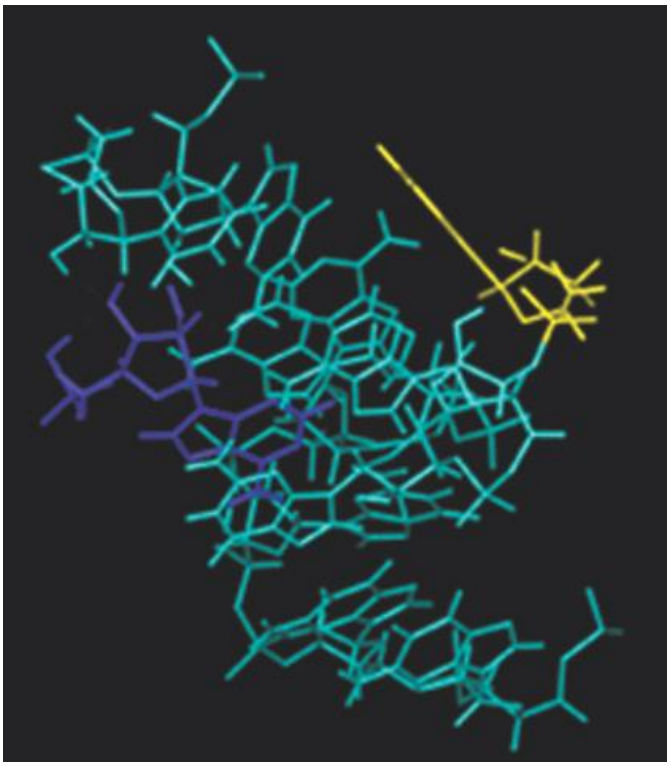

Figure 3-1. (a) Secondary structure of ATP RNA aptamer; (b) Three-dimensional models of ATP RNA aptamers (PDB 1AM0). Bound ATP is shown in purple and residue 13 is shown in yellow.

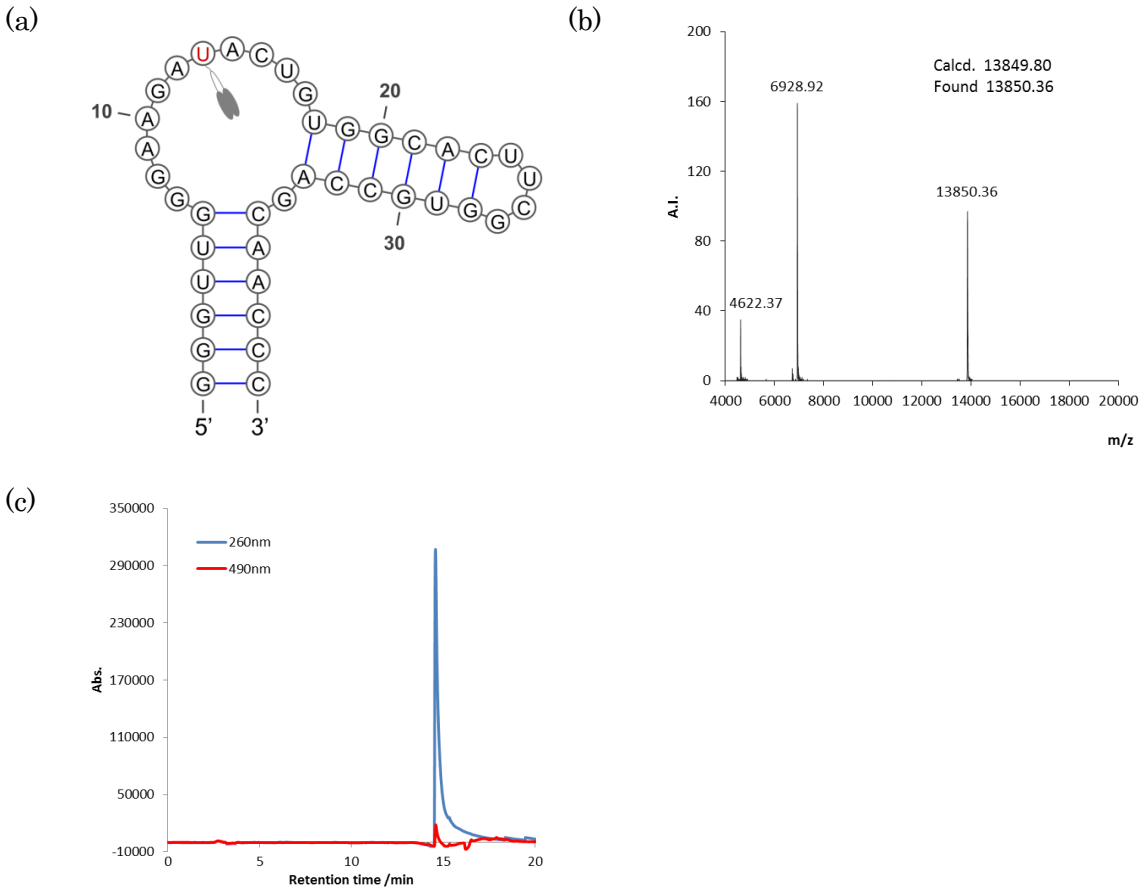

Figure 3-2. Exciton-controlled ATP-sensitive Fluorescent ATP RNA aptamer. (a) Ilustration of the doubly TO-labelled ATP RNA aptamer at site 13 (ATPamer-13); (b) MALDI-TOF mass spectrum showing desired mass value of modified aptamer. (c) HPLC chart of purified aptamer. Condition: gradient 10-30 % in 20min with flow rate of TEAA buffer 1 mL/min.

The absorption and emission properties of the synthesized ATP RNA aptamers, named as ATPatmer-13, were investigated after the addition of different concentration of ATP (Figure 3-3). Two absorption bands were observed for treated samples with the shorter one at nearly 480nm and the longer one at nearly 510 nm. In the sample without ATP addition, the absorption band with shorter wavelength showed more strongly. With the increased addition of ATP, the absorption band of ATPamer-13 with longer wavelength became dominating gradually. The fluorescent emission of these RNA probes were restrained in the ATP-free state, but the fluorescent intensity increased after ATP addition and exhibited a concentration-dependent fluorescence enhancement. As shown in the absorption spectra, two typical absorption bands at approximately 480nm and 510nm apparently shifted before and after addition of ATP. The absorption band with shorter wavelength is similar with the band observed at the monomeric TO while the absorption band with longer wavelength at the homodimeric TO that suggest TO intercalation into RNA duplex to disrupt dye H-aggregation might be the suppression mechanism. With the newly designed fluorescent ATP aptamer, a clear fluorescent response was displayed and a fluorescent variation ratio up to 2.6 times was observed when 1000 mM ATP was added. These obvious signal enhancement for TO homodimer-labeled aptamer (45 % for acridine-conjugated aptamer and 160 % for TO homodimer-labeled aptamer) illustrated that the exciton controlling approach is fit for aptamer based biosensors with high sensitivity.

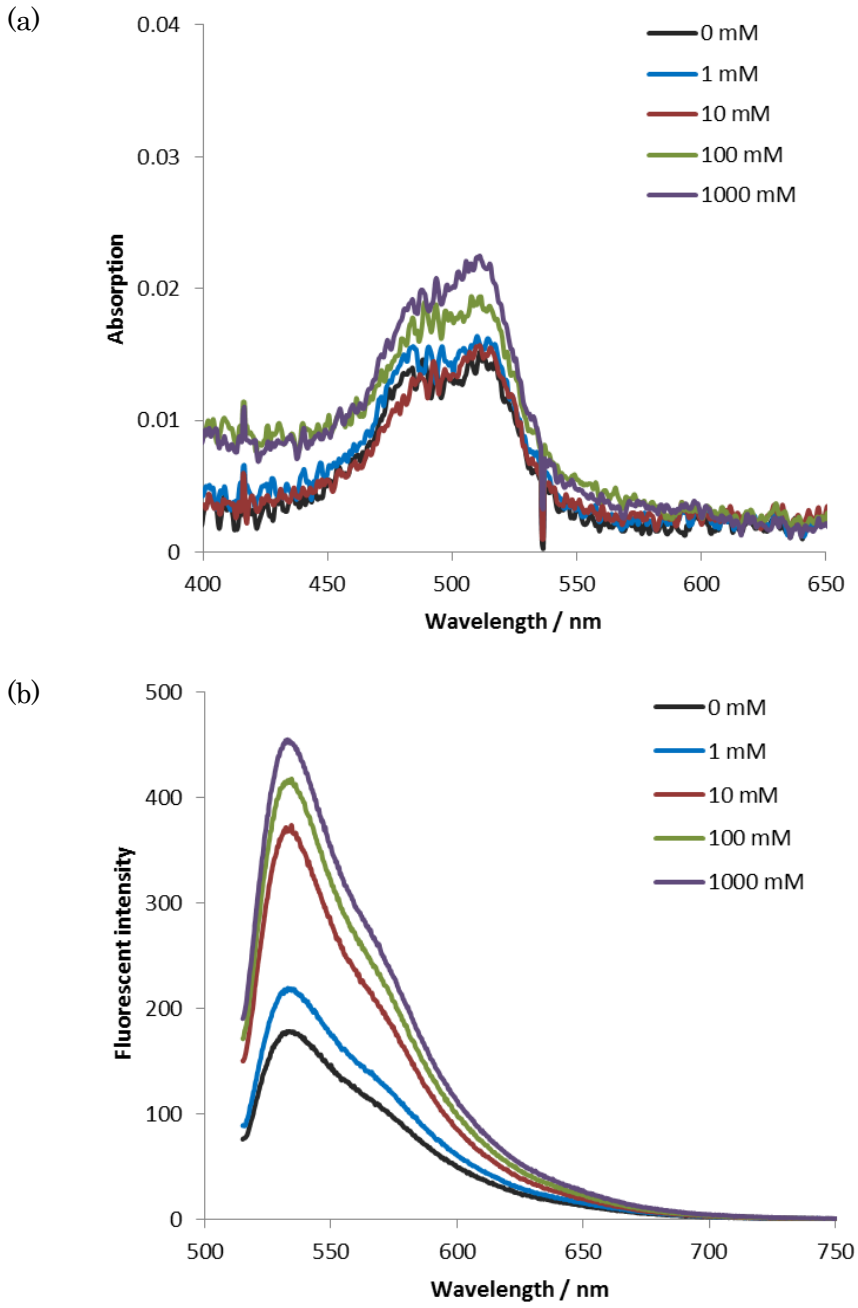

Figure 3-3. The absorption (a) and emission (b) spectra of ATPamer-13 in the presence of ATP with concentrations from 0 mM to 1000 mM. The spectra of ATPamer-13 (20 nM) were measured in buffer containing 300 mM NaCl, 20 mM Tris-HCl and 5 mM $MgCl_2$ (pH 7.6). Before measurement, the mixed solution was incubated at 65 ^{o}C for 3 min and then gradually decreased to room temperature. The emission spectra were measured with excitation at 510 nm and both of the excitation and emission bandwidths were 3.0 nm.

To assess the specificity of exciton-controlled ATPater-13 for ATP, changes in fluorescence were also measured in the presence of CTP, UTP, GTP, ADP and AMP. No significant increases in fluorescence for these molecules were observed (Figure 3-4). Thus, The ATP ligand-dependent fluorescent responsiveness suggested that the TO homodimer conjugation into site 13 of aptamer did not influence the specific recognition of ATP RNA aptamer to ATP.

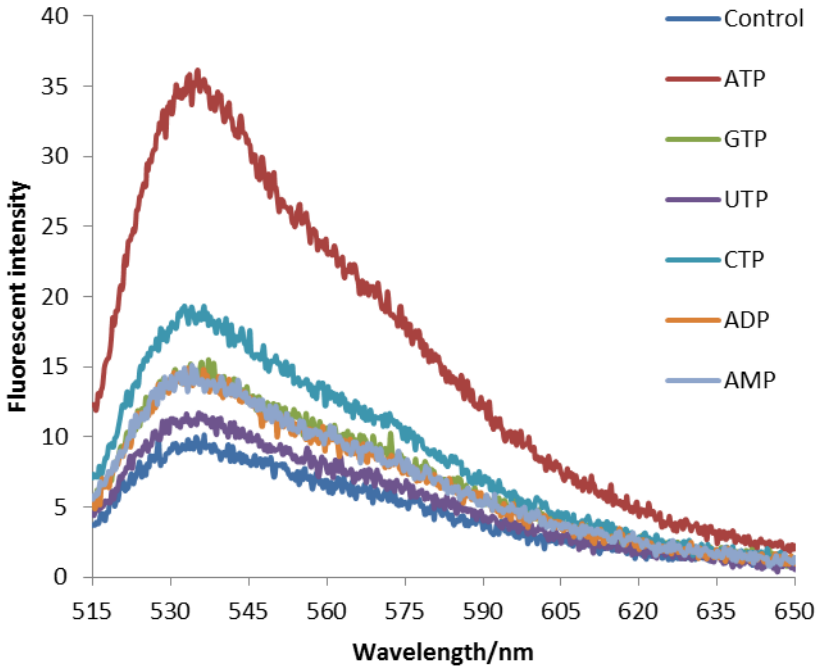

Figure 3-4. Specificites of exciton-controlled aptamer ATPamer-13 to ATP. The fluorescence spectra of ATPamer-13 (0.5 μM) were measured in the buffer containing 300 mM NaCl, 20 mM Tris-HCl and 5 mM $MgCl_2$ (pH 7.6) in the absence or presence of ATP, GTP, UTP, CTP, ADP and AMP (100 mM). Before measurement, the mixed solution was incubated at 65 ^{o}C for 3 min and then gradually decreased to room temperature. The emission spectra were measured with excitation at 510 nm and both of the excitation and emission bandwidths were 1.5 nm.

3.4 Conclusions

The doubly TO-labeled ATP RNA aptamer, ATPater-13, was designed and synthesized successfully based on the exciton coupling theory. ATPater-13 showed evidently ATP-dependent fluorescence increase and good specificity to ATP. These results indicate that introduction of exciton-controlled dyes into aptamers is a resultful way to detect ATP sensitively and specifically. Future orientation should aim at obtaining modified RNA aptamers resistant to RNases for ATP detection in live cells.

3.5 Experimental procedures

Probe synthesis: The probe was synthesized using a similar RNA probe synthesis method described in Chapter 2. Briefly, RNA oligomers were synthesized by a conventional phosphoramide method using a NTS H-8 DNA/RNA synthesizer using commercially available phosphoramidites from GlenResearch and the synthesized RNA oligomer was cleaved from the support with 28 % aqueous ammonia/40 % methylamine 1:1 (v/v) 20 min, and then oligos were deprotected at 65 ^{o}C for 5 min. After removal of the combined solution under reduced pressure to dryness, 2' silyl groups were removed with triethylamine trihydrofluoride at 65 ^{o}C for 2 h. After diluting with distilled water, RNA was purified by reversed-phase HPLC on a 5-ODS-H column (10 mm x 150 mm, elution with a solvent mixture of 0.1 M triethylamine acetate (TEAA), pH 7.0, linear gradient over 30 min from 5 % to 30 % acetonitrile at a flow rate of 3.0 mL/min). A solution of the succinimidyl ester of TO dye (100 eq. to an active amino group of RNA) in DMF was added to a solution of diamino-modified RNA in 100 mM sodium carbonate buffer (pH = 9.0), and incubated at 25 ^{o}C for 1.5 h. The reaction mixture was diluted with ethanol. After centrifuging at -20 ^{o}C for 20 min, the supernatant was removed. The residue was dissolved in a small volume of water and the solution was passed through a 0.45 um filter. The product was purified by reversed-phase HPLC on a 5-ODS-H column (10 mm x 150 mm, elution with a solvent mixture of 0.1 M TEAA, pH 7.0, linear gradient over 30 min from 5 % to 30 % acetonitrile at a flow rate of 3.0 mL/min). The concentration of the fluorescent RNA was determined at nanodrop 1000 spectrophotometer. The fluorescent RNA was identified by MALDI–TOF mass spectrometry.

Absorbance and fluorescence spectra measurements

Absorption and fluorescence spectra of the fluorescent probes were measured in the buffer containing 300 mM NaCl, 20 mM Tris-HCl and 5 mM $MgCl_2$ (pH 7.6) in the absence or presence of ATP, GTP, UTP, CTP, ADP and AMP using a cell with a 1 cm path length. Before measurement, the mixed solution was incubated at 65 ^{o}C for 3 min and then gradually decreased to room temperature. The emission spectra were measured with excitation at 510 nm.

3.6 References

1. Cook S.P., Vulchanova L., Hargreaves K.M., Elde R., McCleskey E.W., *Nature.* 1997, 387, 505-508
2. Khakh B.S., North R.A., *Nature*. 2006, **442**, 527-532.
3. Lowe J.E., Cummings R.G., Adams D.H., Hull-Ryde E.A., *Circulation.* 1983, **68**, 190-202.
4. Souslova V., Cesare P., Ding Y., Akopian A.N., Stanfa L., Suzuki R., Carpenter K., Dickenson A., Boyce S., Hill R., Nebenuis-Oosthuizen D., Smith A.J., Kidd E.J., Wood J.N., *Nature.* 2000, **407**, 1015-1017.
5. Gourine A.V., Kasymov V., Marina N., Tang F., Figueiredo M.F., Lane S., Teschemacher A.G., Spyer K.M., Deisseroth K., Kasparov S.. *Science*. 2010, **329**, 571-575.
6. Vlaskovska M., Kasakov L., Rong W., Bodin P., Bardini M., Cockayne D.A., Ford A.P., Burnstock G., *J. Neurosci.* 2001, **21**, 5670-5677.
7. Nurse C.A., *J. Physiol*. 2014, **592**, 3419-3426.
8. Finger T.E., Danilova V., Barrows J., Bartel D.L., Vigers A.J., Stone L., Hellekant G., Kinnamon S.C., *Science.* 2005, **310**, 1495-1499.
9. Leach F.R., *J. Appl. Biochem.* 1981, **3**, 473-517.
10. Xu Z., Singh N.J., Lim J., Pan J., Kim H.N., Park S., Kim K.S., Yoon J., *J. Am. Chem. Soc.* 2009, **131**, 15528-15533.
11. Ojida A., Takashima I., Kohira T., Nonaka H., Hamachi I., *J. Am. Chem. Soc.* 2008, **130**, 12095-12101.
12. Neelakandan P.P., Hariharan M., Ramaiah D., *Org. Lett.* 2005, **7**, 5765-5768.
13. Ojida A., Miyahara Y., Wongkongkatep J., Tamaru S., Sada K., Hamachi I., *Chem. Asian. J.* 2006, **1**, 555-563.
14. Kim H.N., Moon J.H., Kim S.K., Kwon J.Y., Jang Y.J., Lee J.Y., Yoon J., *J. Org. Chem.* 2011, **76**, 3805-3811.
15. Kurishita Y., Kohira T., Ojida A., Hamachi I., *J. Am. Chem. Soc.* 2010, **132**, 13290-13299.
16. Kaur J., Singh P., *Chem. Commun. (Camb).* 2011, **47**, 4472-4474.
17. Moro A.J., Cywinski P.J., Körsten S., Mohr G.J., *Chem. Commun. (Camb).* 2010, **46**, 1085-1087.
18. Sassanfar M., Szostak J.W., *Nature.* 1993, **364**, 550-553.
19. Huizenga D.E., Szostak J.W., *Biochemistry.* 1995, **34**, 656-665.
20. Lin C.H., Patei D.J., *Chem. Biol.* 1997, **4**, 817-832.

21. Sulay D.J., Romy K., Rick C., Emily J.M., Michael B., Robert T.K., Gary G., Andrew D.E., *J. Am. Chem. Soc.* 2000, **122**, 2469-2473
22. Lin C. H., Patel D. J., *Chem. Biol.* 1997, **4**, 817-832.
23. Jiang F., Kumar R. A., Jones R. A., Patel D. J., *Nature.* 1996, **382**, 183-186.
24. Ikeda S., Okamoto A., *Chem. Asian J.* 2008, **3**, 958-968.
25. Ikeda S., Kubota T., Yuki M., Okamoto A., *Angew. Chem., Int. Ed.* 2009, **48**, 6480-6484.

Chapter 4

Novel Exciton-controlled Hybridization-Sensitive Fluorescent Probes for Two-photon Imaging of Nucleic Acid

4.1 Abstract

Exciton-controlled hybridization-sensitive fluorescent oligonucleotide (ECHO) probe is a powerful nucleic acid detection tool used in real time PCR, point of care testing (POCT), fluorescent in situ hybridization (FISH), live cell imaging and tissue slice imaging. Although widely used, applications of ECHO probes are limited in tubes and single cells. Here we developed a novel two-photon-excited ECHO probe. Nine kinds of candidates of two-photon-excited ECHO probes were synthesized successfully and exhibited good hybridization-based fluorescent turn-on properties towards complementary DNAs or RNAs. Importantly, the probes conjugated with indole-based dyes showed excellent target RNA response that are highly improved compared with previous developed ECHO probes. Live cell imaging experiments demonstrated that three types of newly designed probes are suitable for RNA two-photon imaging when excited at 1030 nm and one probe was successfully used for two-photon RNA imaging in mouse embryo brain. These probes are also applicable for DNA FISH imaging in fixed cells or tissue slices in a simple way without stringent washing step. Our new fluorescence controllable probes provided the potential for RNA imaging *in vivo* and tools for understanding the RNA spatial regulation.

4.2 Introduction

Nucleic acids, DNAs and RNAs, are basic genetic materials in organisms. The spatial organization of DNAs and the dynamic interactions between DNAs and proteins or RNAs regulate the genetic functional output. For example, the subnuclear positioning of genomic elements can modulate gene expression, heterochromatin formation, and DNA replication[1-2]. Intracellular RNAs are dynamically regulated that are related to many biological processes, such as chromosomal structural and functional regulation, mRNA generation and editing and protein translation[3-8]. Consequently, exploring the spatiotemporal regulation of intracellular DNAs or RNAs is rather crucial to understand the dynamics in versatile physiological contexts and detailedly verify the relationship between nucleic acid distribution and the physiological performance.

Generally the localizations of many DNAs or RNAs in specific subcellular regions have been studied by immunostaining, fluorescent in situ hybridization or artificial tagging methods[9-10]. To visualize specific genomic loci in live cells, fluorescently tagged DNA-binding proteins are mostly used[11-13]. Two types of improved RNA imaging methods have been recently developed to image the dynamic transportation of single mRNA molecules in vivo using a mouse model[14-15]. To visualize the dynamics of endogenous RNA in living cells and provide more information about life, many methods for RNA imaging have been designed, such as molecular beacons, MS2-GFP fusion proteins, GFP reconstitution, quenched autoligation probes, and dye-binding aptamers[16-21]. These approaches are greatly advantageous due to the native physiological environment for observing the endogenous nucleic acids. However, none of these methods have been applied to studying the nucleic acid dynamics in vivo or in tissues.

Given various problems of developed methods, such as the low availability, limitations in sequence design, slow response in terms of reactivity or conformation change, high background fluorescence, or low fluorescence reversibility, a new kind of fluorescent controllable probes, called exciton-controlled hybridization-sensitive fluorescent oligonucleotide (ECHO) probes, have been developed for effective in vivo RNA

imaging[22]. Despite of these advantages, ECHO-liveFISH is only suitable for the thin tissue sections due to the limited permeability of visible light and does not meet the requirement to monitor the extracellular autonomous functions[23-24] and signal transformation between long neurons[25]. Two-photon-excited fluorescence microscopy (TPM) has advantages over conventional one-photon-excited techniques such as lower photo-damage, reduced photo-bleaching and higher detection sensitivity[26-31]. Also decreased cell damaging can be obtained due to the longer wavelength excitation light in TPM[32]. This technique also reduces out-of-focus irradiations[33-34]. Therefore, here we developed a series of novel two-photon-excited hybridization-sensitive fluorescent oligonucleotide probes. These probes showed dual photophysical functions: hybridization-sensitive fluorescent turn-on and two-photon-excited fluorescence emission. Three newly designed probes have been two-photon-excited for RNA visualization in live Hela cells.

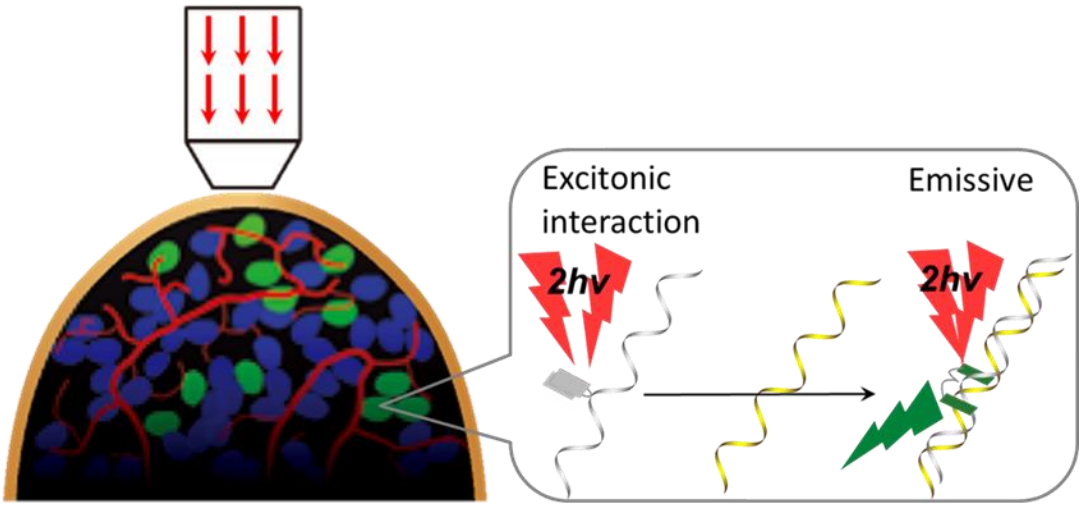

Figure 4-1. Illustration of RNA visualization in tissue by two-photon-excited hybridization-sensitive fluorescent probes

4.3 Results and discussion

Molecular design

The ECHO probe is a doubly thiazole orange-labeled probe to achieve high fluorescence intensity for a hybrid with the target DNA or RNA, and effective quenching for a single-strand state of the probe[35-37]. Emission from the probe was controlled by excitonic interaction of dyes. The clear change in fluorescence intensity depending on hybridization is useful for visible RNA analysis in cells and tissue slices[19]. To develop two-photon-excited hybridization-sensitive probes for visualizing RNA in deep tissues, we focused on two kinds of cyanine dyes: styryl cyanine dyes and indole-based dyes. Styryl cyanine dyes and indole-based dyes have been widely used for two-photon nucleic acid imaging and exhibited perfect two-photon absorption ability[37-38]. On the other hand, some derivatives of these dyes have been effectively quenched through excitonic interaction[39-40]. Therefore, we rationally predicted the styryl cyanine dyes and indole-based cyanine dyes may be two-photon-excited while maintain their exciton interaction when these dyes are doubly labelled to oligonucleotides (Figure 4-1). We designed a series of new fluorescent cyanine units that may possess dual functions. Styryl cyanine dyes $\mathbf{D_{539}}$, $\mathbf{D_{570}}$, $\mathbf{D_{590}}$ and $\mathbf{D_{600}}$ were synthesized in our lab's previous work[37]. Indole-based cyanine dyes **T1**, **T2**, **T3**, **T4** and **T5** were compounds having an indole subunit as a core with a carboxylate-terminated alkyl linker (Scheme 4-1 and Scheme 4-2) and synthesized successfully. The carboxylate end of the alkyl linker of the dyes was activated by succinimidylation, and two molecules of the activated dye were subsequently incorporated into an oligodeoxyribonucleotide (ODN) containing 2'-deoxyuridine with two amino ends[32].

Hybridization–based fluorescent control

The absorption and emission of the ODN strands doubly labeled with nine different dyes, 5'-d(TTTTTT**D**TTTTTT)-3' (where doubly fluorescent dye labeled nucleotides are shown as **D**), were investigated before and after hybridization with the complementary DNA strands (Figure 4-2 and Table 4-1). Fluorescence emission was observed immediately after the addition of the labelled ODN to a solution of the complementary nucleic acid. The emission was suppressed in the nonhybridized state. The source of the fluorescence behaviour

was confirmed by the absorption spectra. The absorption band of the nonhybridized probe appears at a shorter wavelength than that of the hybrid. This blue shift suggested the splitting of the excited state because of H aggregation of the dyes[35]. H aggregation allowed only transitions to the upper excitonic level. The excited state was rapidly transferred to the lower level, but the path from this energy level to the ground state was not emissive. The fluorescence from the fluorescent ODNs was suppressed by an excitonic interaction of dyes in the nonhybridized state. Hybridization with the target nucleic acid resulted in a great enhancement of emission with dissociation of the aggregate. This exciton-controlled fluorescence behavior was also observed for doubly labeled ODNs with other unrepeated sequences (Figure 4-3 and Table 4-2).

Control of fluorescence emission by an excitonic interaction was also evident when the target was RNA (Figure 4-4, Figure 4-5, Table 4-1 and Table 4-2). Several versatile dye-labeled nucleotides exhibited a shift of the absorption bands and the switching of fluorescence intensity upon hybridization with the complementary RNA strands. However, inefficient exciton control was observed in some nucleotides with styryl cyanine dyes. The nucleic acid duplex-binding ability of styryl cyanine dyes is known to be inherently lower than that of thiazole orange dyes[37]. The small shift in the absorption band suggests that the dissociation of the dye aggregate is inefficient in the hybrid with RNA, and that it is difficult for the dyes to bind independently to the hybrid structure. Otherwise, the marked red shift of absorption maxima of oligonucleotides labeled with indole-based dyes was observed in the hybridized state in contrast to that in the nonhybridized state and can be explained by the superior RNA sensitivities of indole-based dyes[38], which is robustly contributed to the dissociation of H-aggregation of dyes. For this reason, the ratio of the fluorescence intensity of the hybrid to that of the unhybridized strands in these nucleotides was divergent due to the different controllable excitonic interactions and could inspire us for much better rational designs of fluorescence controllable probes.

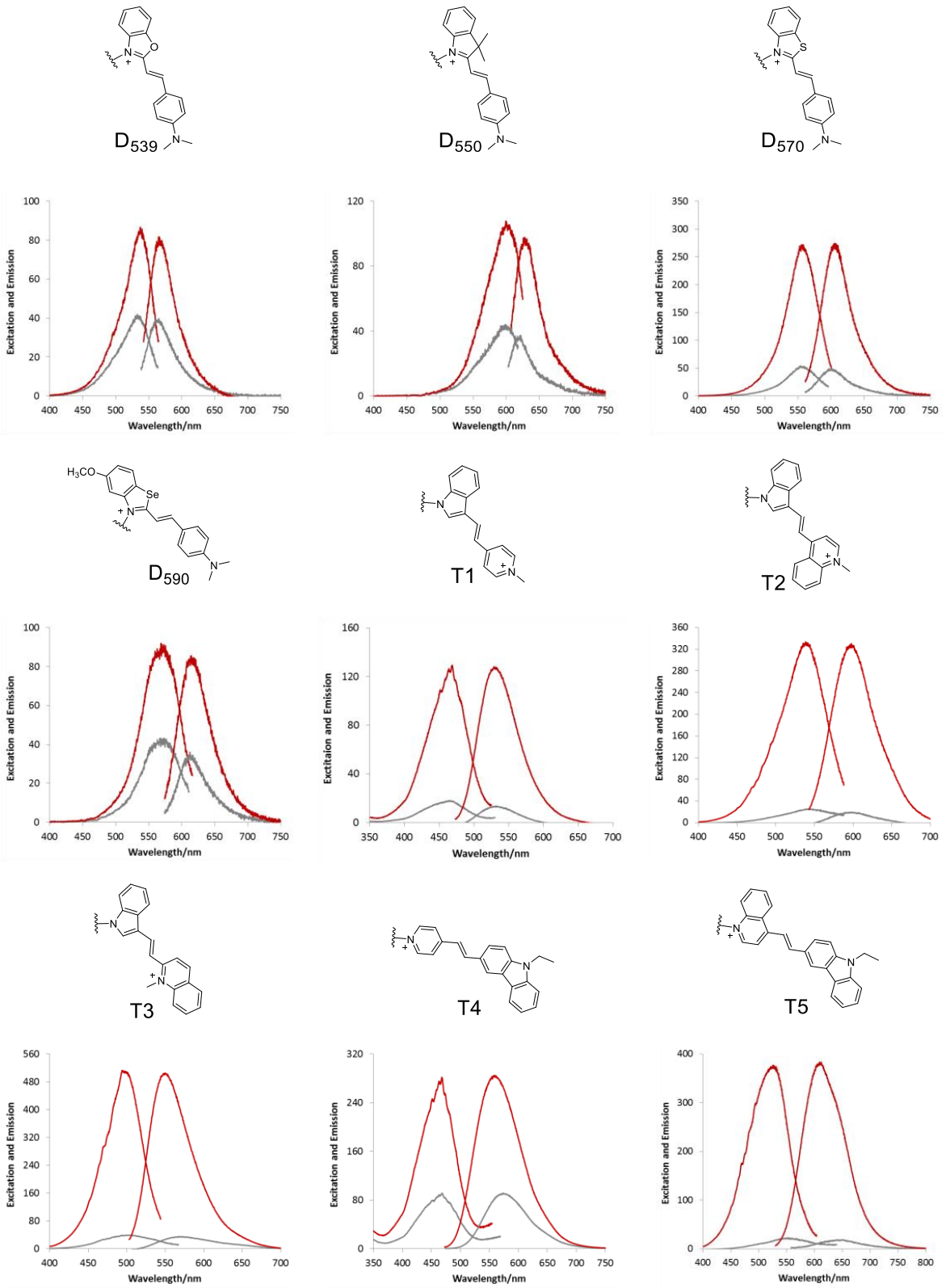

Figure 4-2. Excitation and emission of excitonic-interaction-controlled fluorescent probes before and after hybridization with the complementary DNA. Excitation (shorter wavelength) and emission (longer wavelength) spectra are indicated by grey and red lines for the nonhybridized probe and the hybrid, respectively. The following nucleic acid sequences were used: 5'-d(TTTTTT**D**TTTTT)-3'/5'-d(AAAAAAAAAAAAA)-3'. **D** means the fluorescent modified deoxyuridine. Photophysical data are given in Table 1.

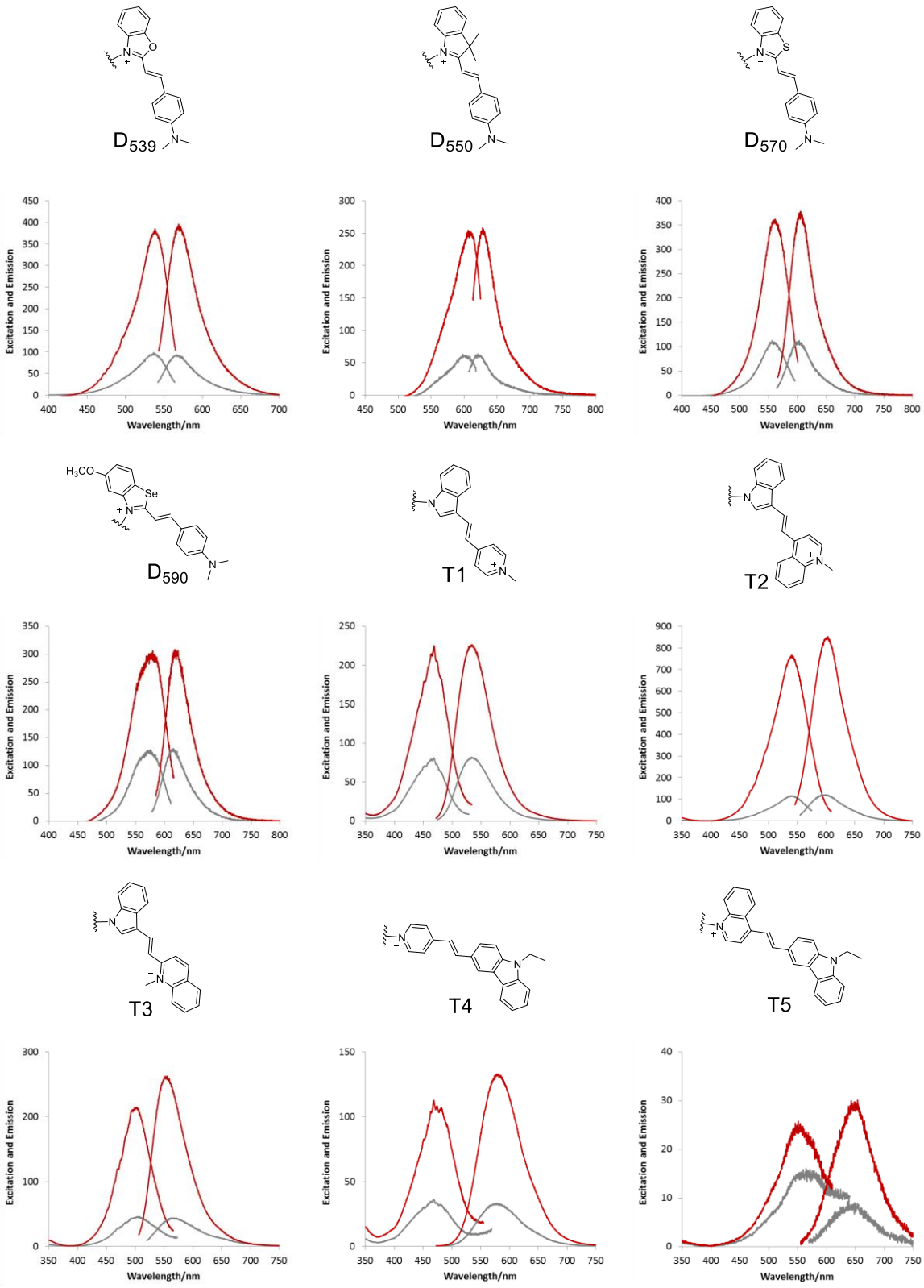

Figure 4-3. Excitation and emission of excitonic-interaction-controlled fluorescent probes before and after hybridization with the complementary DNA. Excitation (shorter wavelength) and emission (longer wavelength) spectra are indicated by grey and red lines for the nonhybridized probe and the hybrid, respectively. The following nucleic acid sequences were used: 5'-d(TACCAG**D**CACCAT)-3'/5'-d(ATGGTGACTGGTA)-3'. **D** means the fluorescent modified deoxyuridine. Photophysical data are given in Table 2.

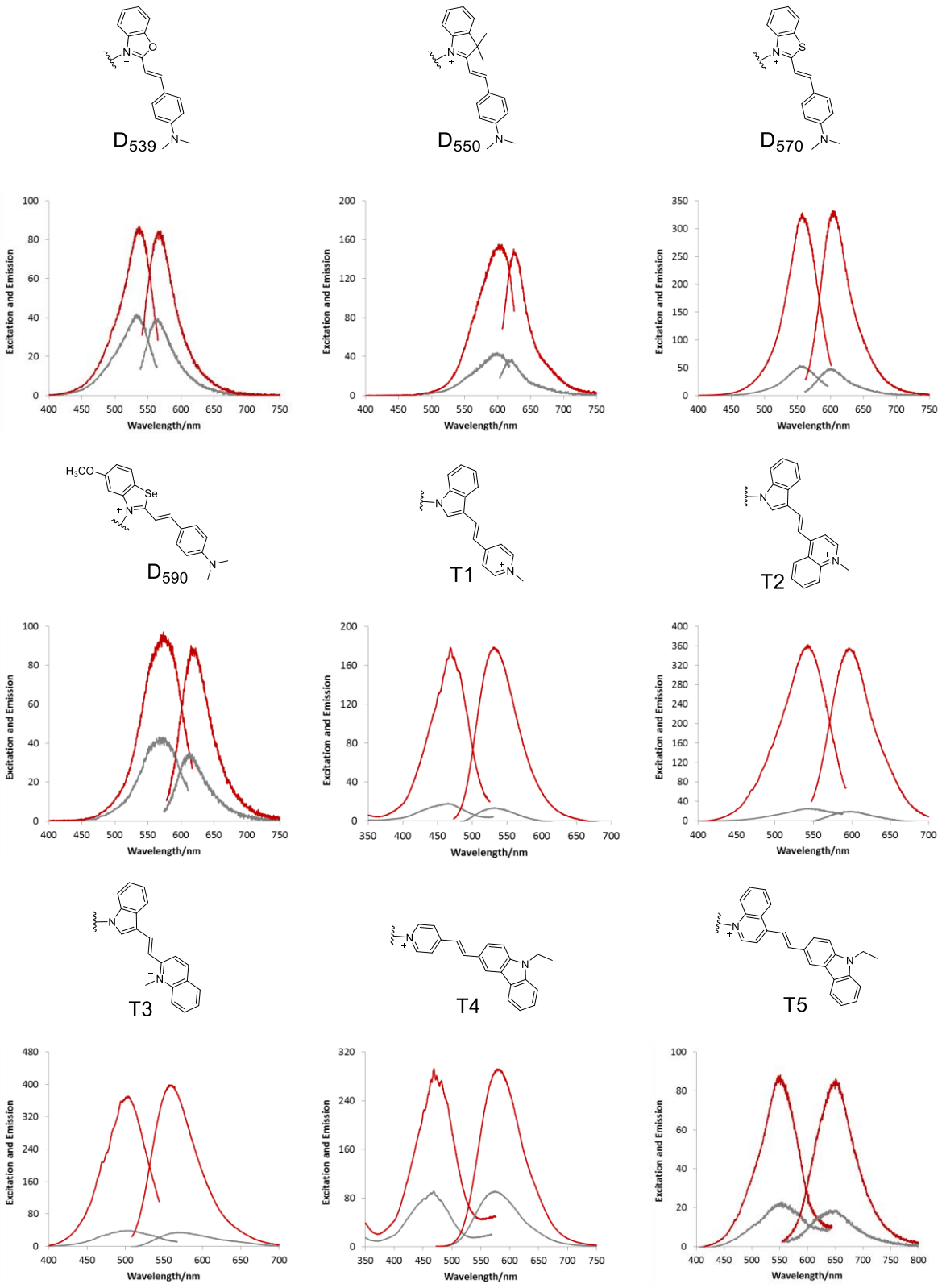

Figure 4-4. Excitation and emission of excitonic-interaction-controlled fluorescent probes before and after hybridization with the complementary RNA. Excitation (shorter wavelength) and emission (longer wavelength) spectra are indicated by grey and red lines for the nonhybridized probe and the hybrid, respectively. The following nucleic acid sequences were used: 5'-d(TTTTTT**D**TTTTT)-3'/5'-r(AAAAAAAAAAAAA)-3'. **D** means the fluorescent modified deoxyuridine. Photophysical data are given in Table 1.

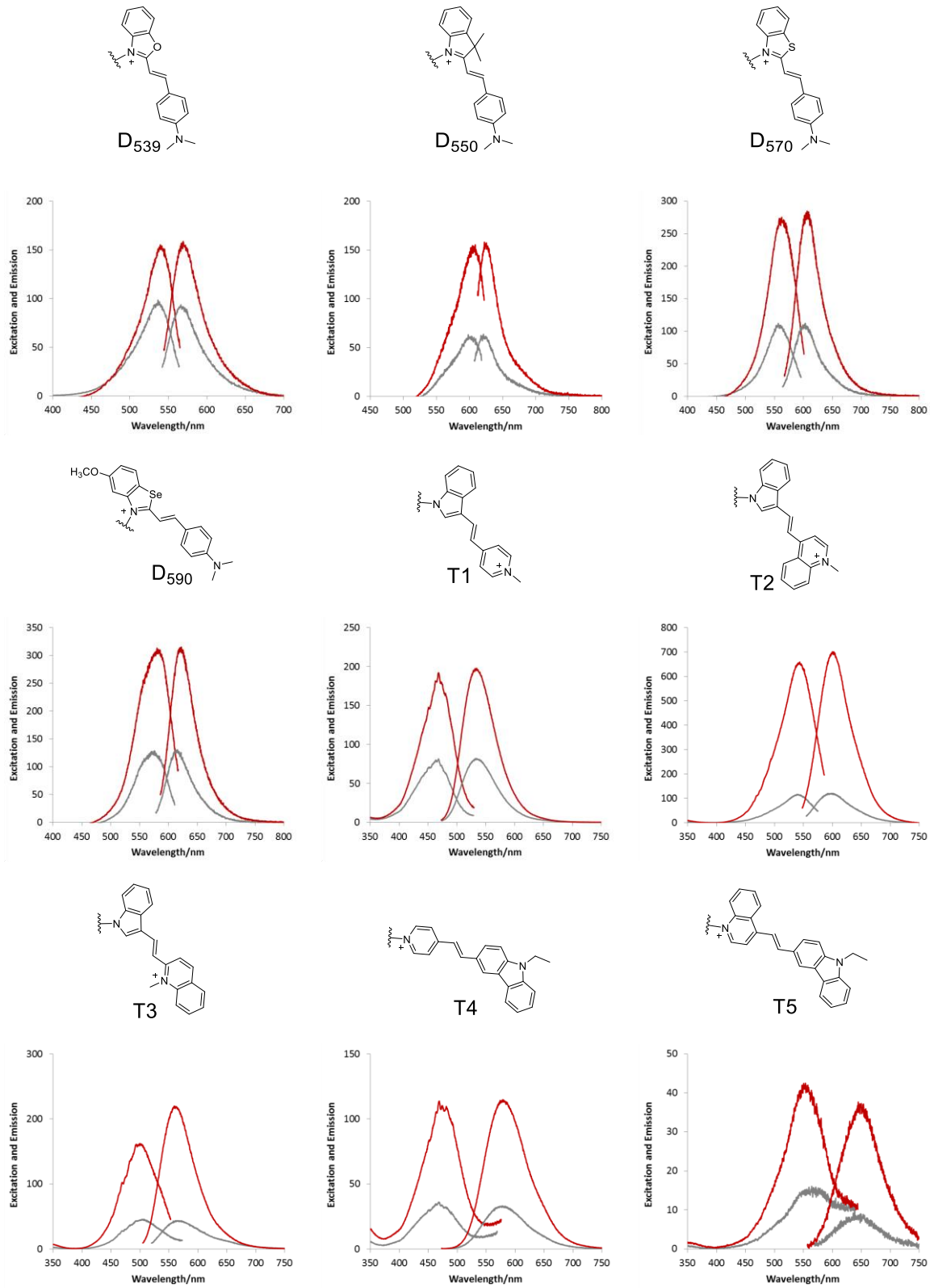

Figure 4-5. Excitation and emission of excitonic-interaction-controlled fluorescent probes before and after hybridization with the complementary RNA. Excitation (shorter wavelength) and emission (longer wavelength) spectra are indicated by grey and red lines for the nonhybridized probe and the hybrid, respectively. The following nucleic acid sequences were used: 5'-d(TACCAG**D**CACCAT)-3'/5'-r(ATGGTGACTGGTA)-3'. **D** means the fluorescent modified deoxyuridine. Photophysical data are given in Table 2.

However, among the nine nucleotides considered, the ODNs containing **T3**, **T4** or **T5** showed relatively strong blue shift in the hybridization duplex of the probe and their complementary DNA in their excitation and emission spectra, although excellent hybridization based fluorescent increase could also observed. The phenomenon was properly contradictory with other dye-conjugated ODNs and difficult to be explained in term of exciton coupling theory. The pull-push structure in cyanine dyes indicates that these dyes may be sensitive to the local environment of nucleic acid duplex. Therefore, the excitation and emission spectra of dye T5', a derivative of **T5**, were measured at various water/glycerol mixtures (Figure 4-6). The enhancement of excitation intensity and the blue shift of excitation maxima were observed with the increase of glycerol proportion in the mixture; that is, this dye emits a strong fluorescence and excited at a shorter wavelength in a high viscosity state, whereas the fluorescence of the dye is weaker and excitation peak appears at a longer wavelength in a relatively low viscosity state. This behaviour is controlled by the restriction of rotation around the conjugated chain linking between the two heterocyclic systems of cyanine dyes. In the case of ODNs with **T3**, **T4** and **T5**, the blue-shifted absorption and emission spectra suggested the existence of dye intercalation into the formed DNA duplex. On the contrary, the blue shifts were not found when these ODN probes hybridized with complementary RNAs indicating that these dyes may interact with DNA/RNA duplex through other mechanisms, for example, groove binding. This hypothesis was further confirmed by the circular dichroism (CD) data of ODN probes hybridized with complementary DNAs or RNAs (Figure 4-7). In these CD spectra, the induced CD peaks in the range of 450 to 550 nm that are characteristic signals of intercalation were only observable when ODNs with **T3**, **T4** and **T5** hybridized with complementary DNAs other than RNAs. This result suggested that the dyes of **T3**, **T4** and **T5** nucleotide were controlled simultaneously by two distinct mechanisms: exciton coupling and the restriction of rotation.

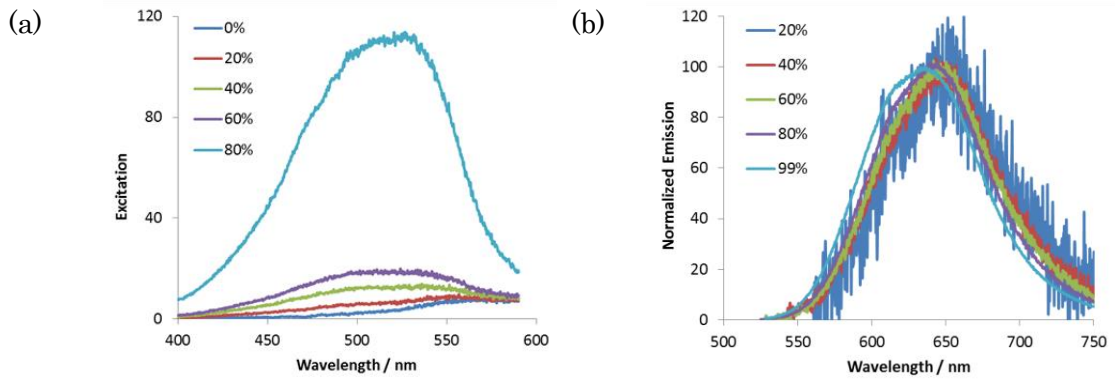

Figure 4-6. Excitaiton and emission spectra of T5' in the water/glycerol mixtures. (a) Excitaiton spectra of T5' in the water/glycerol mixture; (b) Emission spectra of T5' in the water/glycerol mixture. The fluorescent emissions in different mixtures were normalized to have maximum fluorescent emission 100. Labels in the figures mean the percentage of glycerol.

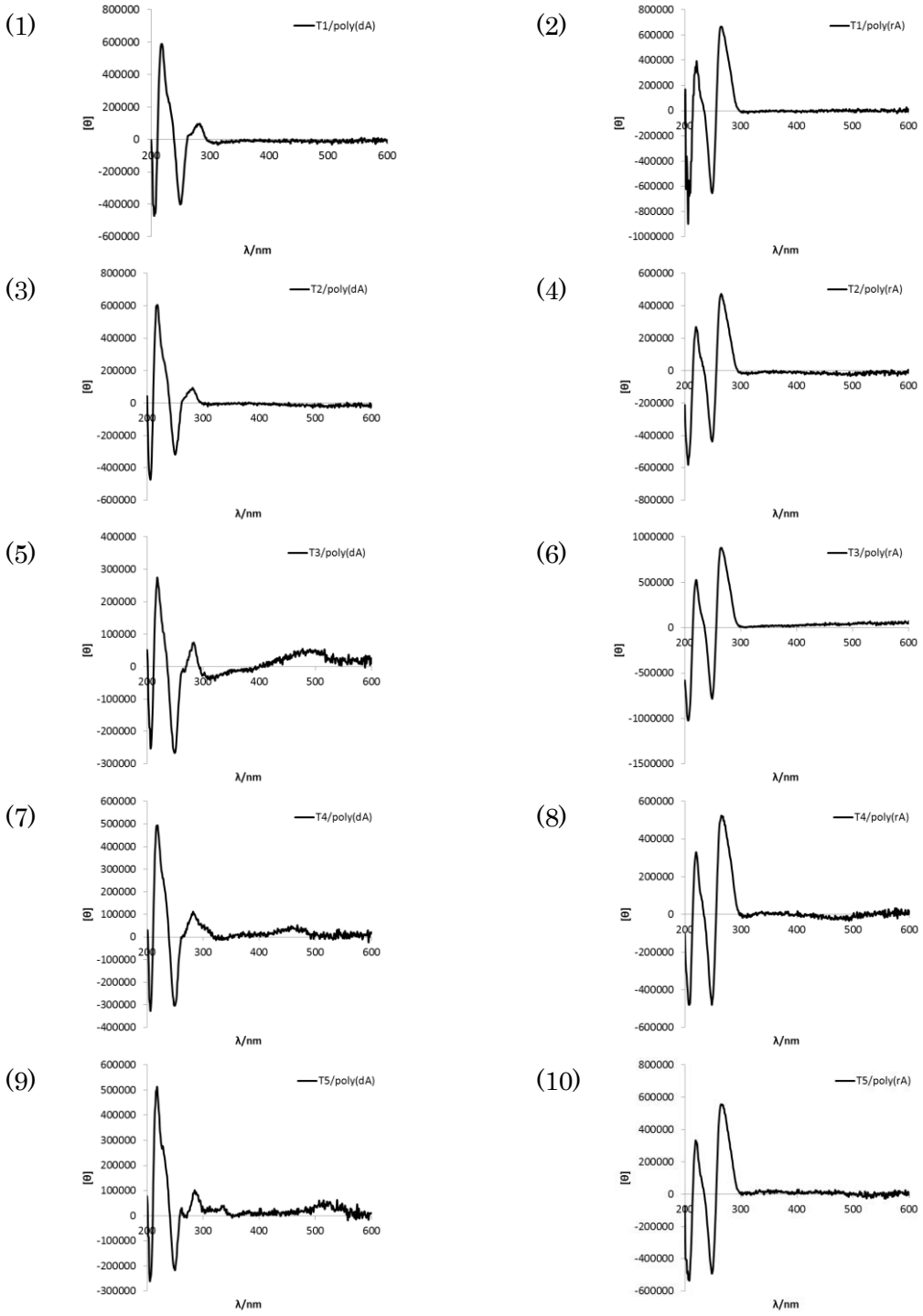

Figure 4-7. Circular dichroism spectra of excitonic-interaction-controlled fluorescent probes after hybridization with the complementary DNA or RNA. The following probe sequences were used: 5'-d(TTTTTT**D**TTTTT)-3'. **D** means the fluorescent modified deoxyuridine.

The doubly dye-labeled ODN probes achieved high fluorescence intensity for a hybrid with the target DNA or RNA, and effective quenching for a single-strand state of the probe. However, the probes have a 2'-deoxyribose backbone and will therefore be unstable under conditions where nucleases are present. For the long-term observation of target RNA in living cells and tissues, the new kind of probes with a 2'-OMe RNA structures were introduced. However, the maintaining of the hybridization-sensitive fluorescent on-off property should also be carefully assessed. We synthesized the newly hybridization-sensitive probes with a 2'-O-methylribose backbone. Next we measured the absorption, excitation, and emission spectra of 2'-OMe RNA probes before and after hybridization with the complementary DNA or RNA strands (Figure 4-8, Figure 4-9 and Table 4-3). Absorption spectra of the 2'-OMe RNA probes showed the red-shift of maximum peaks after hybridization. The strong emission of the hybrid of the 2'-OMe RNA probe and DNA was at similar level to that of DNA probes. Interestingly, the 2'-OMe RNA probes displayed a much better fluorescence ratio when hybridized with the complementary RNA compared to corresponding DNA probes. This should be attributed to the more tight binding ability of 2'-OMe RNA to complementary RNA sequences than analogous DNA oligomers[41-42]. Consequently, the modification of the sugar moiety from a hydrogen atom to a methoxy group did not inhibit fluorescence control by the excitonic interaction of dyes in a probe and had a better fluorescent control for RNA imaging.

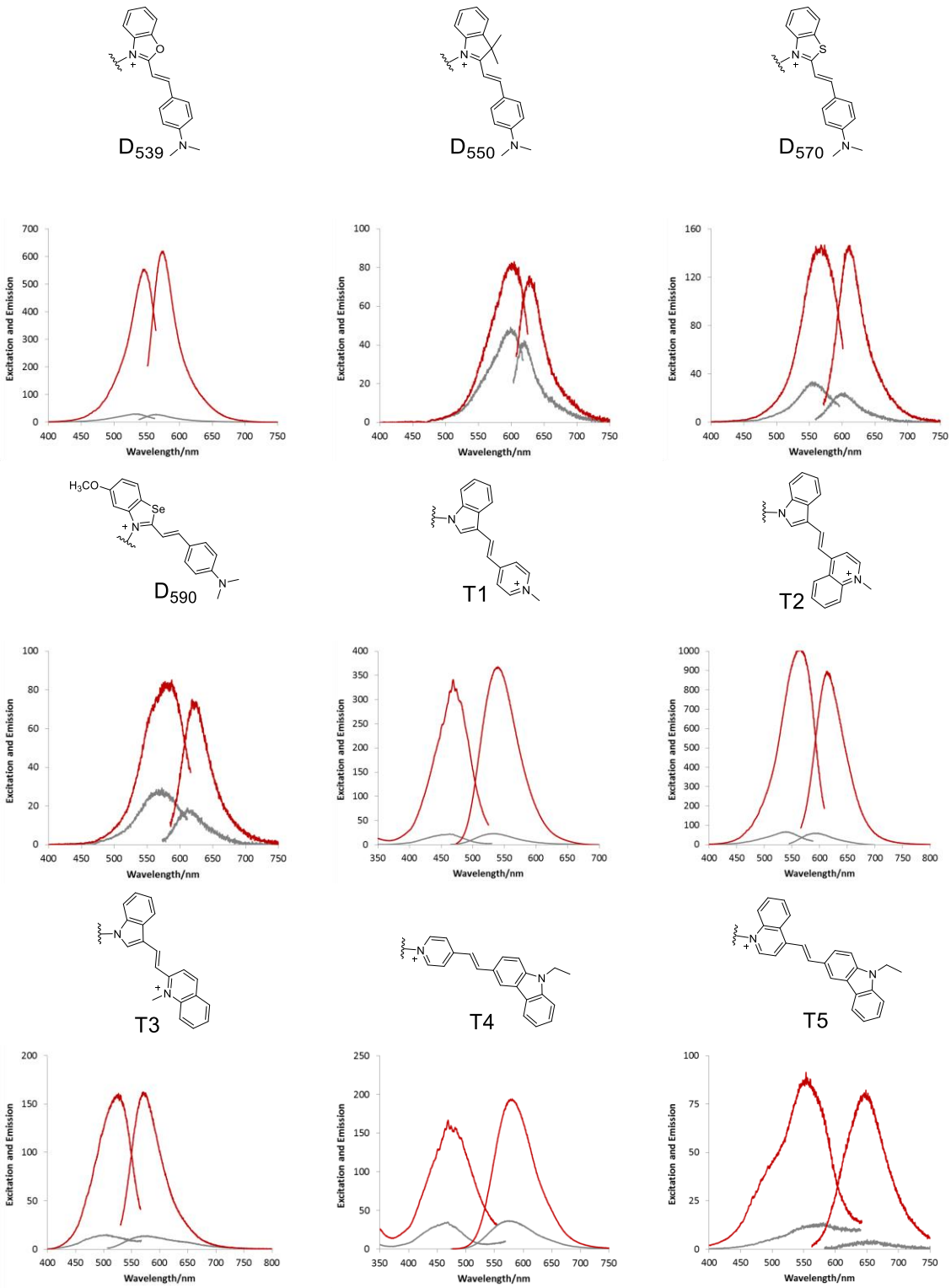

Figure 4-8. Excitation and emission of excitonic-interaction-controlled fluorescent probes before and after hybridization with the complementary DNA. Excitation (shorter wavelength) and emission (longer wavelength) spectra are indicated by grey and red lines for the nonhybridized probe and the hybrid, respectively. The following nucleic acid sequences were used: 5'-mUmUmUmUmUmU**D**mUmUmUmUmUmU-3'/5'-d(AAAAAAAAAAAAA)-3'. **D** means the fluorescent modified deoxyuridine and mU strands for 2'-OMe-Uridine. Photophysical data are given in Table 3.

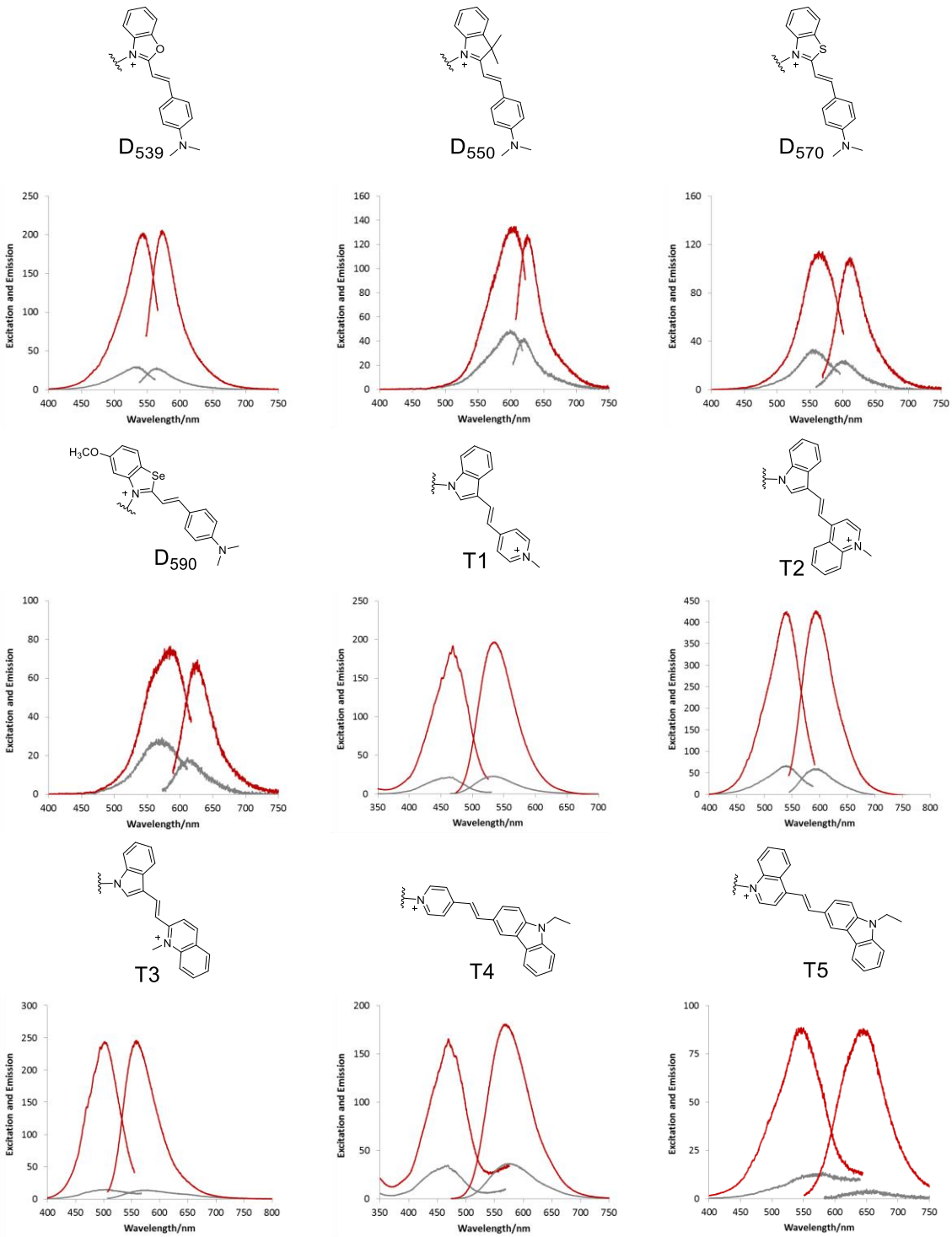

Figure 4-9. Excitation and emission of excitonic-interaction-controlled fluorescent probes before and after hybridization with the complementary RNA. Excitation (shorter wavelength) and emission (longer wavelength) spectra are indicated by grey and red lines for the nonhybridized probe and the hybrid, respectively. The following nucleic acid sequences were used: 5'-mUmUmUmUmUmU**D**mUmUmUmUmUmU-3'/5'-r(AAAAAAAAAAAAA)-3'. **D** means the fluorescent modified deoxyuridine and mU strands for 2'-OMe-Uridine. Photophysical data are given in Table 3.

Table 4-1. Photophysical data of 5'-d(TTTTTT**D**TTTTTT)-3' and hybrids with the complementary DNAs or RNAs. **D** means the fluorescent modified deoxyuridine.

Dyes	Hybridization state	λ_{abs} /nm (ε)	λ_{em} /nm (λ_{ex} /nm)	Φ	$I_{hybrid}/I_{nonhybrid}$ (λ nm)
	nonhybrid	513 (12000)	563 (533)	0.49	–
D_{539}	hybrid with DNA	512 (14000)	566 (537)	0.75	2.1 (566)
	hybrid with RNA	514 (19000)	567 (536)	0.58	2.2 (567)
	nonhybrid	504 (73000)	600 (556)	0.25	–
D_{570}	hybrid with DNA	549 (67000)	606 (556)	0.72	6.1 (606)
	hybrid with RNA	549 (65000)	604 (557)	0.89	7.1 (604)
	nonhybrid	533 (22000)	613 (569)	0.26	–
D_{590}	hybrid with DNA	563 (20000)	615 (569)	0.63	2.6 (615)
	hybrid with RNA	562 (20000)	618 (573)	0.63	2.7 (618)
	nonhybrid	555 (130000)	609 (548)	0.065	–
D_{550}	hybrid with DNA	557 (98000)	607 (552)	0.13	3.2 (627)
	hybrid with RNA	560 (100000)	605 (552)	0.20	4.6 (625)
	nonhybrid	442 (33000)	535 (463)	0.014	–
T1	hybrid with DNA	451(34000)	530 (468)	0.18	9.6 (530)
	hybrid with RNA	455 (33000)	530 (468)	0.23	13.5 (530)
	nonhybrid	495 (57000)	593 (542)	0.034	–
T2	hybrid with DNA	514 (58000)	597 (538)	0.51	17.7 (597)
	hybrid with RNA	516 (66000)	596 (542)	0.50	19.0 (596)
	nonhybrid	476 (83000)	572 (502)	0.033	–
T3	hybrid with DNA	492 (75000)	549 (498)	0.33	19.4 (549)
	hybrid with RNA	493 (86000)	558 (503)	0.24	12.8 (558)
	nonhybrid	443 (52000)	574 (469)	0.11	–
T4	hybrid with DNA	451 (59000)	560 (468)	0.31	3.4 (560)
	hybrid with RNA	456 (58000)	581 (468)	0.28	3.3 (581)
	nonhybrid	511 (37000)	645 (553)	0.050	–
T5	hybrid with DNA	500 (49000)	609 (525)	0.58	31.9 (609)
	hybrid with RNA	518 (39000)	649 (549)	0.16	4.5 (649)

Table 4-2. Photophysical data of 5'-d(TACCAG**D**CACCAT)-3' and hybrids with the complementary DNAs or RNAs. **D** means the fluorescent modified deoxyuridine.

Dyes	Hybridization state	λ_{abs} /nm (ε)	λ_{em} /nm (λ_{ex} /nm)	Φ	I_{hybrid} /$I_{nonhybrid}$ (λ nm)
	nonhybrid	483 (67000)	567 (537)	0.35	–
D_{539}	hybrid with DNA	525 (64000)	569 (538)	0.79	4.4 (569)
	hybrid with RNA	486 (76000)	571 (539)	0.56	1.7 (571)
	nonhybrid	511 (63000)	603 (559)	0.30	–
D_{570}	hybrid with DNA	553 (61000)	605 (561)	0.68	3.5 (605)
	hybrid with RNA	517 (56000)	606 (562)	0.84	2.7 (606)
	nonhybrid	535 (54000)	614 (573)	0.30	–
D_{590}	hybrid with DNA	575 (55000)	619 (580)	0.52	2.4 (619)
	hybrid with RNA	540 (52000)	622 (581)	0.69	2.5 (622)
	nonhybrid	559 (41000)	601 (551)	0.25	–
D_{550}	hybrid with DNA	558 (66000)	608 (558)	0.70	4.6 (628)
	hybrid with RNA	555 (51000)	605 (557)	0.56	2.6 (625)
	nonhybrid	445 (60000)	534 (469)	0.071	–
T1	hybrid with DNA	454 (76000)	534 (467)	0.13	2.8 (534)
	hybrid with RNA	454 (62000)	533 (468)	0.14	2.4 (533)
	nonhybrid	502 (75000)	598 (541)	0.092	–
T2	hybrid with DNA	517 (81000)	603 (541)	0.50	7.3 (603)
	hybrid with RNA	513 (81000)	601 (543)	0.39	6.0 (601)
	nonhybrid	479 (53000)	566 (504)	0.048	–
T3	hybrid with DNA	492 (53000)	553 (502)	0.19	6.7 (553)
	hybrid with RNA	494 (47000)	560 (500)	0.18	5.2 (560)
	nonhybrid	451 (42000)	578 (468)	0.060	–
T4	hybrid with DNA	455 (46000)	580 (468)	0.19	4.1 (580)
	hybrid with RNA	455 (42000)	580 (468)	0.19	3.6 (580)
	nonhybrid	496 (41000)	644 (564)	0.04	–
T5	hybrid with DNA	518 (49000)	648 (550)	0.07	4.2 (648)
	hybrid with RNA	528 (52000)	645 (552)	0.20	4.8 (645)

Table 4-3. Photophysical data of 5'-mUmUmUmUmUmU**D**mUmUmUmUmUmU-3' and hybrids with the complementary DNAs or RNAs. **D** means the fluorescent modified deoxyuridine.

Dyes	Hybridization state	λ_{abs} /nm (ε)	λ_{em} /nm (λ_{ex} /nm)	Φ	I_{hybrid} /$I_{nonhybrid}$ (λ nm)
	nonhybrid	479 (170000)	564 (533)	0.02	–
D_{539}	hybrid with DNA	480 (120000)	574 (546)	0.36	26.1 (574)
	hybrid with RNA	484 (140000)	572 (543)	0.15	8.1 (572)
	nonhybrid	505 (80000)	600 (554)	0.10	–
D_{570}	hybrid with DNA	508 (65000)	611 (566)	0.42	7.4 (611)
	hybrid with RNA	513 (68000)	610 (564)	0.30	5.5 (610)
	nonhybrid	533 (43000)	613 (568)	0.13	–
D_{590}	hybrid with DNA	556 (37000)	621 (580)	0.50	4.5 (621)
	hybrid with RNA	570 (33000)	624 (584)	0.53	4.6 (624)
	nonhybrid	555 (150000)	600 (558)	0.09	–
D_{550}	hybrid with DNA	556 (120000)	608 (552)	0.12	2.2 (628)
	hybrid with RNA	561 (120000)	605 (552)	0.19	3.6 (625)
	nonhybrid	436 (26000)	534 (460)	0.026	–
T1	hybrid with DNA	453 (28000)	539 (469)	0.31	16.4 (539)
	hybrid with RNA	454 (27000)	535 (469)	0.18	8.7 (535)
	nonhybrid	493 (30000)	594 (540)	0.071	–
T2	hybrid with DNA	527 (26000)	614 (561)	0.85	19.7 (614)
	hybrid with RNA	510 (28000)	591 (539)	0.43	7.2 (591)
	nonhybrid	472 (27000)	578 (502)	0.027	–
T3	hybrid with DNA	491 (24000)	571 (525)	0.22	11.6 (571)
	hybrid with RNA	488 (25000)	558 (502)	0.24	19.6 (558)
	nonhybrid	445 (54000)	575 (469)	0.061	–
T4	hybrid with DNA	455 (50000)	579 (472)	0.26	5.3 (579)
	hybrid with RNA	455 (62000)	568 (470)	0.21	5.0 (568)
	nonhybrid	501 (58000)	653 (578)	0.011	–
T5	hybrid with DNA	494 (49000)	647 (558)	0.20	23.7 (647)
	hybrid with RNA	517 (65000)	645 (546)	0.13	42.2 (645)

Two-photon imaging of RNA in living Hela cells and mouse embryo brain

The rational dye arrangement at the single-strand oligonucleotide is the key point to control dye aggregation state and response target sequences sensitively and specifically via a hybridization way. Likewise, the sufficient two-photon absorbance of hybridization-sensitive fluorescent probes is crucial to excite dissociated dyes using an infrared light source on account of the limited light power. We developed a series of hybridization-sensitive fluorescent probes that cover the excitation-wavelength range 460 - 600 nm. To estimate the possibility of RNA imaging in live Hela cells using a two-photon microscope with a 1030 nm excitation laser source, We designed a model experiment using probes doubly labelled with $\mathbf{D_{539}}$, $\mathbf{D_{570}}$, **T2**, **T3** and **T5** as candidates. These probes can emit highly hybridization-sensitive fluorescence and be excited at 500- 550 nm by one-photon absorption that indicates dyes in these probes own the most suitable feasibility to realize the two-photon excitation in 1030 nm. The probes capable of binding to the poly-A tail of mRNA with a sequence 5'-mUmUmUmUmUmU**D**mUmUmUmUmUmU-3', were transfected to HeLa cells with the common transfection reagent Lipofectamine^{TM} 3000. After incubation for 1 h and washing, fluorescence emission was observed from the cells transfected with **T2**, **T3** or **T5** labelled probes (Figure 4-10). The fluorescence can only be observed from **T2**, **T3** and **T5** doubly labelled probes at a local observation field indicating that two-photon excited emission strictly occurred at the focus of laser beam. The fluorescence from $\mathbf{D_{539}}$ and $\mathbf{D_{570}}$ was not observed in cells suggesting two presuppositions: 1) two-photon excitation of $\mathbf{D_{539}}$ and $\mathbf{D_{570}}$ may not be suitable at 1030 nm; 2) the two-photon absorption ability of these dyes may be too weak to be excited by the high-power laser. These two presuppositions should be further confirmed by the two-photon cross-section measurement.

To visualize RNA distribution in a more actual physiological context, we transfected the mouse embryo brain with the T2 modified probes with the sequence 5'-mUmUmUmUmUmU**D**mUmUmUmUmUmU-3' using *in vivo* Magnetofection Kit. After treatment with magnet for 10 min, clear fluorescence emission from mouse embryo was observed at the two-photon microscope. Fluorescence signals at different depth of the mouse embryo brain showed varied distribution indicating RNAs could be monitored in several cells of the mouse embryo brain along the incident light beam (Figure 4-11). The observation depth

was up to 50 um to 60 um suggesting the high permeability of NIR light at 1030 nm and good excitability of ECHO probes conjugated with T2.

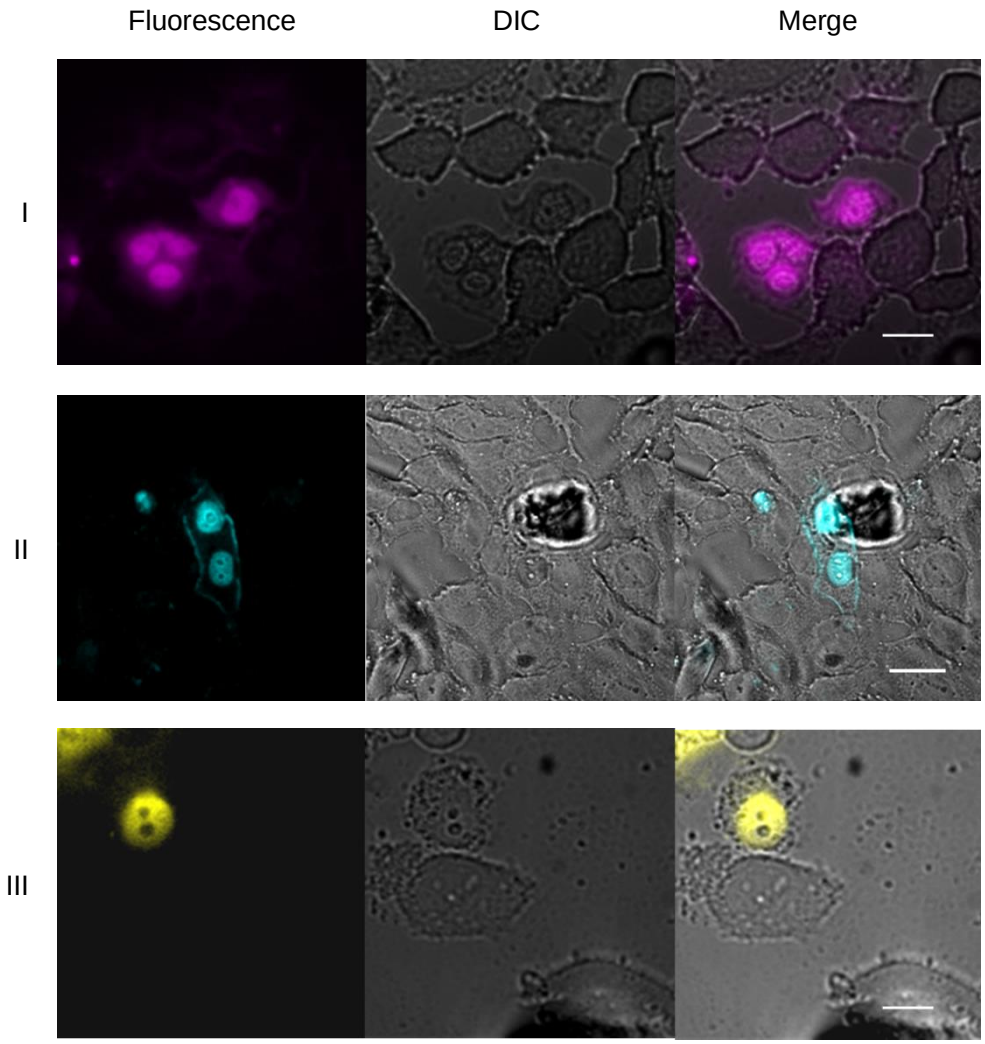

Figure 4-10. Two-photon-excited fluorescence images of mRNA polyA tail in Hela cells. DIC: differential interference contrast images. Scale bar: 50 μm. Excitation wavelength: 1030 nm. I) mUmUmUmUmUmU**T2**mUmUmUmUmUmU; II) mUmUmUmUmUmU**T3**mUmUmUmUmUmU; III) mUmUmUmUmUmU**T5**mUmUmUmUmUmU.

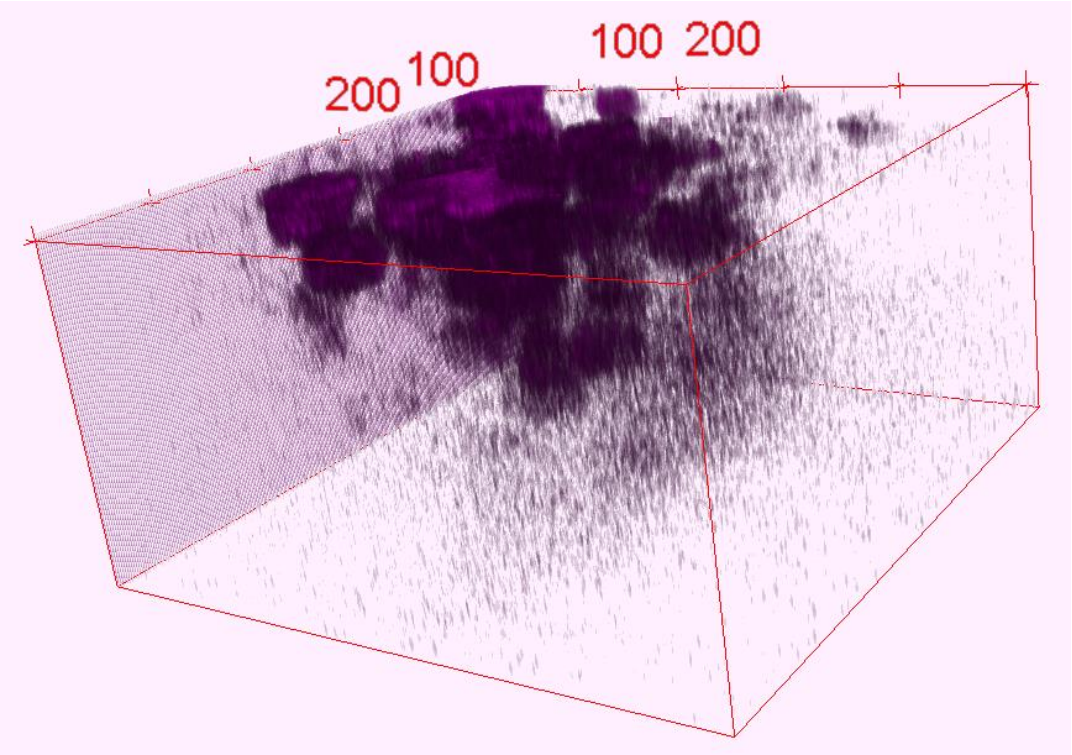

Figure 4-11. Two-photon fluorescence imaging of RNAs with poly-A tails in an embryonic mouse brain. Excitation wavelength: 1030 nm. Probe: mUmUmUmUmUmU**T2**mUmUmUmUmUmU. The numbers in the figure mean figure pixel numbers that are 4 times of the actual lengths in μm. The height of imaging box is 60 μm.

Simple FISH imaging of DNA in fixed cells and brain sections

Due to the high fluorescent ON/OFF ratio of the novel ECHO probes, the cumbersome and time-consuming washing step may be able to be avoided. To compare the probe behavior to conventional FISH probes, we synthesized and applied Telo-FAM-S and Telo-T2 in parallel experiments. Telo-FAM-S revealed noisy images with no telomere localization pattern to be recognized while Telo-T2 showed dispersed fluorescent spots when a simple FISH protocol was conducted without washing steps. Characteristic fluorescent distribution patterns were observed no matter the washing step was conducted or not when probes Telo-T2 were applied. To test the stringency of the fluorescent signals, we introduced complementary telomere probes Telo-FAM-L and Telo-T2 into fixed MEF7 cells. Telo-FAM-L in situ hybridization used a conventional FISH protocol with the stringent washing while Telo-T2 a simple FISH protocol without washing (Figure 4-12). After Telo-T2 was co-applied with Telo-FAM-L in the FISH protocol, we detected colocalized FISH signals indicating the signals of Telo-T2 in simple FISH are derived from telomere hybridization (Figure 4-13).

Simultaneous imaging of multiple chromatin domains or genes is critical for studying chromatin interactions. Using Telo-T2, MajSat-T3 and MinSat-T5 probes, we produced three-color imaging of telomeres, centromeres and pericentromeres in cells with a one-step method in which the three color probes are applied to the cell simultaneously (Figure 4-14). There was no detectable cross-reactivity between the three imaging channels. Thus we demonstrated that ECHO probes with T2, T3 and T5 could be used for imaging multiple sequence-specific genomic regions with multiple colors.

To explore the possibility of applying novel ECHO probes in tissue slice for two-photon-excited FISH imaging, we introduced Telo-T2 into adult mouse brain slice with a simple FISH protocol. We found the changed positions of fluorescent spots in different depths of the brain slice in the two-photon microscope (Figure 4-15). In the defined regions, characteristic telomere distribution patterns were also observed. Therefore, the simple FISH protocol is also suitable for DNA imaging in tissue slices.

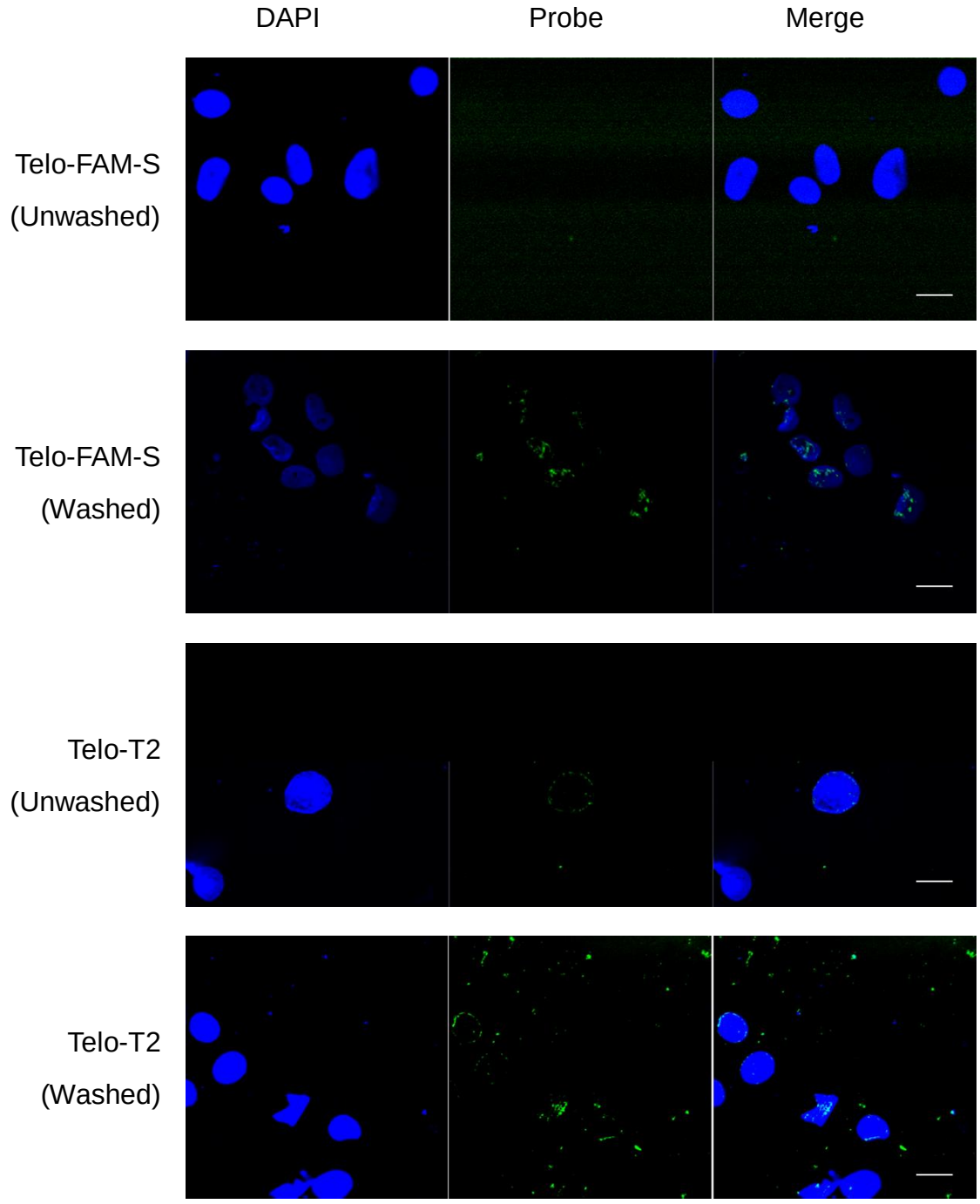

Figure 4-12. FISH images of telomeres in MEF cells using probes Telo-FAM-S and Telo-T2. Both probes show consistent signals (green). DNA was stained with DAPI (blue). Telo-FAM-S: 5'-CCC TAA CCC TAA CCC TAA-**FAM**-3'; Telo-T2: 5'-CCC TAA CCC **T2**AA CCC TAA-3'. Bars =20 μm.

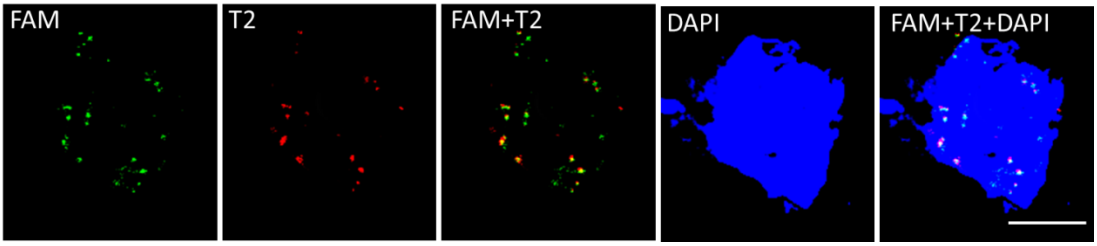

Figure 4-13. FISH images of telomeres in MEF cells using complementary probes Telo-FAM-L and Telo-T2. Both probes show consistent signals (green and red). DNA was stained with DAPI (blue). Telo-FAM-L: 5'-GGG TTA GGG TTA GGG TTA GGG TTA GGG TTA -**FAM**-3'; Telo-T2: 5'-CCC TAA CCC **T2**AA CCC TAA-3'. Bars =20 μm.

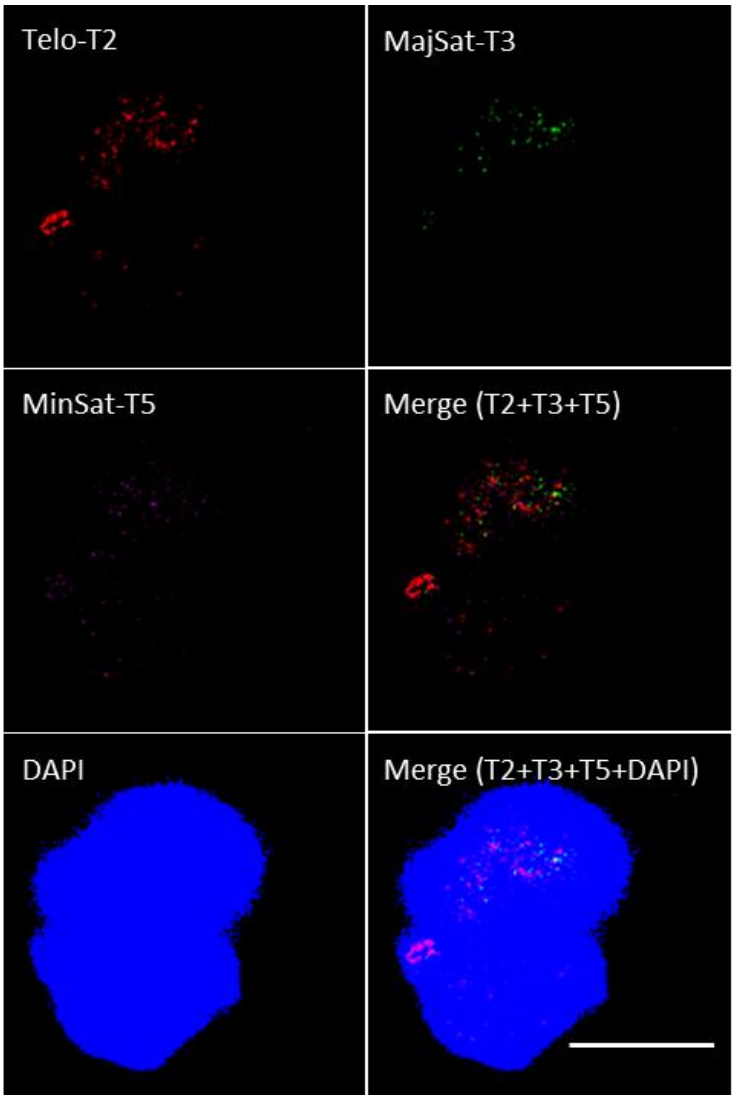

Figure 4-14. FISH images of telomeres, centromeres and pericentromeres in fixed MEF cells using the probe mixture. Probes show consistent signals (green, red and purple). DNA was stained with DAPI (blue). Telo-T2: 5'-CCC TAA CCC **T2**AA CCC TAA-3', MajSat-T3: 5'-CCA TAT **T3**CC ACG TCC TAC AG-3'; MinSat-T5: 5'-ATC TAA TA**T5** GTT CTA CAG TG-3'. Bars =20 μm.

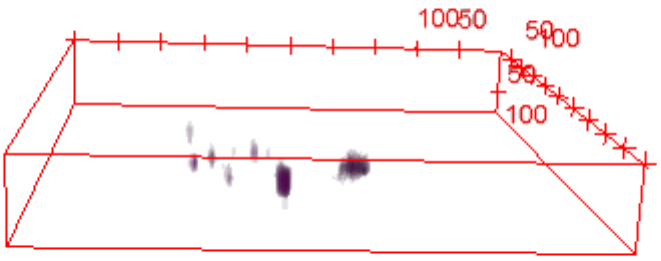

Figure 4-15. Two-photon fluorescence imaging of telomeres in an adult mouse brain slice. Excitation wavelength: 1030 nm. Telo-T2: 5'-CCC TAA CCC **T2**AA CCC TAA-3'. The numbers in the figure mean figure pixel numbers that are 4 times of the actual lengths in μm.

4.4 Conclusions

In conclusion, we have designed a series of novel fluorescent probes based on the concept of exciton-controlled quenching and observed two-photon-excited fluorescence from live Hela cells. The hybridization-sensitive, quencher-free fluorescent probes have also been excited in a two-photon-excited way in the embryonic mouse brain or adult mouse brain slices which facilitate the imaging of intracellular DNA or RNA in deep tissues. Further aspects need to be examined, such as the two-photon absorption ability of these probes and the practical applications in the native body. We anticipate that these new two-photon-excited hybridization-sensitive probes based on photochemical techniques will provide more nucleic acid information in a more actual physiological context, such as live tissues and render a more accurate diagnostics for patients.

4.5 Experimental procedures

General. ^{1}H and ^{13}C NMR spectra were measured with a a Bruker Avance 600 (600 MHz). Coupling constants (J value) are reported in hertz. The chemical shifts are shown in ppm, using residual dimethylsulfoxide (δ = 2.48 in ^{1}H NMR, δ = 39.5 in ^{13}C NMR) as an internal standard. Electrospray ionization mass spectra ESI-MS spectra were recorded by a Bruker microTOF II-NAC. DNA was synthesized on a NTS H-8 DNA/RNA synthesizer (Nihon Techno Service). Reversed-phase HPLC was performed on CHEMCOBOND 5-ODS-H columns (10 × 150 mm) with a Gilson Chromatograph, Model 305, using a UV detector, Model 118, at 260 nm. MALDI TOF mass spectra were measured with a Bruker microflex-NAC. UV and fluorescence spectra were recorded on Shimadzu UV-2550 spectrophotometer and RF-5300PC spectrofluorophotometer, respectively.

Compound 3.

To a solution of indole-3-carbaldehyde (585 mg, 4 mmol) in THF (20 mL) at 0 ^{o}C was slowly added NaH (192 mg, 4.8 mmol). After refluxing for 0.5 h, ethyl 5-bromopentanoate (768 μL, 4.8 mmol) was added dropwise. The resulting mixture was heated to reflux overnight. After cooling down to 0 ^{o}C, the reaction mixture was carefully quenched with water and extracted with ethyl acetate three times. The combined organic phase was washed with brine. Then the organic layer was dried over anhydrous sodium sulfate and the solvent was removed. The residue was purified by silica gel chromatography using hexane and ethyl acetate as eluent to afford yellow oil. Yield: 80 %. ^{1}H NMR (600 MHz, DMSO-*d6*) δ 9.92 (s, 1H), 8.32 (s, 1H), 8.15 (s, 1H), 7.63 (s, 1H), 7.31 - 7.27 (s, 2H), 4.30 (d, 2H, J = 7.04 Hz), 4.01 (d, 2H, J = 7.04 Hz), 2.33 (d, 2H, J = 7.33 Hz), 1.83 (s, 2H), 1.52974 (s, 2H), 1.13 (t, 3H, J = 7.04 Hz); ^{13}C NMR (150 MHz, DMSO-*d6*) δ 185.2, 173.4, 163.1, 141.4, 137.8, 125.6, 124.3, 123.2, 121.9, 118.0, 111.8, 60.5, 46.8, 36.5, 33.7, 29.5, 22.5, 14.8. ESI-MS $[M+H]^{+}$ 274.1365 (calcd.), 274.1304 (found).

Compound 4.

To a solution of ethanol (16 mL) and NaOH 2.5 M (2 mL) was added **3** (3 mmol). After refluxing for 4 h, 11 mL water was added and extracted with ethyl acetate (5 mL, twice) to remove unreacted ester. HCl (2.8 M) wad added slowly to the water phase. After pH become 4.0, the reaction mixture was extracted with ethyl acetate three times. The combined organic phase was washed with brine. Then the organic layer was dried over

with anhydrous sodium sulfate and the solvent was removed. The residue was purified by silica gel chromatography using hexane and ethyl acetate as eluent to afford white powder. Yield: 84 %. ^{1}H NMR (600 MHz, DMSO-*d6*) δ 12.07 (s, 1H), 9.92 (s, 1H), 8.36 (s, 1H), 8.13 (d, 1H, J = 7.62 Hz), 7.66 (d, 1H, J = 7.92 Hz), 7.33 (d, 1H, J = 7.62 Hz), 7.27 (d, 1H, J = 7.33 Hz), 4.31 (d, 2H, J = 7.04 Hz), 2.27 (d, 2H, J = 7.33 Hz), 1.84 (d, 2H, J = 7.62 Hz), 1.50 (d, 2H, J = 7.62 Hz); ^{13}C NMR (150 MHz, DMSO-*d6*) δ 12.07, 9.92, 8.36, 8.13, 8.12, 7.66, 7.65, 7.33, 7.32, 7.27, 7.26, 4.31, 4.30, 2.27, 2.26, 1.84, 1.82, 1.50, 1.49; ESI-MS $[M+H]^+$ 246.1052 (calcd.), 246.0964 (found).

Compound 6.

0.1 mmole of 4-picoline (10 mL) and 0.11 mmole of 2-iodomethane (7.04 mL) were dissolved in toluene and stirred for 4 hours, thereafter refluxed 30 min. After cooling and filtrating, the resulting solid were washed with ether three times. White powder was obtained. Yield: 93 %. ^{1}H NMR (600 MHz, DMSO-*d6*) δ 8.86 (d, 2H, J = 5.86 Hz), 7.98 (d, 2H, J = 5.86 Hz), 4.29 (s, 3H), 2.60 (s, 3H); ^{13}C NMR (150 MHz, DMSO-*d6*) δ 159.0, 145.3, 128.8, 48.1, 22.2; ESI-MS $[M]^+$ 108.0808 (calcd.), 108.0728 (found).

Compound T1.

A solution mixture of **6** (118mg, 1.1 mmol), **4** (343 mg, 1.4 mmol) and piperidine (0.2 mL) in ethanol (20 mL) under sealed tube condition was heated at 90 ^{o}C overnight. After cooling down to room temperature, the residue was filtered, washed with ethanol, ethyl acetate, and petroleum ether to afford a yellow solid. Yield: 86 %. ^{1}H NMR (600 MHz, DMSO-*d6*) δ 8.67 (d, J = 6.9 Hz, 2H), 8.21 (d, J = 16 Hz, 1H), 8.17 (d, J = 7.3 Hz, 1H), 8.12 (d, J = 7.0 Hz, 1H), 7.98 (s, 1H), 7.64 (d, J = 7.5 Hz, 1H), 7.33-7.25 (m, 3H), 4.43 (t, J = 5.0 Hz, 2H), 4.17 (s, 3H), 3.79 (t, J = 5.2 Hz, 2H), 3.52-3.50 (m, 2H), 3.38-3.37 (m, 2H), 3.17 (s, 3H). ^{13}C NMR (150 MHz, DMSO-*d6*) δ 176.1, 154.9, 145.0, 138.1, 136.4, 135.4, 126.4, 123.8, 122.5, 122.2, 121.4, 117.7, 113.5, 111.9, 47.1, 46.7, 45.3, 35.8, 30.1, 24.7, 23.8, 23.3; ESI-MS $[M]^+$ 335.1754 (calcd.), 335.1476 (found).

Compound 8.

0.1 mmole of **7** (13.6 mL) and 0.11 mmole of 2-iodomethane (7.04 mL) were dissolved in toluene and stirred for 4 hours, thereafter refluxed 30 min. After cooling and filtrating, the resulting solid were washed with ether three times. Yellow powder was obtained. Yield: 87 %. ^{1}H NMR (600 MHz, DMSO-*d6*) δ 9.38 (d, 1H, J = 6.16 Hz), 8.55 (d, 1H, J = 8.50 Hz), 8.49 (d, 1H, J = 8.80 Hz), 8.28 (t, 1H, J = 8.21 Hz), 8.09 -8.06 (m, 2H), 4.59 (s, 3H),3.01 (s, 3H); ^{13}C NMR (150 MHz, DMSO-*d6*) δ 159.0, 149.8, 138.5, 135.8,

130.5, 129.3, 127.6, 123.3, 120.4, 45.9, 20.5; ESI-MS $[M]^+$ 158.0964 (calcd.), 158.0975 (found).

Compound T2.

A solution mixture of **8** (118 mg, 1.1 mmol), **4** (343 mg, 1.4 mmol) and piperidine (0.2 mL) in ethanol (20 mL) under sealed tube condition was heated at 90 ^oC overnight. After cooling down to room temperature, the residue was filtered, washed with ethanol, ethyl acetate, and petroleum ether to afford a red solid. Yield: 65 %. ^1H NMR (600 MHz, DMSO-*d6*) δ 9.1 (s, 1H), 8.97 (s, 1H), 8.56 (d, 1H, J = 15.55 Hz), 8.44 (d, 2H, J = 7.04 Hz), 8.34 (d, 1H, J = 8.80 Hz), 8.27 (d, 1H, J = 7.33 Hz), 8.21 (s, 1H), 8.03 - 7.99 (2H), 7.67 (d, 1H, J = 7.62 Hz), 7.34 (d, 2H, J = 7.04 Hz), 4.44 (s, 3H), 4.32 (s, 2H), 2.25 (t, 2H, J = 7.33 Hz), 1.88 (d, 2H, J = 9.68 Hz), 1.52 (s, 2H); ^{13}C NMR (150 MHz, DMSO-*d6*) δ 154.3, 147.5, 139.6, 138.6, 138.1, 135.7, 135.4, 129.4, 126.9, 126.2, 124.0, 122.5, 121.3, 119.9, 114.6, 114.3, 113.6, 112.0, 46.9, 44.7, 34.6, 29.9, 22.9; ESI-MS $[M]^+$ 385.1911 (calcd.), 385.1726 (found).

Compound 10.

0.1 mmole of **9** (13.6 mL) and 0.11 mmole of 2-iodomethane (7.04 mL) were dissolved in toluene and stirred for 4 hours, thereafter refluxed 30 min. After cooling and filtrating, the resulting solid were washed with ether three times. Yellowish powder was obtained. Yield: 87 %. ^1H NMR (600 MHz, DMSO-*d6*) δ 9.13 (d, 1H, J = 8.50 Hz), 8.61 (d, 1H, J = 8.80 Hz), 8.42 (d, 1H, J = 8.21 Hz), 8.24 (t, 1H, J = 7.04 Hz), 8.15 (d, 1H, J = 8.51 Hz), 8.00 (t, 1H, J = 7.33 Hz), 4.46 (s, 3H), 3.09 (s, 3H); ^{13}C NMR (150 MHz, DMSO-*d6*) δ 162.0, 146.3, 140.1, 135.9, 131.2, 129.8, 128.6,126.0, 119.8, 24.0; ESI-MS $[M]^+$ 158.0964 (calcd.), 158.0948 (found).

Compound T3.

A solution mixture of **10** (118 mg, 1.1 mmole), **4** (343 mg, 1.4 mmole) and piperidine (0.2 mL) in ethanol (20 mL) under sealed tube condition was heated at 90 ^oC overnight. After cooling down to room temperature, the residue was filtered, washed with ethanol, ethyl acetate, and petroleum ether to afford a red solid. Yield: 58 %. ^1H NMR (600 MHz, DMSO-*d6*) δ 8.83 (s, 1H),8.64 (s, 2H), 8.48 (s, 2H), 8.25 (s, 2H), 8.10 (s, 1H), 7.86 (s, 1H), 7.70 (s, 1H), 7.58 (s, 1H), 7.36 (s, 2H), 4.47 (s, 3H), 4.36 (s, 2H), 2.28 (s, 2H), 1.88 (s, 2H), 1.53 (s, 2H); ^{13}C NMR (150 MHz, DMSO-*d6*) δ 175.2, 157.5, 142.9, 142.5, 140.06, 138.2, 137., 134.9, 130.6, 128.7, 127.5, 126.8, 124.3, 123.0, 121.3, 120.8, 119.6, 114.5, 112.5, 112.3, 55.8, 47.0, 44.7, 34.2, 29.8, 22.7; ESI-MS $[M]^+$ 385.1911 (calcd.),

385.0984 (found).

Compound 13.

4-Methylquinoline (15.9 mL, 120 mmole) and 5-bromovaleric acid (18.1 g, 100 mmole) were stirred at 150 ^{o}C for 5 min under microwave irradiation (100 W). The reaction mixture was added to dichloromethane (1 L) with vigorous stirring. After cooling to room temperature, the solution was sonicated to obtain a white precipitate. The precipitate was filtered and dried *in vacuo*. The white powder was washed with diethyl ether (100 mL), filtered and dried *in vacuo* to give **13** as a white powder. Yield: 53 %. ^{1}H NMR (600 MHz, DMSO-*d6*) δ 12.16 (s, 1H), 8.95 (s, 2H), 8.01 (s, 2H), 4.54 (s, 2H), 2.61 (s, 3H), 2.28 (s, 2H), 1.90 (s, 2H), 1.46 (s, 2H); ^{13}C NMR (150 MHz, DMSO-*d6*) δ 174.9, 159.5, 149.2, 137.6, 135.9, 130.4, 129.9, 128.0, 123.5, 120.2, 57.5, 33.7, 29.6, 22.1, 20.5; ESI-MS $[M]^{+}$ 194.1176 (calcd.), 194.1408 (found).

Compound T4.

A solution mixture of **13** (118 mg, 1.1 mmol), **14** (343 mg, 1.4 mmol) and piperidine (0.2 mL) in ethanol (20 mL) under sealed tube condition was heated at 90 ^{o}C overnight. After cooling down to room temperature, the residue was filtered, washed with ethanol, ethyl acetate, and petroleum ether to afford an orange solid. Yield: 74 %. ^{1}H NMR (600 MHz, DMSO-*d6*) δ 8.92 (d, 2H, J = 6.45 Hz), 8.59 (s, 1H), 8.23 (m, 4H), 7.92 (d, 1H, J = 8.50 Hz), 7.77 (d, 1H, J = 8.50 Hz), 7.70 (d, 1H, J = 8.21 Hz), 7.54 (m, 2H), 7.30 (t, 1H, J = 7.62 Hz), 4.51 (t, 3H), 2.29 (t, 2H, J = 7.33 Hz), 1.94 (t, 2H, J = 7.62 Hz), 1.52 (m, 2H), 1.35 (t, 3H, J = 7.04 Hz); ^{13}C NMR (150 MHz, DMSO-*d6*) δ 175.0, 154.4, 144.8, 143.5, 141.8, 141.0, 127.3, 127.1, 127.0, 124.0, 123.6, 123.0, 122.1, 121.3, 120.8, 120.6, 110.7, 110.6, 60.0, 38.1, 34.0, 30.8, 21.9, 14.64; ESI-MS $[M]^{+}$ 399.2067 (calcd.), 399.2151 (found).

Compound 16.

15 (15.9 mL, 120 mmole) and 5-bromovaleric acid (18.1 g, 100 mmole) were stirred at 150 ^{o}C for 5 min under microwave irradiation (100 W). The reaction mixture was added to dichloromethane (1 L) with vigorous stirring. After cooling to room temperature, the solution was sonicated to obtain a white precipitate. The precipitate was filtered and dried *in vacuo*. The white powder was washed with diethyl ether (100 mL), filtered and dried *in vacuo* to give **16** as a white powder. Yield: 37 %. ^{1}H NMR (600 MHz, DMSO-*d6*) δ 12.14 (s, 1H), 9.43 (d, 1H, J = 5.86 Hz), 8.61 (d, 1H, J = 8.80 Hz), 8.56 (d, 1H, J = 8.21 Hz), 8.27 (t, 1H, J = 7.04 Hz), 8.09 (d, 1H, J = 5.86 Hz), 8.0671 (t, 1H, J =

7.33 Hz), 5.03 (t, 2H, J = 6.74 Hz), 3.01 (s, 3H), 2.29 (t, 2H, J = 7.04 Hz), 1.97 (s, 2H), 1.60 (d, 2H, J = 7.33 Hz); ^{13}C NMR (150 MHz, DMSO-*d6*) δ 174.9, 159.5, 149.2, 137.6, 135.9, 130.4, 129.9, 128.0, 123.5, 120.1, 57.5, 33.7, 29.6, 22.1, 20.5; ESI-MS $[M]^+$ 244.1332 (calcd.), 244.1388(found).

Compound T5.

A solution mixture of **16** (118 mg, 1.1 mmole), **14** (343 mg, 1.4 mmole) and piperidine (0.2 mL) in ethanol (20 mL) under sealed tube condition was heated at 90 ^{o}C overnight. After cooling down to room temperature, the residue was filtered, washed with ethanol, ethyl acetate, and petroleum ether to afford an orange solid. Yield: 52 %. ^{1}H NMR (600 MHz, DMSO-*d6*) δ 9.45 (s, 1H), 9.24 (s, 1H), 8.98 (s, 1H), 8.64 - 8.46 (m, 4H), 8.35 (s, 2H), 8.23 (s, 1H), 8.14 (s, 1H), 7.89 (d, 1H), 7.81 (d, 1H), 7.65 (s, 1H), 7.43 (s, 1H), 5.06 (s, 2H), 4.62 (s, 2H), 2.32 (s, 2H), 2.06 (s, 2H), 1.71 (s, 2H), 1.46 (d, 3H); ^{13}C NMR (150 MHz, DMSO-*d6*) δ 175.5, 154.1, 147.7, 146.0, 142.1, 141.0, 138.7, 135.8, 129.6, 128.4, 127.6, 127.5, 127.3, 123.7, 123.1, 122.8, 121.4, 120.6, 119.9, 117.0, 116.0, 110.6, 110.6, 56.9, 38.1, 35.1, 29.8, 22.8, 14.6; ESI-MS $[M]^+$ 449.2224 (calcd.), 449.1977 (found).

Compound T5'.

A solution mixture of **8** (285 mg, 2 mmol), **14** (223 mg, 2.4 mmol) and piperidine (0.4 mL) in ethanol (40 mL) under sealed tube condition was heated at 90 ^{o}C overnight. After cooling down to room temperature, the residue was filtered, washed with ethanol, ethyl acetate, and petroleum ether to afford an orange solid. Yield: 93 %. ^{1}H NMR (600 MHz, DMSO-*d6*) δ 9.30 (d, 1H), 9.15 (d, 1H), 8.88 (s, 1H), 8.52 (d, 1H), 8.44 (3H), 8.39-8.07 (4H), 7.79 (d, 1H), 7.71 (d, 1H), 7.56 (t, 1H), 7.33 (t, 1H), 4.52 (t, 5H), 1.37 (t, 3H); ^{13}C NMR (150 MHz, DMSO-*d6*) δ 153.9, 148.4, 145.7, 142.1, 141.1, 139.7, 135.7, 129.8, 128.4, 127.5, 127.4, 127.3, 127.0, 123.7, 123.1, 122.7, 121.4, 120.6, 120.1, 117.0, 115.9, 110.7, 45.2, 38.1, 14.6; ESI-MS $[M]^+$ 363.1856 (calcd.), 363.1920 (found).

Compound 18.

17 (8.0 mL, 50.0 mmole) and 5-bromovaleric acid **12** (18.1 g, 100 mmole) were suspended to 20 mL of 1,2-dichlorobenzene. The mixture was stirred at 120 ℃ for 16 h. The reaction solution was cooled to 25 ℃. To the reaction mixture, dichloromethane (300 mL) was added and mixed. The resultant suspension was left for 2 h at 25 ℃. The precipitation was filtered, washed with dichloromethane, and dried under reduced pressure to give **18** as a white powder. Yield: 23 %. ^{1}H NMR (600 MHz, DMSO-*d6*) δ

12.12 (s, 1H), 8.01 (d, 1H), 7.87 (t, 1H), 7.65 (q, 2H), 4.52 (t, 2H), 2.87 (s, 3H), 2.33 (t, 2H), 1.89 (m, 2H), 1.68 (m, 2H), 1.55 (s, 6H); ^{13}C NMR (150 MHz, DMSO-*d6*) δ 197.5, 174.9, 142.7, 142.0, 130.2, 129.8, 124.4, 116.3, 55.0, 48.1, 33.9, 27.5, 22.9, 22.3, 14.9; ESI-MS $[M]^+$ 260.1645 (calcd.), 260.2518 (found).

Compound D_{550}.

Compounds **18** (1020 mg, 3.00 mmole) and **19** (521 mg, 3.50 mmole) were suspended to 30 mL of acetic anhydride. The resultant suspension was stirred at 120 ^{o}C for 30 min. 10 mL of distilled water was slowly added to the reaction mixture and further stirred at 120 ^{o}C for 30 min. After the solvent was evaporated, acetone (100 mL) was added to the residue. The precipitation was filtered, washed with acetone, dried under reduced pressure to give $\mathbf{D_{550}}$ as a purple powder. Yield: 61 %. ^{1}H NMR (600 MHz, DMSO-*d6*) δ 12.11 (s, 1H), 8.38 (d, 1H), 8.14 (d, 2H), 7.81-7.75 (2H), 7.57-7.49 (2H), 7.30 (d, 1H), 6.91 (d, 2H), 4.57 (t, 2H), 3.21-3.18 (8H), 2.34 (q, 2H), 1.84 (7H), 1.69 (2H). ^{13}C NMR (150 MHz, DMSO-*d6*) δ 180.2, 175.0, 155.5, 143.5, 142.0, 129.6, 128.3, 123.6, 123.2, 114.4, 113.1, 105.4, 51.8, 49.4, 45.6, 33.9, 31.5, 28.1, 27.4, 22.3; ESI-MS $[M]^+$ 391.2380 (calcd.), 391.3380 (found).

Succinimidylation of dyes (D_{539}, D_{570}, D_{590}, D_{600}, T1, T2, T3, T4 or T5).[32]

N-Hydroxysuccinimide (4.6 mg, 40 μmole) and 1-ethyl-3-(3-dimethylaminopropyl)carbodiimide hydrochloride (7.7 mg, 40 μmole) were added to a solution of synthesized dyes (20 μmole) in DMF (0.50 mL) and stirred at 25 ℃ for 16 h. The reaction mixture was used for the next reaction with DNA oligomers without further purification.

Probe synthesis.

DNA oligomers were synthesized by a conventional phosphoramidite method using a NTS H-8 DNA/RNA synthesizer (Nihon Techno Service). Commercially available phosphoramidites were used for dA, dG, dC, and dT. The diamino-modified nucleoside phosphoramidite was synthesized as described in our previous report[32]. The synthesized DNA oligomer was cleaved from the support with 28% aqueous ammonia, then deprotected at 55 °C for 5 h, or at 25 °C for 16 h. After removal of ammonia from the solution under reduced pressure, the DNA was purified by reversed-phase HPLC on a 5-ODS-H column (10 mm × 150 mm, elution with a solvent mixture of 0.1 M S8 triethylamine acetate (TEAA), pH 7.0, linear gradient over 30 min from 5% to 40% acetonitrile at a flow rate of 3.0 mL/min).

A solution of the succinimidyl ester of dyes (100 eq. to an active amino group of DNA) in N,N-dimethylformamide was added to a solution of diamino-modified RNA in 100 mM sodium carbonate buffer (pH 9.0), and incubated at 25 ^{o}C for 1.5 h. The reaction mixture was diluted with ethanol. After centrifuging at −20 ^{o}C for 20 min, the supernatant was removed. The residue was dissolved in a small volume of water and the solution was passed through a 0.45 um filter. The product was purified by reversed-phase HPLC on a 5-ODS-H column (10 mm x 150 mm, elution with a solvent mixture of 0.1 M TEAA, pH 7.0, linear gradient over 30 min from 5% to 30% acetonitrile at a flow rate of 3.0 mL/min). The concentration of the fluorescent DNA was determined at Nanodrop 1000 spectrophotometer. The fluorescent DNA was identified by MALDI–TOF mass spectrometry. (Here, the molecular weight of the counter anions of dyes is not included in the value of M.): TTTTTT**D**$_{539}$TTTTTT, calcd for ([M − H]$^{-}$) 4766.6, found 4783.3; TTTTTT**D**$_{550}$TTTTTT, calcd for ([M − H]$^{-}$) 4825.2, found 4826.2; TTTTTT**D**$_{570}$TTTTTT, calcd for ([M − H]$^{-}$) 4798.6, found 4802.6; TTTTTT**D**$_{590}$TTTTTT, calcd for ([M − H]$^{-}$) 4953.6, found 4959.4; TTTTTT**D**$_{550}$TTTTTT, calcd for ([M − H]$^{-}$) 4869.6, found 4868.1; TTTTTT**T1**TTTTTT, calcd for ([M − H]$^{-}$) 4704.6, found 4706.2; TTTTTT**T2**TTTTTT, calcd for ([M − H]$^{-}$) 4782.6, found 4783.1; TTTTTT**T3**TTTTTT, calcd for ([M − H]$^{-}$) 4782.6, found 4784.3; TTTTTT**T4**TTTTTT, calcd for ([M − H]$^{-}$) 4839.2, found 4839.8; TTTTTT**T5**TTTTTT, calcd for ([M − H]$^{-}$) 4939.2, found 4940.4; TACCAG**D**$_{539}$CACCAT, calcd for ([M − H]$^{-}$) 4811.2, found 4811.4; TACCAG**D**$_{550}$CACCAT, calcd for ([M − H]$^{-}$) 4757.1, found 4759.7; TACCAG**D**$_{570}$CACCAT, calcd for ([M − H]$^{-}$) 4789.1, found 4790.2; TACCAG**D**$_{590}$CACCAT, calcd for ([M − H]$^{-}$) 4745.0, found 4745.6; TACCAG**D**$_{550}$CACCAT, calcd for ([M − H]$^{-}$) 4829.1, found 4830.6; TACCAG**T1**CACCAT, calcd for ([M − H]$^{-}$) 4697.1, found 4697.8; TACCAG**T2**CACCAT, calcd for ([M − H]$^{-}$) 4797.1, found 4798.1; TACCAG**T3**CACCAT, calcd for ([M − H]$^{-}$) 4797.1, found 4798.8; TACCAG**T4**CACCAT, calcd for ([M − H]$^{-}$) 4825.2, found 4826.5; TACCAG**T5**CACCAT, calcd for ([M − H]$^{-}$) 4925.2, found 4926.8; mUmUmUmUmUmU**D**$_{539}$mUmUmUmUmUmU, calcd for ([M − H]$^{-}$) 4961.1, found 4960.4; mUmUmUmUmUmU**D**$_{550}$mUmUmUmUmUmU, calcd for ([M − H]$^{-}$) 5015.2, found 5019.1; mUmUmUmUmUmU**D**$_{570}$mUmUmUmUmUmU, calcd for ([M − H]$^{-}$) 4988.6, found 4990.5; mUmUmUmUmUmU**D**$_{590}$mUmUmUmUmUmU, calcd for ([M − H]$^{-}$) 5161.6, found 5159.7; mUmUmUmUmUmU**D**$_{550}$mUmUmUmUmUmU, calcd for ([M − H]$^{-}$) 5077.6, found 5078.1; mUmUmUmUmUmU**T1**mUmUmUmUmUmU,

calcd for ([M − H]$^+$) 4901.9, found 4905.1; mUmUmUmUmUmU**T2**mUmUmUmUmUmU, calcd for ([M − H]$^-$) 4972.6, found 4971.7; mUmUmUmUmUmU**T3**mUmUmUmUmUmU, calcd for ([M − H]$^-$) 4972.6, found 4972.0; mUmUmUmUmUmU**T3**mUmUmUmUmUmU, calcd for ([M − H]$^-$) 4961.1, found 4960.4; mUmUmUmUmUmU**T4**mUmUmUmUmUmU, calcd for ([M − H]$^-$) 5029.2, found 5028.7; mUmUmUmUmUmU**T5**mUmUmUmUmUmU, calcd for ([M − H]$^-$) 5129.2, found 5129.4. Here all mU mean 2'-OMe-Uridine.

Absorption, fluorescence and circular dichroism spectra measurements.
Absorption and fluorescence spectra of the probes (0.5 μM for both single-stranded and duplex) were measured in 50 mM sodium phosphate buffer (pH = 7.0) containing 100 mM sodium chloride using a quartz cell with a 1 cm path length. The bandwidths of excitation and emission are 1.5 nm. The fluorescence quantum yields (Φ) of probes were calculated using Rhodamine B as a reference which has a known quantum yield Φ= 0.31 in water. The quantum yield was determined as the equation below:

$$\Phi_{(S)}/\Phi_{(R)} = [A_{(S)}/A_{(R)}] * [(Abs)_{(R)}/(Abs)_{(S)}] * [n_{(S)}^2/n_{(R)}^2]$$

Here, $\Phi_{(S)}$ and $\Phi_{(R)}$ mean the fluorescent quantum yields of the sample and the reference, respectively. $A_{(S)}$ and $A_{(R)}$ are the areas under the fluorescent spectra of the sample and the reference, respectively, $(Abs)_{(S)}$ and $(Abs)_{(R)}$ are the optical densities of the sample and the reference solution at the wavelength of excitation, respectively, and $n_{(S)}$ and $n_{(R)}$ are the values of the refractive index for the solvents used for the sample ($n_{(S)}$ = 1.333) and the reference ($n_{(R)}$ = 1.333), respectively.

Circular dichroism spectra measurements. Circular dichroism spectra of the fluorescent probes (1 μM) were measured in 50 mM sodium phosphate buffer (pH 7.0) containing 100 mM sodium chloride using a cell with a 1 cm path length.

Cell culture.
Dulbecco's modified Eagle's medium (DMEM) and fetal bovine serum (FBS) were purchased from GIBCO. HeLa cells were cultured at 37 ˚C in DMEM containing 10 % heat-inactivated FBS, 25 U/mL penicillin and 25 mg/mL streptomycin, under a humidified atmosphere with 5 % CO_2. For imaging usage, cells were cultured in glass-base dishes (Matsunami). Before microscope observation, culture medium was washed and exchanged to phenol red-free DMEM. Cells were maintained in the

culturing condition by an incubation system (INU; Tokai Hit) during the observation.

Imaging.

Images were acquired with a home-made two-photon microscope (at Satoshi Wada Laboratory, RIKEN, Japan) equipped with an objective (25x water immersion lens (N.A=1.1)). The average power after objective lens is approximately 400 mW. Acquired images were analyzed and processed with ImagJ. Probes (50 pmol) were introduced using 2 μL transfection reagent LipofectamineTM 3000 (Invitrogen) following the manufacturer's protocol. After 1 h incubation at 37 °C with the Lipofectamine^{TM} 3000 and a probe, the cells were washed three times with PBS and observed in phenol-red-free DMEM. The excitation wavelength is 1030 nm.

For tissue imaging, probes (50 μg) were introduced using 10 μL transfection reagent in *in vivo* Magnetofection Kit (OZ Biosciences) following the manufacturer's protocol. After 10 min treatment by magnet, the mouse embryo brain was observed in a home-made two-photon microscope (Wada Lab, RIKEN, Japan). The excitation wavelength is 1030 nm.

Fluorescent in situ hybridization (FISH)

For conventional FISH, cells were fixed with Carnoy solution, incubated with 25 % acetic acid, 75 % methnol at RT, washed with 1 × PBS three times, treated with RNase A at 37 ^{o}C for 1h, washed with 2 × SSC and equilibrated with PBS for 5 min. Then cells were treated with 0.002 % pepsin in 0.01M HCl at 37 ^{o}C for 5min and washed with 1 × PBS three times. For dehydration, samples were incubated incubations in 70 %, 85 % and 100 % ethanol for 5 min. After airdrying, FISH probe in hybridizing solution (10 % dextran sulfate, 50 % formamide in 2 × SSC buffer), at a final concentration of 2 ng/μl, were heated at 80 ^{o}C for 10 min and incubated overnight at room temperature. After hybridization, cells were washed with 2 × SSC for three times and finally stained with DAPI. For simple FISH, the washing step was removed.

Images of fixed MEF7 cells were acquired with a motorized inverted microscope (Axio Observer Z1; Zeiss) equipped with an objective (PlanApochromat 63 oil immersion NA 1.4). The T3 probe was detected with a green channel (Ex 514, Em 520-555 nm). The T2 probe was detected with a red channel (Ex 543, Em 560-615 nm). The T5 probe was detected with a purple channel (Ex 633, Em 656-731 nm).

Scheme 4-1. Synthesis of T1, T2 and T3 dye units

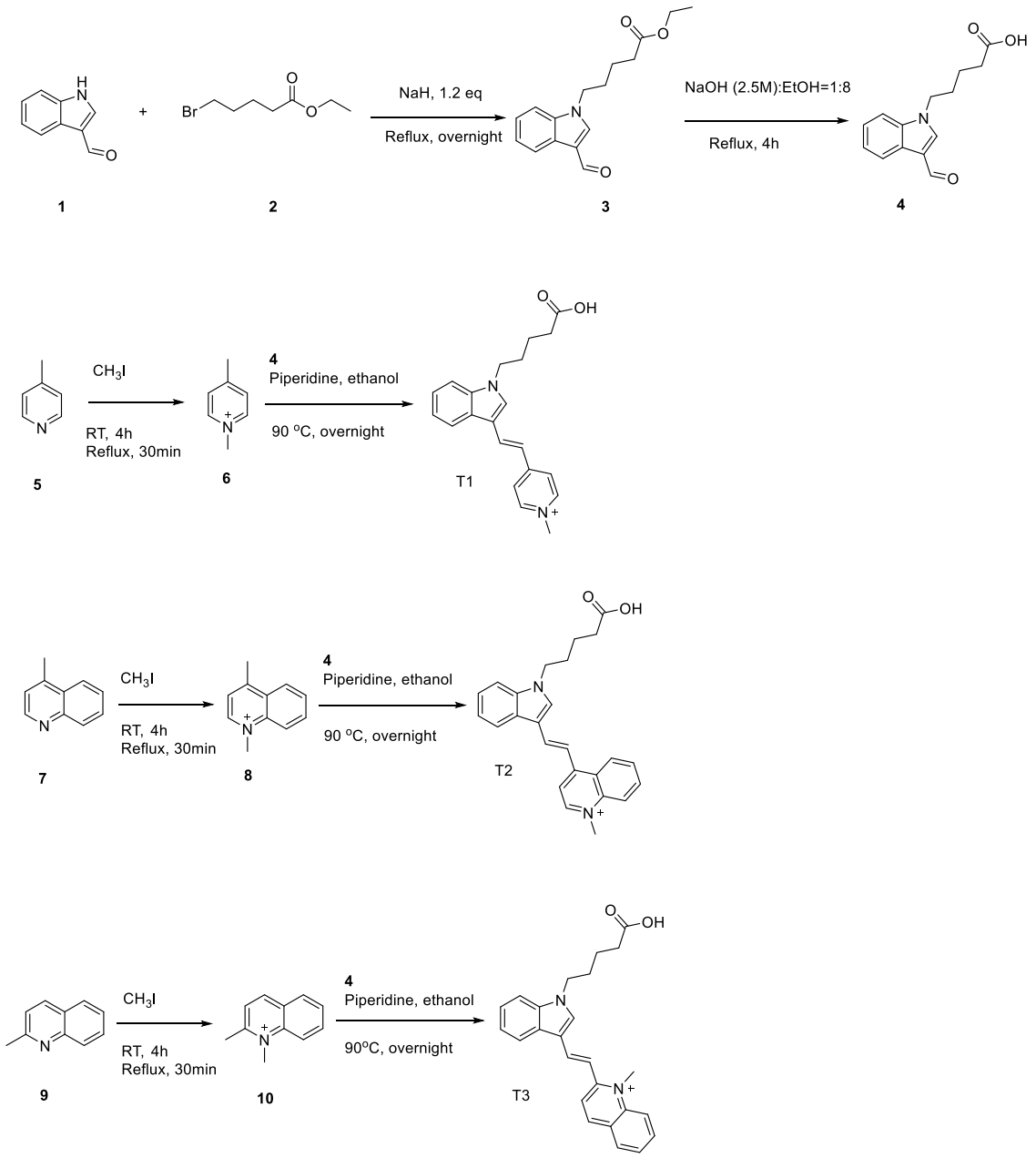

Scheme 4-2. Synthesis of T4 and T5 dye units

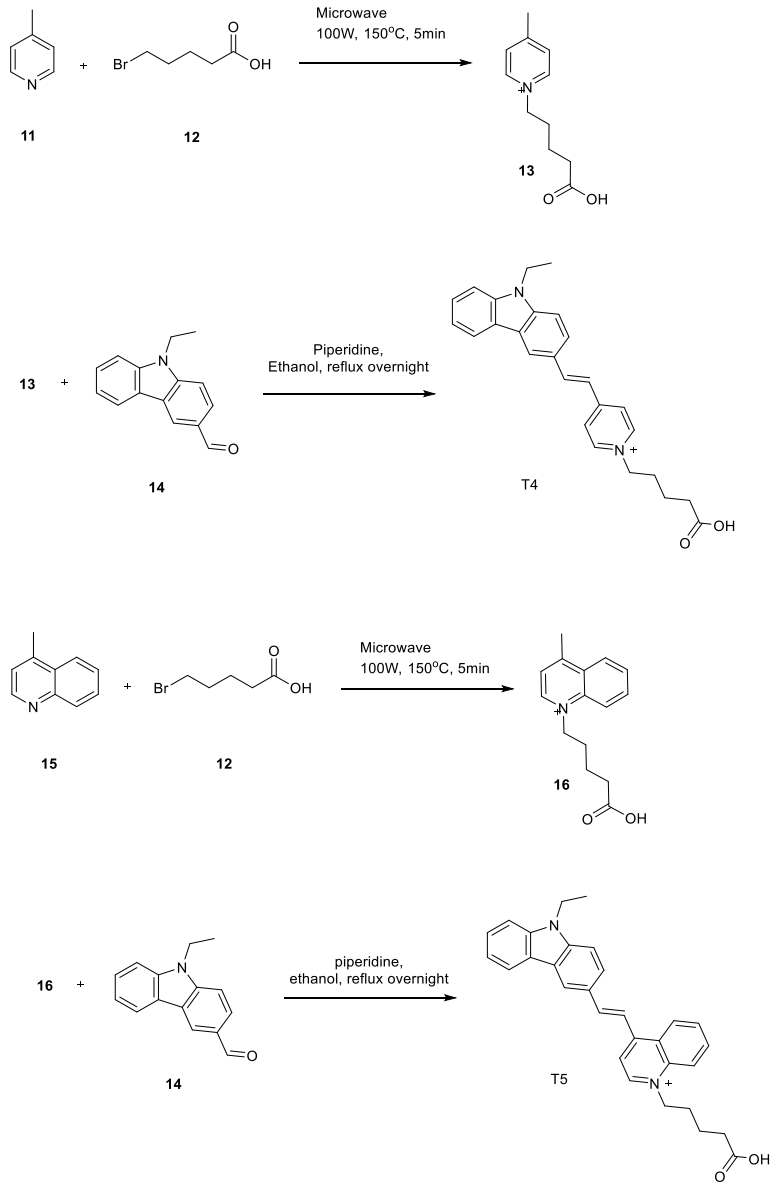

Scheme 4-3. Synthesis of T5' dye

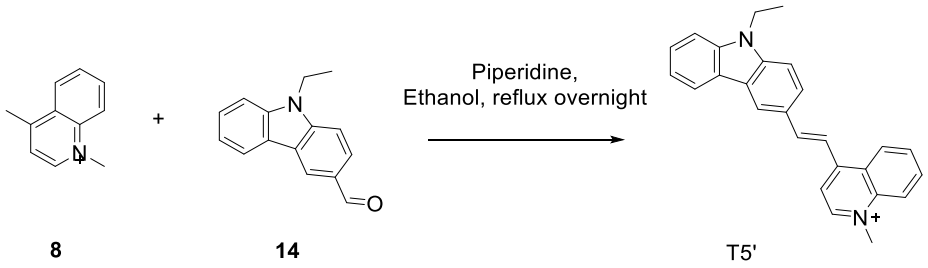

Scheme 4-4. Synthesis of $\mathbf{D_{550}}$ dye unit

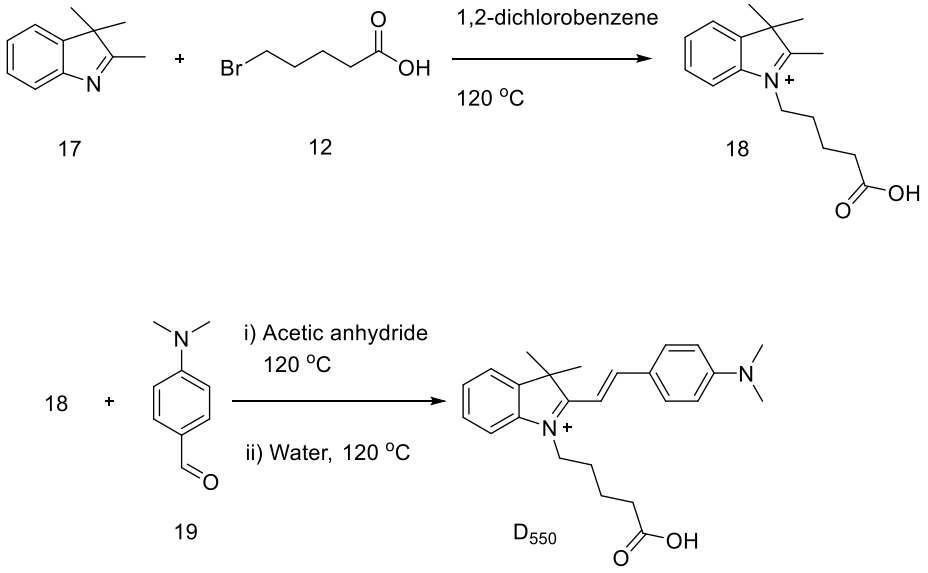

4.6 References

1. Misteli T., *Cell.* 2007, **128**, 787-800.
2. Misteli T., *Cell.* 2013, **152**, 1209-1212.
3. Carter K.C., Taneja K.L., Lawrence J.B., *J. Cell Biol.* 1991, **115**, 1191-1202.
4. McKenna N.J., O'Malley B.W., *Cell*. 2002, **108**, 465-474..
5. Li C.F., Pontes O., El-Shami M., Henderson I.R., Bernatavichute Y.V., Chan S.W., Lagrange T., Pikaard C.S., Jacobsen S.E., *Cell*. 2006, **126**, 93-106.
6. Gubitz A.K., Feng W., Dreyfuss G., *Exp. Cell Res*. 2004, **296**, 51-56.
7. Lafarga M., Tapia O., Romero A.M., Berciano M.T., *RNA Biol.* 2016, **14**, 1-14.
8. Sleeman J.E., Trinkle-Mulcahy L., *Curr. Opin. Cell Biol.* 2014, **28**, 76-83.
9. Fong K.W., Li Y., Wang W., Ma W., Li K., Qi R.Z., Liu D., Songyang Z., Chen J., *J. Cell Biol.* 2013, **203**, 149-164.
10. Raj A., van den Bogaard P., Rifkin S.A., van Oudenaarden A., Tyagi S., *Nat. Methods*. 2008, **5**, 877-879.
11. Robinett C.C., Straight A., Li G., Willhelm C., Sudlow G., Murray A., Belmont A.S., *J. Cell Biol.* 1996, **135**, 1685-1700.
12. Wang X., Kam Z., Carlton P.M., Xu L., Sedat J.W., Blackburn E.H., *Epigenetics Chromatin.* 2008, **1**, 4.
13. Hellwig D., Munch, S., Orthaus S., Hoischen C., Hemmerich P., Diekmann S., *J. Biophotonics.* 2008, **1**, 245-254.
14. Muramoto T., Cannon D., Gierlinski M., Corrigan A., Barton G.J., Chubb J.R., *Proc. Natl. Acad. Sci. USA*. 2012, **109**, 7350-7355.
15. Park H.Y., Lim H., Yoon Y.J., Follenzi A., Nwokafor C., Lopez-Jones M., Meng X., Singer R.H., *Science.* 2014, **343**, 422-424.
16. Rodriguez A.J., Condeelis J., Singer R.H., Dictenberg J.B., *Semin. Cell Dev. Biol.* 2007, **18**, 202-208.
17. Bernacchi S., Mély Y., *Nucleic. Acids Res.* 2001, **29**, E62.
18. Weil T.T., Forrest K.M., Gavis E.R., *Dev. Cell.* 2006, **11**, 251-262.
19. Ozawa T., Natori Y., Sato M., Umezawa Y., *Nat. Methods.* 2007, **4**, 413-419.
20. Sando S., Abe H., Kool E.T., *J. Am. Chem. Soc.* 2004, **126**, 1081-1087.
21. Sando S., Narita A., Hayami M., Aoyama Y., *Chem. Commun. (Camb).* 2008, **33**, 3858-3860.
22. Oomoto I., Suzuki-Hirano A., Umeshima H., Han Y.W., Yanagisawa H., Carlton P., Harada Y., Kengaku M., Okamoto A., Shimogori T., Wang D.O., *Nucleic. Acids Res.* 2015, **43**, e126.

23. Ghildiyal M., Zamore P.D., *Nat. Rev. Genet.* 2009, **10**, 94-108.
24. Chitwood D.H., Timmermans M.C., *Nature.* 2010, **467**, :415-419.
25. Ouzounov D.G., Wang T., Wang M., Feng D.D., Horton N.G., Cruz-Hernández J.C., Cheng Y.T., Reimer J., Tolias A.S., Nishimura N., Xu C., *Nat. Methods.* 2017, **14**, 388-390.
26. Li L., Shen X., Xu Q.H., Yao S.Q., *Angew. Chem. Int. Ed. Engl.* 2013, **52**, 424-428.
27. Oheim M., Michael D.J., Geisbauer M., Madsen D., Chow R.H., *Adv. Drug Deliv. Rev.* 2006, **58**, 788-808.
28. Dedov V.N., Cox G.C., Roufogalis B.D., *Micron.* 2001, **32**, 653-660.
29. Cho E.E., Drazic J., Ganguly M., Stefanovic B., Hynynen K., *J. Cereb. Blood Flow Metab.* 2011, **31**, 1852-1862.
30. Hopt A., Neher E., *Biophys. J.* 2001, **80**, 2029-2036.
31. Potter S.M., *Curr. Biol.* 1996, **6**, 1595-1598.
32. Li C., Liu Y., Wu Y., Sun Y., Li F., *Biomaterials.* 2013, **34**, 1223-1234.
33. Patterson G.H., Piston D.W. *Biophys. J.* 2000, **78**, 2159-2162.
34. van Zandvoort M.A., de Grauw C.J., Gerritsen H.C., Broers J.L., oude Egbrink M.G., Ramaekers F.C., Slaaf D.W., *Cytometry.* 2002, **47**, 226-235.
35. Ikeda S., Okamoto A., *Chem. Asian J.* 2008, **3**, 958-968.
36. Kubota T., Ikeda S., Yanagisawa H., Yuki M., Okamoto A., *Bioconjug. Chem.* 2009, **20**, 1256-1261.
37. Ikeda S., Kubota T., Yuki M., Okamoto A., *Angew. Chem. Int. Ed. Engl.* 2009, **48**, 6480-6484.
38. Guo L., Chan M.S., Xu D., Tam D.Y., Bolze F., Lo P.K., Wong M.S., *ACS Chem. Biol.* 2015, **10**, 1171-1175.
39. Li D., Tian X., Wang A., Guan L., Zheng J., Li F., Li S., Zhou H., Wu J., Tian Y., *Chem. Sci.* 2016, **7**, 2257-2263.
40. Rubner M.M., Holzhauser C., Bohländer P.R., Wagenknecht H.A. *Chemistry.* 2012, **18**, 1299-1302.
41. Inoue H., Hayase Y., Imura A., Iwai S., Miura K., Ohtsuka E., *Nucleic. Acids Res.* 1987, **15**, 6131-6148.
42. Majlessi M., Nelson N.C., Becker M.M., *Nucleic. Acids Res.* 1998, **26**, 2224-2229.

Chapter 5

Conclusion and Prospect

Conclusion

This doctor thesis presented the development of turn-on biosensors by smartly controlling the excitonic states of dyes. Hybridization-based fluorescent control by exciton interaction was introduced to aptamer-based biosensor design replacing the distance-based fluorescent control via energy transfer. A turn-off neomycin B aptamer sensor was designed based on the inhibition of dye intercalation induced by neomycin B binding in Chapter 2. This competition-caused fluorescent turn-on further used for bacterial counting. A turn-on ATP RNA aptamer was created by transducing ATP-binding into duplex recognition by TO homodimer in Chapter 3. The aptamer-based biosensor design in Chapter 2 and Chapter 3 was conversing from a three-dimensional consideration (distance-based) into a two-dimensional attention (duplex-based). The exciton controlling notion was also extended into the usage of two-photon-excitable fluorophores as the two-photon-excitable ECHO probes in Chapter 4. Combination of exciton controlling concept with other biological applications renders biomolecule detection more precisely and effectively.

Chapter 2 focuses on quantification of bacteria population. First, RNA backbone ECHO probes were successfully synthesized and exhibited favorable hybridization based fluorescent turn-on comparable to the previous DNA ECHO probes. Then, the neomycin RNA aptamer was covalently conjugated to two thiazole orange moieties and effectively quenched by neomycin B by inhibiting dye intercalation. As a proof of concept, modified neomycin aptamers in neomycin B-containing solution showed apparently higher fluorescent intensity in the presence of *E. coli* compared to that in the absence of *E. coli*.

Chapter 3 describes an ATP-sensitive fluorescent ATP RNA aptamer. The thiazole orange dimer was covalently conjugated to the site 13 of ATP RNA aptamer that is proximal to the duplex fragment of ATP RNA aptamer after forming the ATP/aptamer complex. The modified RNA aptamer increased the intensity of fluorescence several times in the presence of ATP and displayed the specificity to ATP.

In Chapter 4, two-photon-excitable ECHO probes was achieved by conjugating dyes with dual functions: exciton interaction and two photon excitability. The styryl cyanine probes have higher molar extinction coefficients while the fluorescent ON/OFF ratio of indole-based cyanine probes are more desirable. Interestingly, the indole-based cyanine probes performed excellent RNA sensitivities that have been quite problematic for the previously developed ECHO probes. Probes with **T2**, **T3** and **T5** showed clear images in live Hela cells and mouse embryo brain when excited at 1030nm.

Prospect

I believe that the advances of biosensor design using exciton controlling concept in this doctor thesis are just a start. In future, the breakthroughs below in some techniques for biosensor design may facilitate the practical applications of biosensor in both academic and industrial areas.

1. An ideal modification of RNAs: This method should resist the digestion of RNAs by RNases. Meanwhile, this modification does not affect functions of RNAs seriously.
2. A better hybridization-based design principle: Until now only neomycin aptamer and ATP aptamer were successfully transformed into biosensors using folding based biosensor design. Other strategies, structure-switching, aptamer splitting and aptamer fusing, should also be tested. A more general designing principle is eagerly desired.
3. Effective transportation of sensors into tissues or whole bodies: Transportation of sensors into whole bodies is challenging but quite necessary.

List of Achievements

Publications

1. L. Guo and A. Okamoto. Fluorescence-switching RNA for detection of bacterial ribosome. *Chem. Commun.* 2017. doi: 10.1039/C7CC04818A.
2. L. Guo, Y. Maeda, S. Wada and A. Okamoto. Novel Exciton-Controlled Hybridization-Sensitive Fluorescent Probes for Two-Photon Imaging of Nucleic Acid. In preparation.

Presentations

1. L. Guo and A. Okamoto. Synthesis of Exciton-Controlled Hybridization-Sensitive Fluorescent RNA probes for Monitoring Active RNA states. The 95th CSJ Annual Meeting, Chiba, Japan. 26-29, March, 2015. (Oral)
2. L. Guo and A. Okamoto. Exciton-Controlled Hybridization-Sensitive Fluorescent RNA Probes for the Application of Riboswitch Measurement. The 96th CSJ Annual Meeting, Kyoto, Japan. 24-27, March, 2016. (Oral)
3. L. Guo and A. Okamoto. Novel Exciton-Controlled Hybridization-Sensitive Fluorescent Probes for Two-Photon Imaging of Nucleic Acid. The 97th CSJ Annual Meeting, Yokohama, Japan. 16-19, March, 2017. (Oral)
4. L. Guo and A. Okamoto. Exciton-Controlled Hybridization-Sensitive Fluorescent RNA Probes for Measuring Conformational Change of Riboswitches. The 42nd International Symposium on Nucleic Acids Chemistry, Himeji, Japan. 23-25, September, 2015. (Poster)
5. L. Guo and A. Okamoto. Bacterial population quantification in solid state fermentation by exciton-controlled fluorescent neomycin-competition RNA aptamer. The 18th Tetrahedron Symposium, Budapest, Hungary. 27-30, June, 2017. (Poster)

Acknowledgements

Firstly, I would like to express my deepest gratitude to my supervisor Professor Akimitsu Okamoto. His support and guidance gave me confident in my research. He has provided me a wonderful research environment and many chances to attend conferences and do collaboration researches. His attitude to research and leadership in management made me learn a lot and will benefit to my future career.

I am also grateful to Professor Shinsuke Sando, Professor Kohji Seio, Associate Professor Nozomu Yachie and Lecturer Satoshi Yamaguchi who gave me valued advices and discussions to improve this thesis.

I would like to thank Lecturer Satoshi Yamaguchi and Assistant Professor Gosuke Hayashi for teaching experimental skills, providing valuable suggestions and giving encouragement to me.

I would like to thank other members in Okamoto Lab for thoughtful comments and pleasant life in Okamoto Lab. Particularly, I would like to thank Mr. Hyun Seok Jeong, Ms. Mei Takenaka, Mr. Takuma Sueoka, Mr. Kenta Kohyama, Mr. Masafumi Yanase, Mr. Ryosuke Sakamoto, Mr. Hidefumi Shiota and Mr. Taku Matsushita who taught me many technical skills to promote my research progress.

I would like to thank Secretary Ms. Chie Shishido for giving me useful guides to live in Japan and finish related administration affairs.

I would like to thank Professor Satoshi Wada and Mr. Yasuhiro Maeda who provide the machine for two-photon cross-section measurement and microscope for two-photon-excited imaging used in Chapter 4.

I would like to thank Lecturer Yoshiho Ikeuchi and Mr. Ryuji Misawa for their kind donation of mouse embryo brain used in Chapter 4.

Finally, I want to thank my father Zhaoju Guo, my mother Wenlan Zhang and my girlfriend Jiao Meng for encouraging and supporting me through the research life in the University of Tokyo.